ANNALS

OF THE

UNIVERSITY OF CRAIOVA

Series: AUTOMATION, COMPUTERS, ELECTRONICS and MECHATRONICS

Vol. 11 (38), No. 2, 2014

ISSN 1841-0626

Editura Universitaria Craiova

ANNALS OF THE UNIVERSITY OF CRAIOVA

Series: AUTOMATION, COMPUTERS, ELECTRONICS AND MECHATRONICS

Vol. 11 (38), No. 2, 2014 **ISSN 1841-0626**

Note: The **"Automation, Computers, Electronics and Mechatronics Series"** emerged from **"Electrical Engineering Series" (ISSN 1223-530X)** in 2004.

Address for correspondence:

Vladimir RĂSVAN
University of Craiova
Faculty of Automation, Computers and Electronics
Al.I. Cuza Street, No. 13
RO-200585, Craiova, Romania
Phone: +40-251-438198, Fax: +40-251-438198
Email: vrasvan@automation.ucv.ro

This issue has been published under the responsibility of Emil PETRE.

We exchange publications with similar institutions from country and from abroad

CONTENTS

Mathematical Model of Heat Flows from Shelters for Telecommunications Equipments

Gheorghe Doru Dicu
Doctoral School of the Faculty of Automation, Computers and Electronics
Craiova, Romania
dicu_doru@yahoo.com

Abstract: This paper develops a solution for keeping the ventilation of some isolated rooms (shelters) designed for telecommunications equipment, monitored by a controller which administrates the heating, the cooling and the air exchange with the outside of the room through ventilation. This thing leads to a significant increase of the electricity consumption, to an increase of administration costs which, at present, are very high, but also to an increase of the operational reliability of telecommunications equipments.

Keywords: Parameters, Ambient temperature, Monitoring, Ventilation, Equipment, Telecommunications.

1. INTRODUCTION

The telecommunications equipments installed outside the buildings, in special containers, are called shelters in specialty literature and they need certain temperature and humidity conditions. At present, these conditions shall consider the day/ the night, the season, the climate, the site at the level of the sea or at altitudes higher than 1500 m, where the environment conditions are extreme.

These shelters are in the endowment of the mobile telephony networks Orange, Vodafone, Digi, Telecom, but also in the endowment of the Ministry of Defence, Ministry of Administration and Interior, National Meteorological Administration, of some agencies which deal with the measurement of environment parameters, etc.

The requirements imposed by telecommunications equipments are to keep a temperature between 15ºC and 30ºC, and humidity lower than 90%, which are followed to be automatically ensured by the monitoring and control system.

In order to size the heating/ the cooling equipments, it was taken into consideration the necessary volume of a shelter to host the telecommunications equipments, the heating emanated by these and the thermal transfer of the shelter with the outside environment.

In the first part, is described the structure of the architecture used, insisting on the hardware components, then is presented the mathematical model of a shelter, both the dynamic model resulting from the balance equation for the air volume submitted to the monitoring and control, and the stationary model including the energetic balance of the shelter.

According to the law no. 199 from 13th of November 2000 regarding the efficient use of the energy, the consumers using more than 1.000 tones of oil equivalent per year have the obligation to appoint a responsible for energy, to perform an energetic balance every year, realized by an authorized individual or legal person, to elaborate measurement programs in order to reduce the energetic consumptions, including also investments for which various feasibility studies are carried out. These objectives can be realized through a monitoring and control management of the environment parameters with minimum costs, which shall lead to the decrease of the energy consumption, but also to the decrease of the costs with the maintenance personnel (Law no.199 / 2000).

All these coordination measures will lead to the decrease of the risk of occurring operational failures of the telecommunications equipments, to the extension of the life both of telecommunications equipments and of the ventilation equipments.

The equipments operational safety decreases the number of alarms and accidental stops, leading to an increase of the voice and data communications efficiency and, implicitly, of the gains for the operators of these shelters.

The coordination refers to the monitoring, in real time, of the environment parameters both from the inside and from the outside, then it follows the management activity located at a superior level in respect to the coordination, realizing the keeping of a prescribed temperature and humidity, and, at the same time trying to meet a performance maximum level of the maintenance. This desideratum can be implemented only through an advanced monitoring, control and management system realized by means of a controller.

The monitoring and control system has also the facility to archive the operational data, allowing the putting at the operator's disposal, who can analyze the operation of the ventilation process and which he can optimize in time.

The most important objectives of a management system of the environment parameters control are:

» the decrease of the electricity consumption for ventilation equipments;

» the decrease of the electricity consumption for telecommunications equipments;

» the decrease of the number of failures for ventilation equipments;

» the decrease of the number of failures for telecommunications equipments;

» the decrease of the expenses with the equipments maintenance, but also with the maintenance personnel (Vînătoru and Iancu, 1999).

The meeting of these objectives contributes to the increase of the efficiency for the shelters owners (time and fuel economy, reduction of electricity consumption and, implicitly, decrease of the environment pollution), the increase of the comfort through data and voice services without interruptions for the consumers.

Starting from these objectives, we can map out the essential functions to be fulfilled by the monitoring and control system:

» monitoring of study parameters;

» purchase and transmission of possible alarms in real time to the closest analysis and control centre;

» establishment of optimal orders for keeping the environment parameters;

» procurement of an operational history of the monitoring and control system for statistics and for previous analysis of alarms causes;

» possibility of interconnection with telecommunications equipments;

» evaluation of operational efficiency, in order to elaborate reports;

2. SHELTER'S STRUCTURE AND HEAT FLOWS

The electronic way for shelter's monitoring and control (SMC-01) is a digital system installed inside the shelter with the main charge of optimizing the equipments operation, which ensures the climatic conditions inside the shelter, the monitoring of its functioning, the storage conditions of the events leading to the overtaking of optimal temperature regimes and the launching of alarms corresponding to each event.

SMC-01 module is based on a microcontroller and the module programming has as an objective to get optimal functioning conditions of telecommunications equipments installed inside the shelter. The interconnections of SMC-01 module with the temperature sensors and with the equipments whose operation they handle are presented in figure 1. (Ciobanu, 2006).

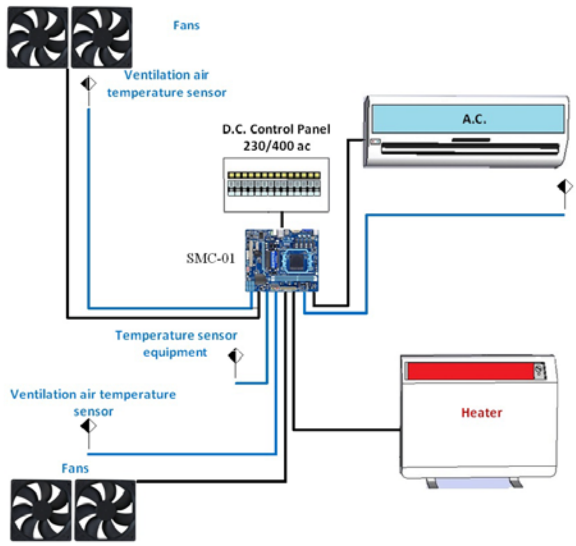

Figure 1. The interconnection chart of the elements handled by the monitoring and control system.

SMC-01 measures the inside/ outside temperature in various points and then it orders the ventilation elements from the shelter.

Depending on the power dissipated inside the shelter and on the outside temperature, SMC-01 activates at most one of the ventilation elements mentioned above.

In figure 2 is presented the shelter's structure and the heat flows from the inside and from the outside of the shelter.

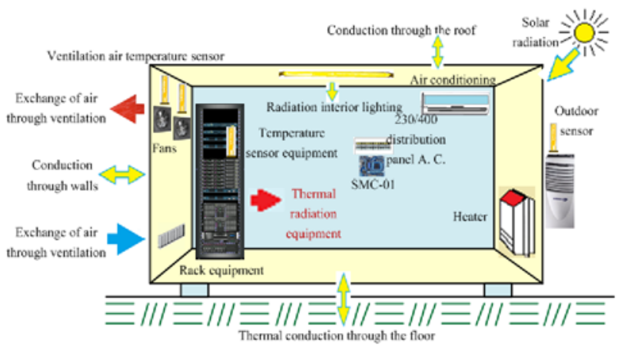

Figure 2. Main ventilation elements and heat flows of a shelter.

The shelter is fitted with the following ventilation elements:

» the heating source used when the outside temperature is lower than 15^0C and the temperature inside the shelter inclines to decrease under 15^0C;

» the air conditioning source (cooling source) used when the outside temperature is higher than 30^0C and the temperature inside the shelter inclines to increase over 30^0C;

» ventilation system for the introduction of the air from the outside if the outside temperature is between 15^0C and 30^0C, in forced regime when the temperature exceeds 35^0C, if the voltage 220 V c.a is interrupted or if the air conditioning doesn't stand.

3. HEAT, AIR AND HUMIDITY FLOWS THROUGH THE COVER OF A SHELTER

3.1 The cover of the construction:

The cover of a building is composed of all surfaces, marginal construction elements, which delimit the inside volume (heated or cooled) from the outside environment or from the unconditional spaces from the outside of the building. The cover of the building separates out the inside volume of the building from:

- the outside air;

- the ground (at plates in direct contact with the ground, located either over the height of the systematized land or under this height, and also at the walls in contact with the ground). (Vînatoru et al. 2008).

The cover protects the inside of the building against sun rays, wind, rain and snow. Moreover, it gives the structural support for walls and roof, protects the structure against deterioration, and allows the use of natural light and the access in the building.

The surface of the cover of the building (A) – represents the amount of all surfaces of marginal construction elements of the building through which takes place the thermal transfer and which is calculated with the formula:

$$A = \sum A_j, [m^2\ ] \tag{2.1}$$

where: Aj represents the surfaces of construction elements which form the cover of the building.

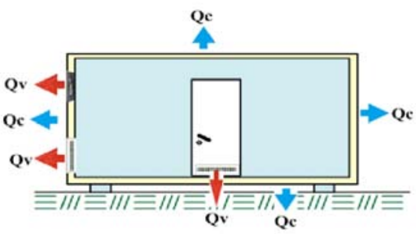

Figure 3. The temperature flows in a telecommunications shelter.

A global approach of the cover represents the key of a performing thermal isolation. For an efficient isolation of the cover, we shall take into account all its parts. But in practice is not so simple giving the fact that these parts shall meet various and distinct requirements (transparency, mobility, mechanic characteristics). Often, an equilibrated isolation of all the parts is impossible. The keeping of climatic conditions wanted for the inside is realized through the control of heat, air and humidity flows between the inside and the outside of the building. The presence of these flows is illustrated in figure 3, where the heat flows Q_C (losses through the walls) are different from the air and humidity flows realized through ventilation Q_V.

3.2 The cover and the heat flow.

An important condition for meeting the inside comfort is represented by the endowment of the building with a heating system which provide heat during the cold season. The heat supplied shall be kept at the inside of the building, thus the electricity consumption of the heating system be minimum necessary.

The transfer mechanisms (or ways) of the heat are the thermal conduction, the thermal convection and the thermal radiation. The heat flow through the cover can be realized through one, two or through all the tree ways.

The thermal radiation is showed at any temperature level and, as opposed to conduction and convection, it doesn't need a transporting agent.

Through the walls, it takes place a heat transfer from the outside environment, through convection and radiation from the air and the sun, through conduction in the shelter's walls and through convection from the walls to the inside air. The directions of the heat flows depend on the difference of temperature according to the second thermodynamics principle.

This heat exchange shall be globally approached with an exchange sent through convection directly between the temperature of the outside and the inside air, approximated with a relation in the form:

$$Q_{conv} = \sum h_i A_j (T_z - T_{ext}) \tag{2.2}$$

where A_j are the surfaces of the shelter's walls, and h_i are the global convection coefficients.

The reduction of the heat flow through the cover is realized by choosing a good thermal isolator material (Iancu and Vinatoru 2003).

4. MATHEMATICAL MODEL OF THE SHELTER

4.1. Mathematical model of the equipments rack

As it can be noticed from figure 2, inside the shelter is the Rack board, with the telecommunications equipments. This is the main source of heat from the inside of the shelter which shall be evacuated to the outside. That is why a first study will be realized on the Rack board.

A. Dynamic model of the Rack board. The Rack board measures 300x800x1700 mm and hosts the telecommunications equipments having a total mass (rack + equipments) m = 100 kg.

The air from the inside is returned through a system of two cooling fans (nominal voltage range 36 ... 60 V, 180mA).

The mathematical model corresponding to the thermal transfer is determined according to the thermal balance equation of the type:

$$mC_p \frac{dT_{ra}}{dt} = Q_{ec} - (h_a A_r (T_{ra} - T_z)) - F_{vr} \rho_a C_a (T_{ra} - T_z) \tag{2.3}$$

Where m is the mass of the board and of the equipments from the inside, m=100 kg;

C_p – is the specific heat of the board and of the equipment support equivalent with C_p = 890 J/kgK;

Q_{ec} – the heat generated by the telecommunications equipments. Q_{ec} = 7x200w = 1400 w;

h_a – the coefficient of heat transfer through convection through the walls of the board. h_a = 1,15w/m^2 k;

A_r – is the total surface of the board. A_r =4,22 m^2;

F_{vr} – is the air supply transferred by the cooling fans from the board and will be taken as a control input in order to ensure the temperature;

C_a – is the specific heat of the air. C_a = 1011 J/kg K

ρ_a – is the air density . ρ_a = 1,2047 kg/m^3;

T_z – is the temperature of the air from the shelter considered in accordance with the standards between 15ºC and 25ºC;

T_{ra} – is the air temperature from the inside of the Rack board which shall be kept lower 30 ºC.

The term $mC_p \frac{dTra}{dt}$ represents the quantity of the heat accumulated by the materials from the inside of the rack, where was neglected the heat accumulated by the air from the inside, this being lower in comparison with the heat accumulated in the board and equipments mass.

B. Stationary model of the Rack board.

According to the equation (2.1) in stationary regime (T_{ra} = ct.).

Is determined the temperature T_{ra} depending on F_{vr} and T_z.

$$(h_a A_r + F_{vr}\rho_a C_a)T_{ra} = Q_{ec} + (h_a A_r + F_{vr}\rho_a C_a)T_z \quad (2.4)$$

$$T_{ra} = T_z + Q_{ec}/(h_a A_r + F_{vr}\rho_a C_a) \quad (2.5)$$

$$T_{ra} = T_z + 1400/(4{,}22\times 1{,}15 + 1{,}2047\times 1011\times F_v)$$

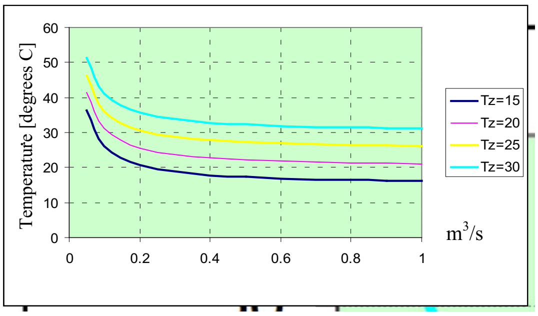

Figure 4. Temperature variation in Rack board

In figure 4 and in table 4.1 are presented the variations of the temperature T_{ra} in the rack of equipments, depending on the variation of the air input returned through the own cooling fans of the rack. It can be noticed that the temperature T_{ra} is higher than the temperature T_Z inside the shelter. As a conclusion, in order to keep the temperature in the rack board lower than 30^0 C, we shall keep the temperature from the inside of the shelter lower than de 29^0 C.

Table 4.1. Model of Rack board

Tz	15	20	25	30
Fv	Tz=15	Tz=20	Tz=25	Tz=30
0.05	36.29258622	41.29258622	46.29258622	51.29258622
0.1	26.05424579	31.05424579	36.05424579	41.05424579
0.2	20.63508766	25.63508766	30.63508766	35.63508766
0.3	18.78134625	23.78134625	28.78134625	33.78134625
0.4	17.84533368	22.84533368	27.84533368	32.84533368
0.5	17.28076605	22.28076605	27.28076605	32.28076605
0.6	16.90314612	21.90314612	26.90314612	31.90314612
0.7	16.63280694	21.63280694	26.63280694	31.63280694
0.8	16.4297176	21.4297176	26.4297176	31.4297176
0.9	16.27156029	21.27156029	26.27156029	31.27156029
1	16.14490891	21.14490891	26.14490891	31.14490891

Herewith, from the chart results that the air input of the Rack board cooling fan shall be higher than 0,2 m^3/s (F_r > 0,2 m^3/s). (Vinatoru 1993).

4.2. Mathematical model of the shelter

Considering that the temperature in the Rack Board is stabilized very quickly to a normal operation of own cooling fans, the study of the temperature variation inside the shelter will be realized by considering the Rack Board as a constant heat source Q_{ec} = 1400 w, corresponding to seven telecommunications equipments installed and we'll take into account only the heat flows from the inside of the shelter's structure, as resulting from figure 2.

Dynamic model of the shelter:

The dynamic model of the shelter results from the thermal balance equation for the air volume "V" of the shelter according to the figure 3 and has the form:

$$V_s\rho_a C_a \frac{dTz}{dt} = \sum Q_{echip} + \alpha_v F_V C_a (T_z - T_{ex}) + \alpha_r F_r C_a$$
$$(T_r - T_z) + \alpha_{ac} F_{ac} C_a (T_{ac} - T_z) + \sum_i h_P A_{pi} (T_{ex} - T_z) \quad (2.6)$$

where the following terms appear:

$\sum Q_{echip}$ - the amount of internal heat sources flows (lighting, electric equipments, people);

$h_P A_{pi}(T_{ex} - T_z)$ - the equivalent heat transfer through convection from the outside air with the temperature T_{ex} at the interior volume of the shelter with the temperature T_z through the surfaces A_i of the shelter;

$Q_v = \alpha_v F_V C_a (T_z - T_{ex})$ - the heat transfer through the air return cooling fans from the shelter;

$Q_{rad} = \alpha_r F_V C_a (T_z - T_{ex})$ - is the heat transfer from the heating radiator of the shelter used during the cold seasons, which introduces air with the

temperature $T_r > T_z$;

$Q_{ac} = F_{ac} C_a (T_{ac} - T_z)$ – is the heat transfer from the air conditioning which introduces air at the temperature $T_{ac} < T_z$. In the mathematical model, were introduced the coefficients for the use of the heat sources α_v, α_r, α_{ac}, which have values equal to 1 if the source is used and equal to zero if the source is not used.

According to the operational rules of the shelters, the values of these coefficients, depending on the outside temperature T_{ex} , are presented in table 4.2.

Table 4.2 Values of α coefficient

Temperatura exterioara	α_v	α_r	α_{ac}
$T_{ex} < 15^0C$	0	1	0
$15^0C < T_{ex} < 25^0C$	1	0	0
$T_{ex} < 25^0C$	0	0	1

In order to study the efficiency of heating or cooling sources of the shelter, from the equation (2.6) it results the variations of the temperature T_z inside the shelter, for various variation fields of the outside temperature T_{ex} . (Vinatoru 1993).

Stationary model for 15 ºC < T_{ex} < 35 ºC .

In this case, according to the operational instructions mentioned in table 4.2, the adjustment of the air temperature in the shelter's space is ensured only by the cooling fans which evacuate the air from the shelter, being replaced with an outside air with the temperature T_{ex}. In the equation (2.6.), appears also the term Q_{ec} = 1400 w and the term $h_P A_{pi} (T_{ex} - T_z)$ corresponding to the heat transfer through convection (shelter's walls).

Depending on the sizes and the materials of which shelters are usually made of, it was considered:

$A_{pi} = 3 \times 10 \times 18 = 48 m^2$ and h_p = 1,15 W/K/m^2

(usually for the conditions from our country h_p = 0.28-1.4 W/K/m^2) .

Under these conditions from the equation (2.6) in stationary regime ($dT_z / dt = 0$) results:

$$Q_{ec} + h_p A_{pi} (T_{ex} - T_z) - F_v \rho_a C_a (T_z - T_{ex}) \qquad (2.7)$$

or $$T_Z = T_{ex} + Q_{ec} / (h_p A_{pi} + F_a C_a \rho_a F_V) \qquad (2.8)$$

$$T_Z = T_{ex} + 1400 / (1{,}15 \times 48 + 1011 \times 1{,}2047 \times F_V)$$

By the help of Excel program, using the formula (2.8) it was mapped out the chart of the variation of temperature T_z depending on the air input F_v of cooling fans presented in figure 5 for various values of temperature T_{ex} .

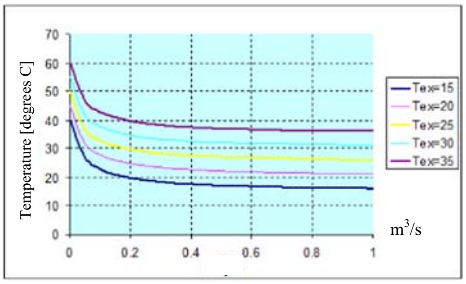

Figure 5. Variation of shelter's temperature for $15^0C < T_z < 35^0C$

From the relation (2.8) and from the charts from figure 5, it results that the inside temperature T_z is higher than the outside temperature T_{ex} .

Also, from the same chart, it results that in order to keep inside the shelter a temperature T_z < 40 ºC the minimum input of cooling fans shall be F_v > 0,2 m^3 / s.

Stationary model for -15 ºC < T_{ex} < 10 ºC

In this case, according to the operational rules, the adjustment of the temperature is realized through the heating radiator which transfers a heat flow: $Q_{rad} = F_v C_a \rho_a (T_r - T_z)$.

The balance equation becomes:

$$Q_{ec} - h_p 48 (T_z - T_{ex}) + F_v C_a \rho_a (T_r - T_z). \qquad (2.9)$$

From (2.9) it results the variation of the temperature T_z depending on the input F_v for various values of the temperature T_{ex} :

$$T_z = (Q_{ec} + 48 \times 1{,}15 \times T_{ex} + 1011 \times 1{,}2047 \times F_v T_r) / (48 \times 1{,}15 + 1011 \times 1{,}2047 \times F_v). \qquad (2.10)$$

From the fire prevention conditions is considered that the temperature T_r = 100 ºC of the air delivered by the forced convection air heater.

In figure 6 are presented the variations of the air temperature from the shelter for various values of the outside air temperature T_{ex}.

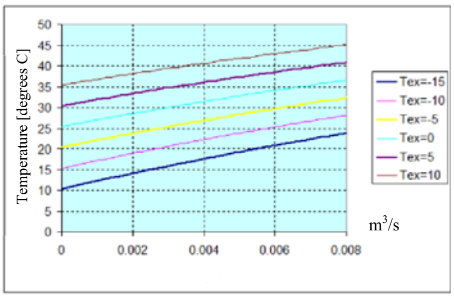

Figure 6. Variation of shelter's temperature for $-15^0C < T_z < 10^0C$

It results that for outside temperature higher than 0ºC to a zero air input of the forced convection air heater, the temperature from the inside of the shelter is higher than 25ºC. This thing comes from the fact that the thermal isolation of the shelter's walls is very good and the heat exchange through the shelter's walls is very low.

From this study, it results that the operational instructions of the shelter shall be changed, in the sense that the using field of cooling fans shall be also extended for outside temperatures under 15 ºC .

For temperatures between 0 ºC and 15 ºC, the study results are presented in figure 6.

From this figure, it can be noticed that, if it is accepted an inside temperature higher than 20ºC, the temperature adjustment through cooling fans can be kept even for values of the outside temperature up to -5ºC, and the heating system will operate only for temperatures under -5 ºC.

Stationary model for $T_{ex} \geq 35$ ºC.

In this case, according to the operational rules from table 4.1, the adjustment of the temperature is realized by the help of the air conditioning equipment which provides the cold air flow $Q_{ac} = C_a \rho_a (T_{ac} - T_z)$, where F_{ac} is the cold air flow input considered variable, with the temperature $T_{ac} = 10$ ºC.

The thermal balance equation in stationary regime becomes:

$$Q_{ec} = h_p 48(T_z - T_{ex}) + F_{ac} C_a \rho_a (T_{ac} - T_z) \quad (2.11)$$

From (2.11) it results the variation of the temperature T_z depending on the input T_{ac} for various temperatures T_{ex} = [35, 40, 45]

$$T_z = (Q_{ec} + F_{ac} C_a \rho_a T_{ac} + h_p 48 T_{ex}) / (h_p 48 + F_{ac} C_a \rho_a) \quad (2.12)$$

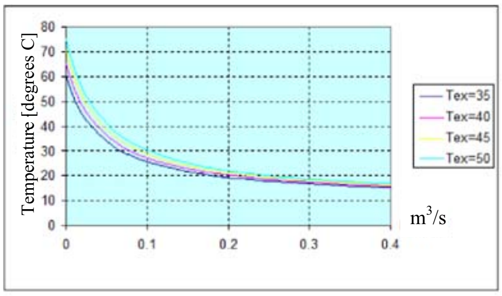

Figure 7. Temperature variation of the shelter for $T_{ex} > 35^0$C.

In figure 7 are presented the variations of the air temperature from the shelter for various temperatures of the outside air.

From figure 7 it can be noticed that the temperature from the inside of the shelter can be kept under 40ºC for an air input of the air conditioning system $F_{ac} \geq 0{,}05$ m^3/s.

Emergency operation study

In the operational instructions of the shelter is mentioned the fact that if the cooling system gets out of order for temperatures higher than 35 ºC, than the temperature control automatic machine shall keep the ventilation system with the maximum debit at cooling fans.

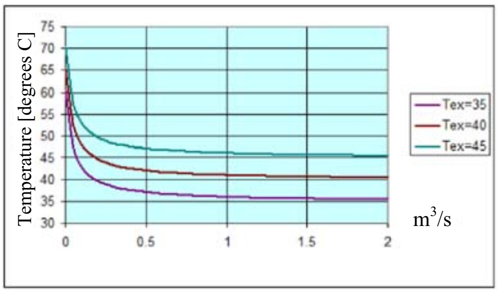

Figure 8. Emergency operation study

For the analysis of this case, the study is restarted, but for T_{ex} = [35, 40, 45] ºC, with T_z given by the relation (2.8).

The results of the study are presented in figure 8.

It can be noticed that the temperature inside the shelter is closer to the outside temperature for a debit of cooling fans $F_v > 1$m^3/s, but it cannot get down.

5. CONCLUSION

The most important thing is the operation of telecommunications equipments in the environment parameters recommended by the manufacturer, fact which leads to their operation in safety, the life extension and the decrease of maintenance costs.

A coherent management of the energy gives the greatest opportunity from the present for the energetic efficiency. From the point of use, the well managed systems will be a significant factor, allowing to the network to make real savings of energy.

The implementation of the sensors network, distributed and managed by microcontroller, leads to the use of the outside temperature of the air (through ventilation) for a better management of the heat flows from the shelter. This working way leads to important improvements of the energetic efficiency in terms of use, costs, security and impact on the environment, to an extension of the life of telecommunications equipments, but also of the ventilation equipments.

REFERENCES

Ciobanu, L. (2006). *Sensors and transducers*, Matrix-Rom, Bucuresti, Romania.

Iancu, E. and Vinatoru, M. (2003). *Analitical Methods for Fault Detection and Isolation – Case Studies*, Universitaria Craiova, Romania.

Vinatoru, M., Iancu, E., Maican, C., and Canureci, G. (2008). *Automatic management of industrial processes,* EUC Universitaria Craiova, Romania.

Vinatoru, M. (1993). *System Theory,* University Typography of Craiova, Romania.

Vinatoru, M. and Iancu, E., (1999). *Fault detection and location in dynamic systems,* SITECH, Craiova, Romania.

Law no. 199 from 13th of November 2000 *regarding the efficient use of the energy* (http://www.legex.ro/Legea-199-2000-21728.aspx).

An Overview of the Hiper-Redundant Robot HIPROB-I

Sorin Dumitru*, Florin Manta,**
Cristina Resceanu***

**Faculty of Automation, Computers and Electronics, University of Craiova*
(Tel: 0744152497; e-mail: dumitru@robotics.ucv.ro).
*** Faculty of Automation, Computers and Electronics, University of Craiova*
(Tel:0740292334; e-mail: manta@robotics.ucv.ro)
**** Faculty of Automation, Computers and Electronics, University of Craiova*
(Tel: 0731466449; e-mail: cristina@robotics.ucv.ro).

Abstract: In these days can be observed a grown in interest regarding the robots with high mobility degree, wanted for their capability to avoid obstacles and reach difficult positions in their working space. One particular class of these robots consists in tentacle robots, biologically inspired by cephalopods. This paper present the steps followed for building a hyper-redundant robotic structure called HIPROB-I. It is shown how the CAD model was made, the preparation and built of the physical robotic structure and the finite-element analysis.

Keywords: hyper-redundant; CAD; finite-element; actuation; flexible.

1. INTRODUCTION

A tentacle manipulator is a hyper-redundant or hyper degree of freedom manipulator. The control of these systems is very complex and a great number of researchers have tried to offer solutions for this difficult problem. Various solution have been tried in order to obtain a fast and accurate control algorithm (Cieslak, 1999), (Hirose, 1993), (Immega, 1995).

The research group from the University of Craiova, Romania started working in the field of hyper redundant robots over 20 years ago. Starting since 2008, the research group designed a new experimental platform for tentacle manipulators.

This new robot, called HIPROB–I, is actuated by stepper motors. The rotation of these motors rotates the cables which, by correlated screwing and unscrewing of their ends, determines their shortening or prolonging, and by consequence, the tentacle curvature. The backbone of the tentacle is an elastic cable made out of steel, which sustains the entire structure and allows the bending. Depending on which cable shortens or prolongs, the tentacle bends in different planes, each one making different angles (rotations) respective to the initial coordinates frame attached to the manipulator segment – i.e. allowing the movement in 3D (Blessing, 2004).

2. CAD MODEL

Taking into consideration the latest research results in the area of hyper-redundant robotic structures, a virtual model of such a robotic unit was elaborated. The robotic system is composed from two units, one with a flexible structure with kinematic possibilities similar with the snake's locomotion and another one for driving.

The poly-articulated unit is composed from three modules with independent driving, that confers a complex 3D configuration, with multiple kinematic possibilities for the working space.

The flexible structure as an integrate system, or as independent modules, is conceived to allow driving in two modes, respectively:

- one with wires and a flexible central column;
- one with flexible vertebrates and a flexible central column;

For the case in which the driving is made by wires, a module has two degrees of freedom and in the case of driving with flexible columns each module has three degrees of freedom.

The mechanical structure for each module is based upon thread transmissions with self decelerations possibilities and adjust of the axial-radial clearances.

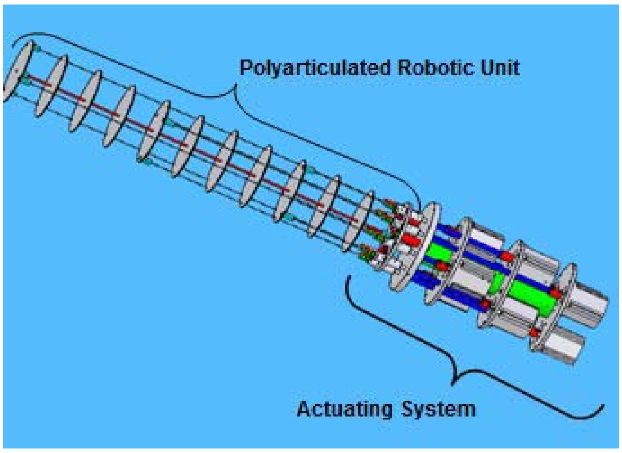

Fig. 1. Virtual model of the polyarticulated robotic unit.

The flexible unit with the snake-like design is composed from a base flange, some intermediary flanges, and four flexible shafts, with high elasticity which will be called vertebral spines. The central shaft is mounted rigidly to all the intermediary flanges, Figure 1. The three super elastic spines are mounted equidistantly upon the central spine.

The vertebrates are connected only to the end flange. The intermediary flanges maintain constant the radial distance between the secondary tubes and the central vertebrate.

By modifying in an active way the length of two of the vertebrate spines, the final flange can be manipulated with two degrees of freedom in any direction.

The actuating spines are rigidly joined only to the end flange; the joint between them and the intermediary flanges is like one translational joint.

In Figure 2 is presented the flexible unit that has a cylindrical form.

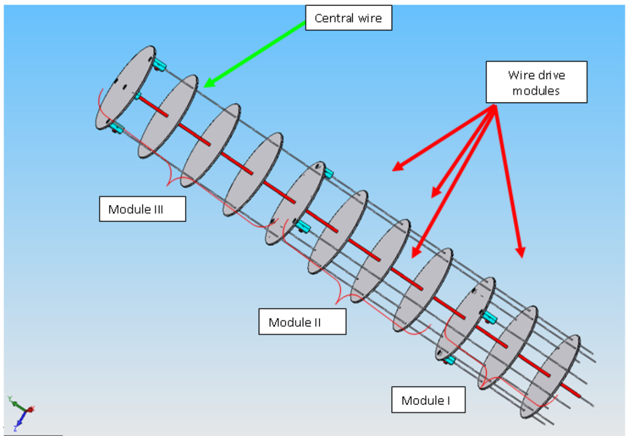

Fig. 2. Flexible robotic unit.

As it was presented above, the actuation of the robotic unit is based upon thread transmissions. The motion of rotation developed by the actuators is transformed into a translation motion due to thread transmission (Figure 3).

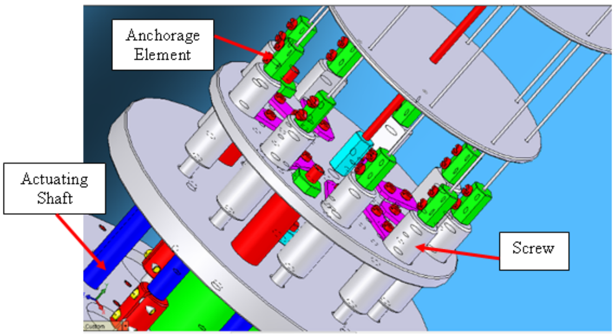

Fig. 3. Virtual model of the actuating shafts.

The shafts that are delivering the motion, unitive with the actuators shafts and using the command unit, are realizing a motion of rotation that encloses the characteristics of the actuators(rotative speed, torque, etc). Moreover, the shafts have at the opposite part a threaded sector that on which is mounted the screw joint that is realizing the motion of translation. Each screw joint is unitive with one actuating cable of the poly-articulated unit.

The stepper-motors are disposed on three superposed levels (three actuators on each level) for the individual actuating of the three modules. In Figure 4 is presented the virtual model of the actuating system together with the identification of it's main elements.

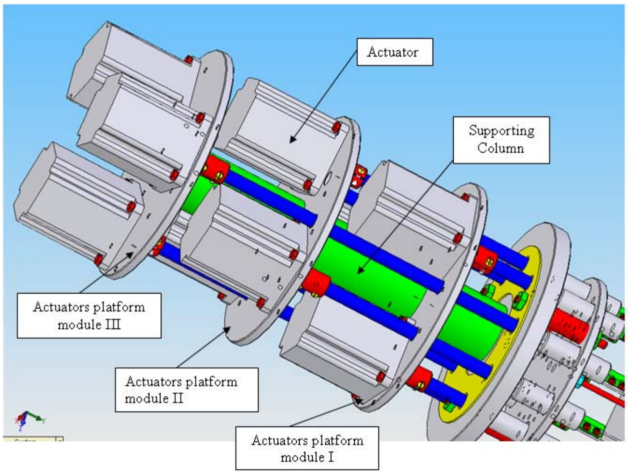

Fig. 4. Virtual model of the actuating system

3. THE VALIDATION OF THE ACTUATING PRINCIPLE OF THE ROBOTIC UNIT

The working principle was verified by importing the vitual model (respectively of the poly-articulated robotic unit) in the virtual simulation environment of the software Visual Nastran 2001. Therefore, it was applied an actuating force of 500N on the 9 actuating cables, on different directions (Figure 5).

The first simulation was realized for one module, some aspects being presented on the following figure. Observing that the simulation produces the bending of one module, it was realized the simulation for the entire robotic structure(some aspects are presented in Figure 6).

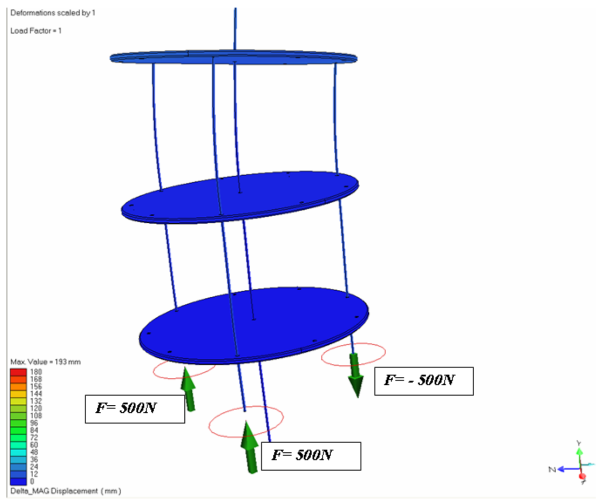

Fig. 5. Virtual simulation for one module (displacements in mm).

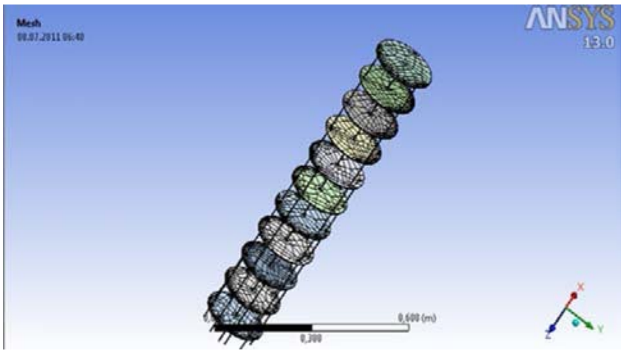

Fig. 6. Virtual simulation for the entire robotic unit.

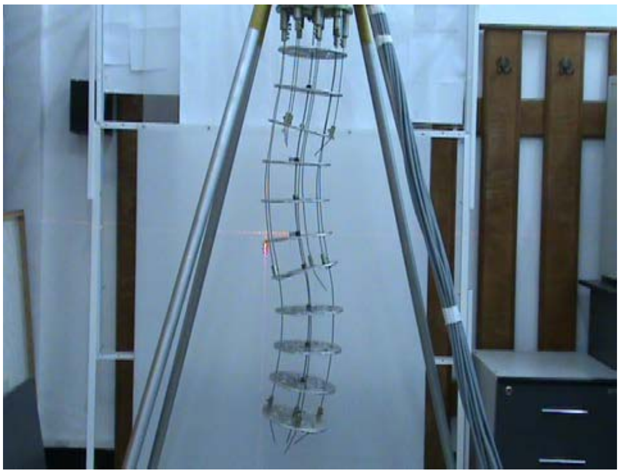

Fig. 7. The experimental model of the robotic structure.

4. THE ACTUATING SYSTEM

The motion is transmitted to the robot's arm using the cables. Each module is actuated using three cables that follow the entire module and are fixed on the last disk of that element. This cables are disposed under an angle of 120˚ from the median longitudinal axis of the element (Figure 7). It has been chosen a number of 3 actuating cables due to the fact that is the minimum number of actuating elements that can confer total mobility and control of the robot's motion.

The block of the actuating elements is shown in Figure 14. The tentacle arm is designed to be actuated by 3-phase stepper motors. The interfaces are pulse direction based without rotation monitoring. Set-point position of the stepper motor is preset as a pulse signal by a controller via signal interface. A pulse corresponds to one step of the motor (0.5 pps-2.4M pps, Max. Acceleration Rate: 737M pps2, Speed resolution: 16-bit). An electronic relay contact reports operating readiness. The nominal torque MN is 2 Nm. Steps per revolution are selectable from 200 to 10000. The step angle α is selectable from 1.8° to 0.036°. Tree stepper motors are used for each segment of the tentacle. 4-Axis Stepper Motion Controller boards are used. It is a pulse train motion controller which provides T/S curve control, on-the-fly speed change, non-symmetric acceleration and deceleration profile control, and simultaneous start/stop functions. This controller also offers card index settings for multiple cards in one IPC system.

Fig. 8. The block of the actuating element (stepper motors).

The boards offer powerful speed change functions that can be executed while the axis is moving. After motion begins, the target speed can be changed as needed according to the application. By using either a software function or external input signal, the controller can perform simultaneously starts and stops on multiple axes in a one-card configuration, or multiple axes in a multiple-card application (in this case). The motion generated by the stepper motors (rotation), is transformed into a motion of translation using the screw joint system (see Figure 9).

Fig. 9. The system that converts the rotation produced by the stepper motors into translation.

In the superior part, it can be observed the screw thread attached to the axis of the motor, and under this is the nut that takes contact with the screw.

It was chosen this kind of actuating system due to the fact that stepper motors are reliable, have a good precision and a very good repeatability of the motion, develops a very large torsion moment, are easy to control and command and the system that converts the rotation into translation motion assures very high precision. The transmission of the motion is expressed through the following expression:

$$\omega = \frac{v}{L} \qquad (1)$$

Where:

- ω is the rotation velocity of the stepper motor;
- v is the linear velocity of the movement of the translation element;
- L is the step of the fillet.

In other words, to every complete rotation of the motor's axis it corresponds a translation equal with the length of the fillet's step. Therefore, (1) can be written under this form:

$$d = L \cdot r \qquad (2)$$

Where:

- d is the translated distance;
- L is the fillet's step;
- r represents the number of complete rotations of the motor's axis.

In conclusion, by selecting for the stepper motor a number of 2000 steps per rotation, it can be obtained a very good precision for the translation. Furthermore, considering the ideal case in which no steps are lost, we can determine using (1) the precise translation per total, without being necessary a supplementary sensorial system for closing the position reaction loop, simplifying like this the command and control system (Ivănescu, 1984, 2004, 2007).

5. FINITE ELEMENT MODELING

In order to demonstrate the viability of the mechanical system, it was realized the modeling and simulating of the functionality using the finite element method.

The parameterized modeling of the flexible system allows the 3D simulation for different versions with one, two or three modules, with gauge dimensions and versions with different materials with full circular spines or tubular.

It is proposed the finite element analyze for the simple case with one robotic system with one module and for a system composed from three modules (Cojocaru et al, 2010).

For the analyze with the finite element method the next important steps have been followed:

- realizing the three-dimensional geometrical model using SolidWorks software, for both of the cases;
- it was defined the interface with a software for simulation and analyze with flexible elements (Ansys, Nastran, Adams,Algor);
- defining the type of finite elements (solid-tetrahedral finite elements);
- defining material properties (longitudinal elasticity module, the coefficient of transversal contraction, material's density, etc);
- digitization the entire structure and building a network of finite elements for each element of the flexible unit (disks, spines);
- introduction of the contour and loading conditions, respectively:
  - fixing the central spine on the intermediary and bottom disks;
  - defining the translation thimbles between the actuating spines and the intermediary disks;
  - fixing the actuating spines to the bottom disk;
  - introducing the single forces that apply on each actuating spine;
  - the first disk, on which are mounted the screwed transmissions, is fixed;
- post processing, respectively:
  - identifying the variation laws for tensions, deformations and displacements.

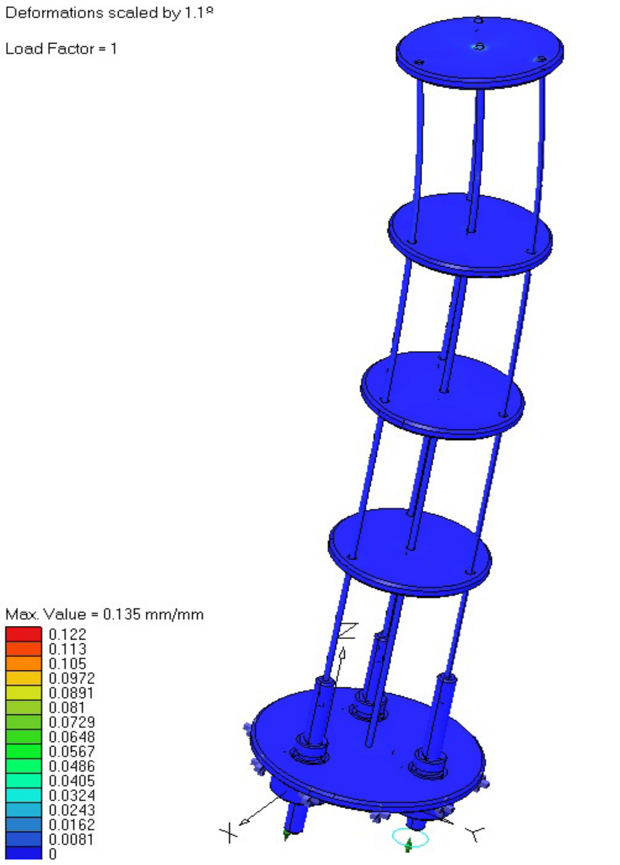

Fig. 10. Distribution of the resulted elastically deformations, for one module, with three flexible spines.

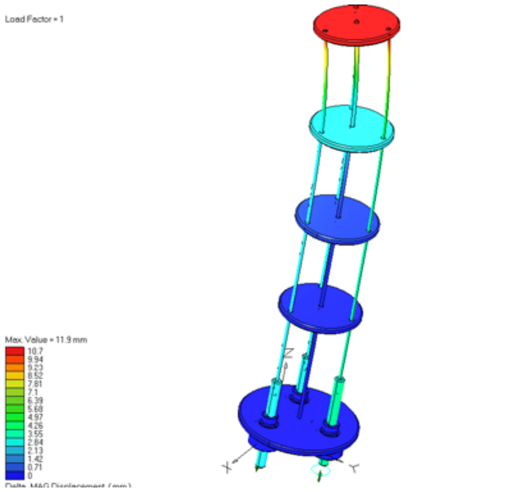

Fig. 11. Distribution of the resulted elastically displacements for one module, with three flexible spines, sequence 1.

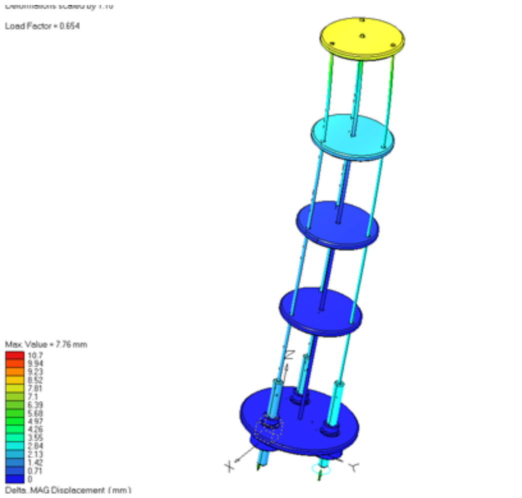

Fig. 12. Distribution of the resulted elastically displacements for one module, with three flexible spines, sequence 2.

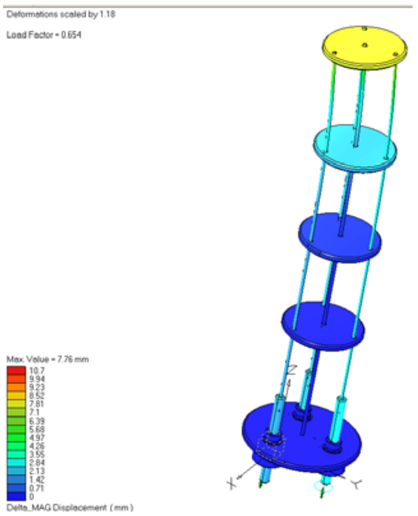

Fig. 13. Distribution of the resulted elastically displacements for one module, with three flexible spines, sequence 3.

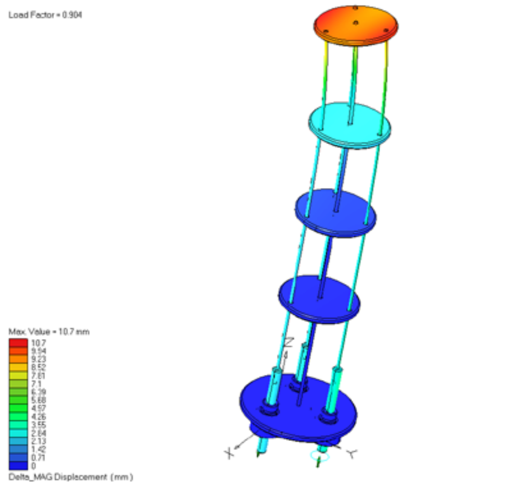

Fig. 14. Distribution of the resulted elastically displacements for one module, with three flexible spines, sequence 4.

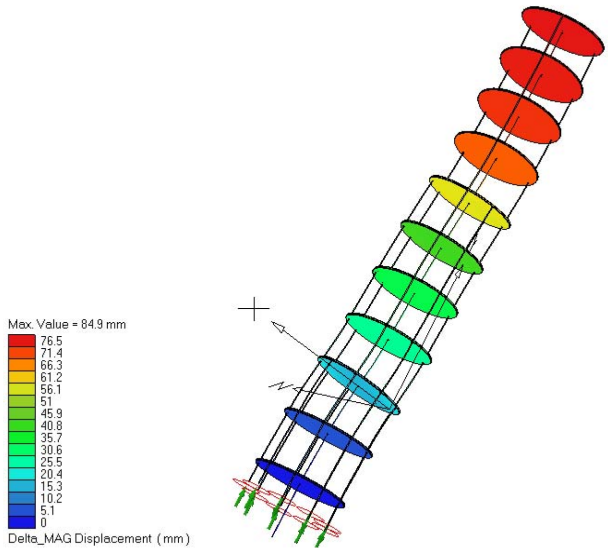

Fig. 15. Distribution of the elastically displacements for a linkage with three modules (sequence 1).

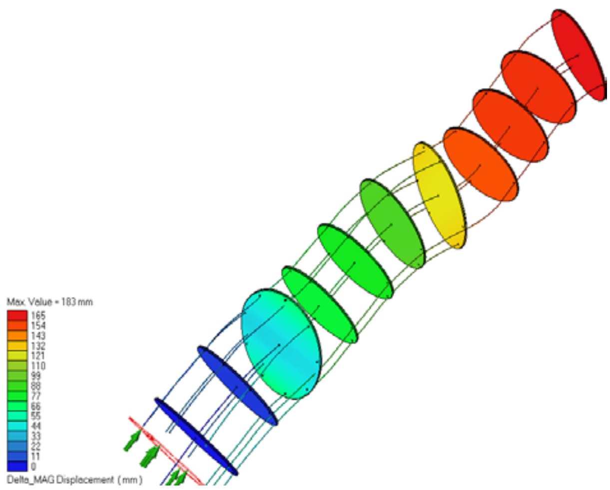

Fig. 16. Distribution of the elastically displacements for a linkage with three modules (sequence 2-rotate view).

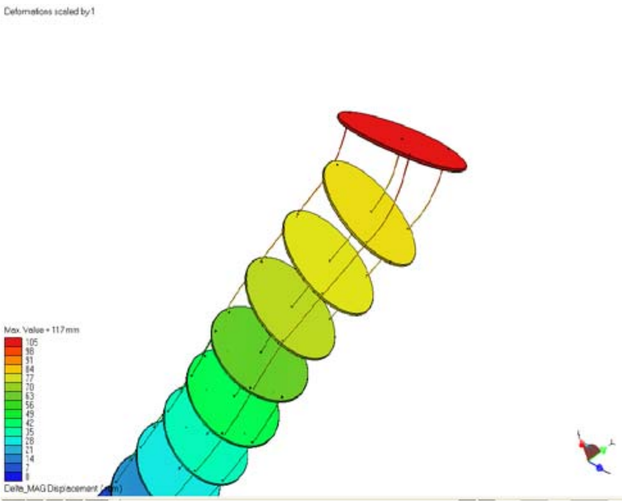

Fig. 17. Distribution of the elastically displacements for a linkage with three modules (sequence 3-in detail).

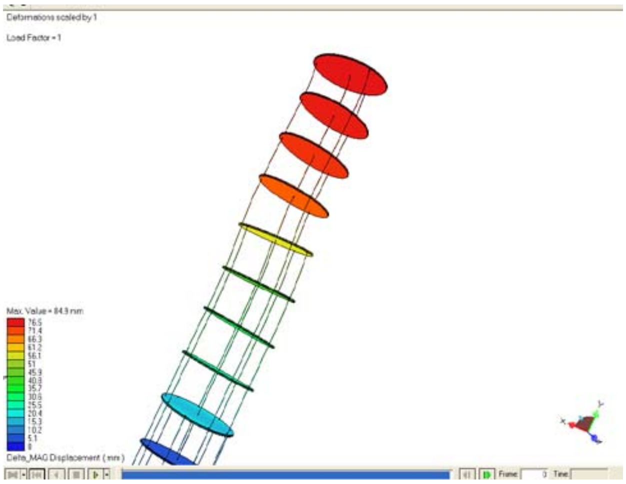

Fig. 18. Distribution of the elastically displacements for a linkage with three modules (sequence 4-in detail).

6. CONCLUSIONS

Due to the fact the robotic unit is composed from three modules HIPROB-I has a larger number of degrees of freedom and a complex spatial configuration for the working space.

Finite element analysis provides a total control of the behaviour of the robotic unit, dynamically from the point of view of displacements, tensions and deformations.

Using the finite-element modeling, we can identify the time variation laws for the dynamic and cinematic parameters, if the actuating forces are time variable (the elastically deformations and displacements for every important point of the system).

The finite-element modeling was done assuming that all the three modules are simultaneously actuated.

Using the interface with the Adams software, on the segment of flexible elements can be realized the cinematic and dynamic response of the system on time segments, when the three modules are working independent or simultaneously.

ACKNOWLEDGMENT

This work was partially supported by the grant number 18C/2014, awarded in the internal grant competition of the University of Craiova.

REFERENCES

Blessing M. and Walker I.D. (2004). *Novel continuum robots with variable length sections*, 55-60. Proc. 3rd IFAC Symp. on Mechatronic Syst., Sydney, Australia.

Cieslak R. and Morecki A. (1999). *Elephant trunk type elastic manipulator*, volume (17), 11-16, Robotics.

Cojocaru D., Ivănescu M., Manta Fl., Dumitru S. and Tănasie T.R. (2010). *Hyper-redundants robots*, Editura Universitaria, ISBN 978-606-510-980-3, Craiova, Romania.

Hirose S. (1993). *Biologically inspired robots*, Oxford University Press.

Immega G. and Antonelli K. (1995). *The KSI tentacle manipulator*, 3149-3154, Proc. 1995 IEEE Conference on Robotics and Automation.

Ivănescu M. (1984). *Dynamic control for a tentacle manipulator*, 315-327, Proceedings International Conference on Robotics and Factory of the Future, Charlotte.

Ivănescu M. (2002). *Position dynamic control for a tentacle manipulator*, A1-15, 1531-1539, Proceedings IEEE International Conference on Robotics and Automation, Washington.

Ivănescu M. and Cojocaru D. (2007). *Visual servoing by artificial potential methods of a hyper-redundant robot*, Proceedings of 16th International Workshop on Robotics in Alpe-Adria-Danube Region - RAAD 2007, Ljubljana, Slovenia.

Lossless Compression in Image Processing Technologies and Applications

Bogdan Popa *, Dan Popescu **,

** Department of Automation and Applied Informatics, University of Craiova, Craiova, Romania (e-mail: bogpo89@yahoo.com)*
*** Department of Automation and Applied Informatics, University of Craiova, Craiova, Romania (e-mail: dpopescu@automation.ucv.ro)*

Abstract: This research work provides lossless data compression methodologies, an extensive research study of methods of compression and image processing algorithms starting from the actual materials and functions made by several processing technologies today, resulting in finding solutions and innovative ways to improve the actual studies . Data compression is a process that reduces the data size, removing the excessive and redundant information. Today there are a lot of different data compression methodologies, which are used to compress different data formats like, video, audio, image files. This study represents a comparison of several compression methods based on previous research and the analysis in the context of their current needs.

Keywords: Data compression; image processing; lossless compression, wavelet transform.

1. INTRODUCTION

Data compression and image processing are old and eternally new research fields. It can be said that the first type of data compression is stenography (or shorthand writing) which is a method that increases the speed and brevity of writing. Today, many problems that occur with printed matters are not related to the production of papermaking, but such physical storage types of the paper require large volumes. Storage requirements for digital images are several orders of magnitude lower than for paper documents. The main goal is the improvement of the information contained images for interpretation by a human subject or by artificial robots.

Image processing is very commonly used today with multiple applications in different areas. Lossless compression (or information storage, or the reverse), compresses data by different techniques, which is the same as its original. Data are represented today as a combination of information and redundancy. Information is the portion of data that must be preserved permanently in its original form, in order to interpret the meaning or purpose of the data. The redundancy of the data is that it can be removed when not needed, or can be used to interpret the data when necessary. In most cases, redundancy is reused to generate original data in its original form. A technique for reusing data redundancy is defined as data compression. Redundancy is reduced representation of the data so that it can subsequently be reintroduced to retrieve the original data, which is called the decompression of the data.

In several technologies there are some applications that need to recover essential or crucial information in it, such an expert in these areas need to process and analyse all the information, for example, in medical imaging, sensing (i.e., satellite imaging), scientific imaging, museums / art machine vision etc., and therefore, it is necessary to perform lossless methods such technology and applications. In research, starting from compression algorithms, compression means, techniques used, all conclude in analysis based on previous articles compared with the results from proposed project.

2. COMPRESSION ALGORITHMS BACKGROUND

Many type of references broke lossless image compression method in two parts: Modelling and Coding [1, 2, 3]. Penrose et al. [4, 5] add mapping stage previous to the modelling stage like in Figure 1. This stage it is less correlated with the original data. It can be said that can be a simple process, for example replacing each pixel with the difference between the current and previous pixel (difference mapping), on the other hand more complex mapping offer better results. It modifies the statistical properties of the data at the pixel level. This can do the data to be encoded closer to being independent, identically distributed (i.i.d.).

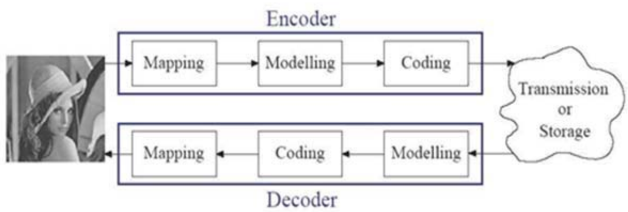

Figure 1: Main model for lossless image compression [4, 5].

Removing or reducing the redundant data is done most often by processing the original data representation to a form or another. Some of the known conversion technologies are discrete cosine transform (DCT) and discrete wavelet transform (DWT). This step leads to the reduction of entropy.

JPEG2000 standard uses image plates. The source image is divided into non-overlapping rectangular blocks in a process called tiling. Application of dimensional changes in the horizontal and vertical forms two-dimensional transforms. This leads to four small blocks of the image; one low resolution to high resolution vertical and horizontal low resolution, a vertical resolution and low and high horizontal resolution, and a high resolution all. This process of applying a one-dimensional filter in both directions is repeated several times on the low resolution image block.

This is called dyadic decomposition, and is shown in Figure 2. An example of the dyadic sub-band decomposition the entire image is dealt with as a piece shown in Figure 2.

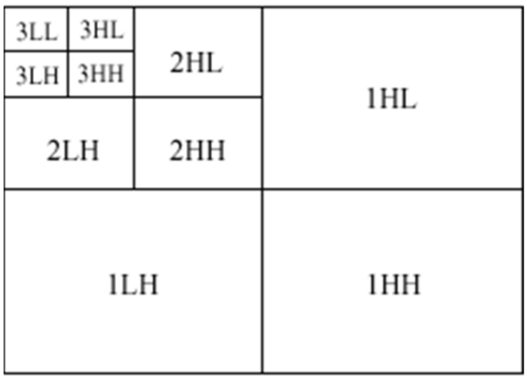

Figure 2: Dyadic decomposition.

3.WAVELET TRANSFORM LIBRARY FOR IMAGE PROCESSING

The Fast Wavelet Transform is a mathematical algorithm designed to turn a waveform or signal in the time domain into a sequence of coefficients based on an orthogonal basis of small finite waves, or wavelets. The transform can be easily extended to multidimensional signals, such as images, where the time domain is replaced with the space domain. The Fast Wavelet Transform is used in image processing tasks like image compression, denoising and fast scaling. It has as theoretical foundation the device of a finitely generated, orthogonal multiresolution analysis (MRA). In the terms given there, one selects a sampling scale J with sampling rate of 2 at J per unit interval, and projects the given signal f onto the space V_J; in theory by computing the scalar products.

$$s_n^{(J)} := 2^J < f(t), \emptyset(2^J t - n) > \quad (1)$$

where ϕ is the scaling function of the chosen wavelet transform; in practice by any suitable sampling procedure under the condition that the signal is highly oversampled, so $P_j[f](x) := \sum_{n \epsilon Z} s_n^{(J)} \emptyset(2^J x - n)$ (2) is the orthogonal projection or at least some good approximation of the original signal in V_J.

The Fast Wavelet Transform is used in image processing tasks like image compression, denoising and fast scaling. The implementation of the FWT with custom filter support and simple in usage was applied in the paper. There are implemented it with known filter families: Daubechies, Coiflets and Biorthogonal wavelets. Discrete wavelet transform (DWT) [6] has gained a great reputation due to its excellent property decorrelation , many systems of modern image and video compression using DWT transform phase [7] .

It is generally recognized that 9/7 filters [8] are among the best image compression filters based DWT [9]. In reality, JPEG2000 image coding standard ["JPEG 2000 Final Committee Draft". Boliek, M. 2000.] has the 9/7 wavelet filters as default filters for lossy compression and 5/3 filters lossless compression.

The capability of a hardware implementation of the bank 9/7 filter (FB) depends on the accuracy with which the filter coefficients are presented. Techniques for lossless image compression find applications in areas such as medical imaging, artwork conservation, remote sensing, etc. Every day discrete wavelet transform (DWT) is becoming more and more popular digital image compression.

Wavelets provide good compression ratios, especially for high resolution images. Wavelets perform much better than competing technologies like JPEG 10 both in terms of signal-to-noise ratio and visual quality. Unlike JPEG, it shows no blocking effect but allow for a graceful degradation of the whole image quality, while preserving the important details of the image. It also makes sense that local features can be described better with wavelets that have local extent.

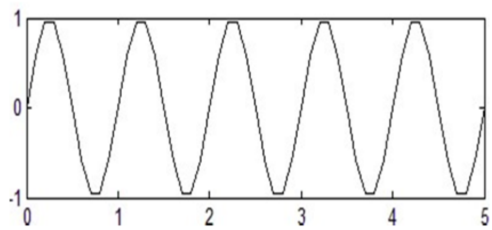

Figure 3: A Wave

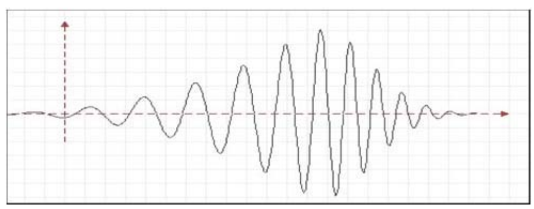

Figure 4: Wavelet

The wavelet as shown in Fig. 3 is a mother wavelet (*h(t)*). The mother wavelet and its scaled daughter functions are used as a basis for a new transform.

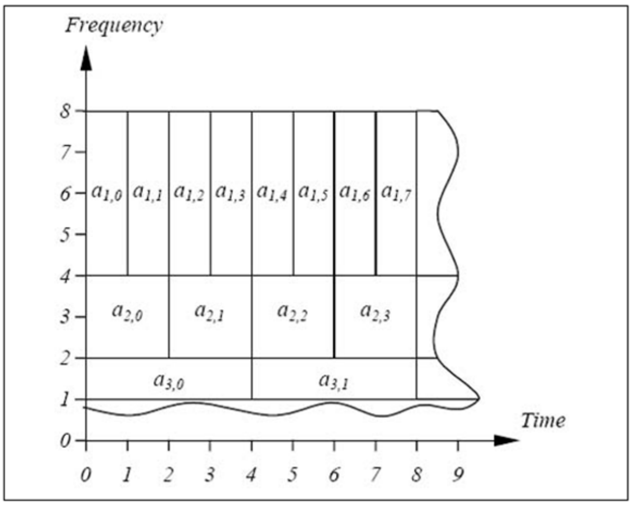

Figure 5: Wavelet Transform

Figure 5 shows a time-scale view for wavelet analysis rather than a time frequency region. Scale is inversely related to frequency. A low-scale compressed wavelet with rapidly changing details corresponds to a high frequency. A high-scale stretched wavelet that is slowly changing has a low frequency application [10].

4. TYPES OF WAVELET FAMILIES

4.1 Biorthogonal Wavelets

This family-linear phase wavelet is used for signal and image reconstruction. In most cases,it uses two wavelets, one for decomposition and the other to recover the image. There are also a number of derived properties.

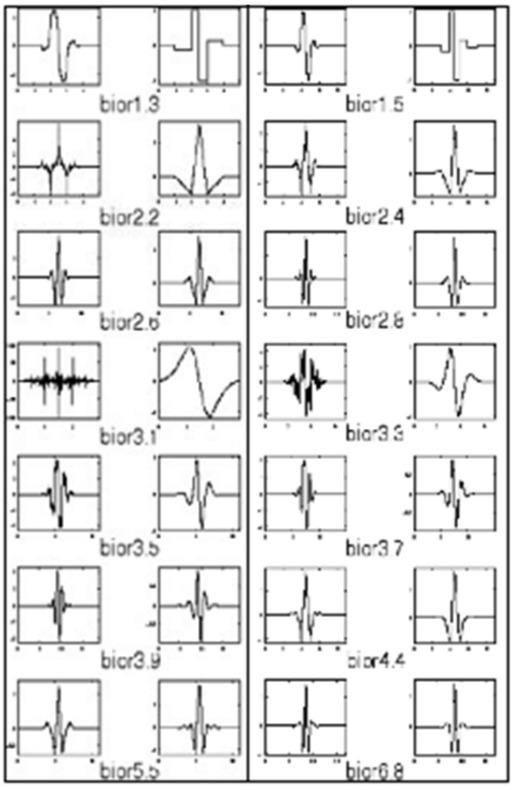

Figure 6: Biorthogonal wavelet Families

4.2 Coiflets Wavelets

The wavelet function has 2N moments equal to 0 and the scaling function has 2N-1 moments equal to 0. The two functions have a support of length 6N-1.

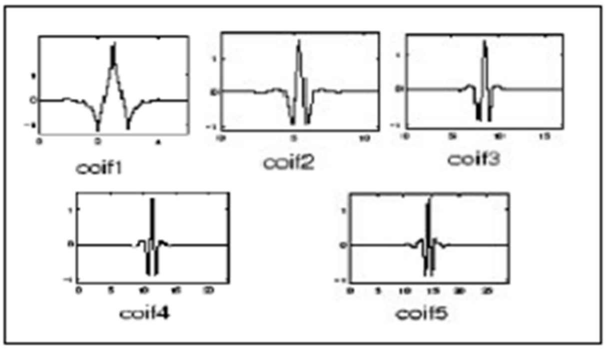

Figure 7: Coiflets Wavelet Families

4.3 Daubechies Wavelets

Ingrid Daubechies, one of the brightest stars in the world of wavelet research, invented what are called compactly supported orthonormal wavelets — thus making discrete wavelet analysis practicable.The names of the Daubechies family wavelets are written dbN, where N is the order, and db the “surname” of the wavelet. The db1 wavelet, as mentioned above, is the same as Haar wavelet. Here is the wavelet functions psi of the next nine members of the family [10]:

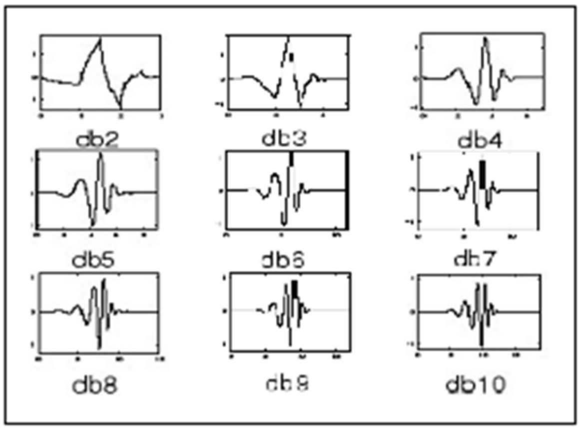

Figure 8: Daubechies Wavelet Families

5. MEASURING COMPRESSION PERFORMANCES

Compression ratio: compression ratio is the ratio between size of compressed file and the size of source file.

$$\textbf{\textit{Compression ratio}} = \frac{\textit{Size after compression}}{\textit{Size before compression}}$$

Compression factor: compression factor is the inverse of compression ratio. That is the ratio between the size of source file and the size of the compressed file.

$$\textbf{\textit{Compression factor}} = \frac{\textit{Size before compression}}{\textit{Size after compression}}$$

Saving percentage calculates the shrinkage of the source file as a percentage.

$$\textit{\textbf{Saving percentage}} = \frac{\textit{Size before compression} - \textit{size after compression}}{\textit{Size before compression}} \%$$

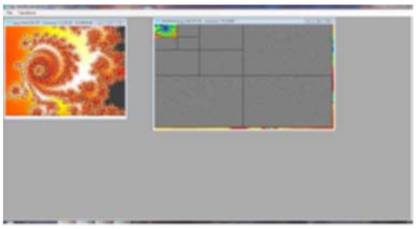

Figure 9: One image after the reconstruction and another image compressed

There are many applications for lossless images such as digital photography, museums or art, publishing, scientific imaging, remote sensing, aerial survey, astronomy, GIS, medical imaging, microscopy, machine vision, quality control, parts inspection, defect tracing, CCTV and security, fingerprint or Forensic and remote operation. Each image has its own characteristics.

Some authors have been developed such a specific method to exploit image nature to obtain better compression performance. Some authors also have analysed a few of lossless image compression for different type of image [11, 12, 13, 14]. Each technique has its advantages and disadvantages, for example Santa Crus in [15] gives a summary of few of image compression techniques as seen in Table 1.

Table 1: Functionality matrix. A "+" indicates that it is supported, the more "+" the more efficiently or better it is supported. A "-" indicates that it is not supported [16].

	JPEG2000	JPEG-LS	JPEG	PNG
lossless compression performance	+++	++++	+	+++
lossy compression performance	+++++	+	+++	-
random access	++	-	-	-
low complexity	++	+++++	+++++	+++
error resilience	+++	++	++	+
non-iterative rate control	+++	+++	++	+++

In order to achieve competitive compression, some authors create a specific method for certain applications. Specific algorithm generally performs better than do general purpose image-data compression algorithms. It exploits the nature of the image to suit the compression methods.

In this work an application for compression and decompression of natural images, was developed, starting from the techniques used by other tools, based on the time and performance capacity.

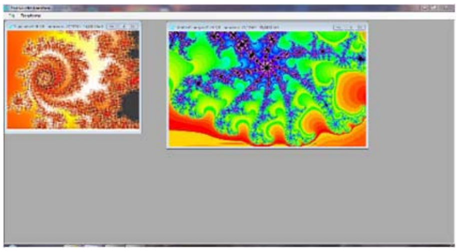

Figure 10: Difference between the filters and the images after the reconstruction

It is particularly used in most test cases, for a better view fractal images. Due to the very complex characteristics of these images, in the different filters used it can be related that it is very difficult, depending on the filter and compression method to recover at the same quality the image.

Considering that the use of these processes for compression and decompression requires many operations and processing techniques for new types of images for evolution systems with high quality, it requires a calculation process much faster.

In these conditions there are more efficient methods of calculation, such as parallel processing or giving up certain features and redundant data, useless depending on compression needs. In this application was tried to use parallel computing to develop faster compression system.

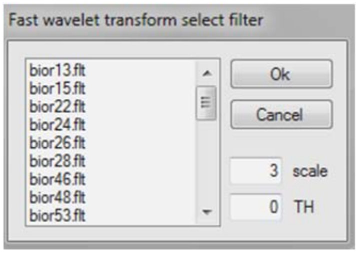

Figure 11: Filter selection panel

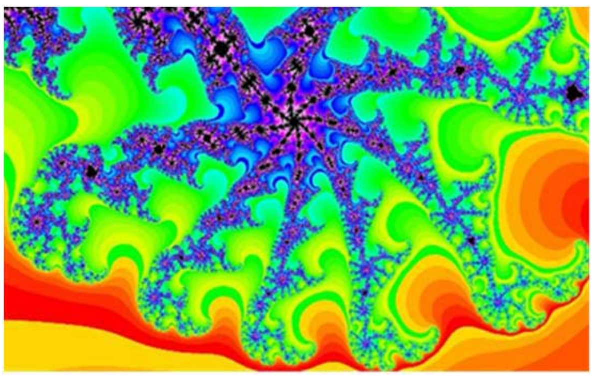

Figure 12: Image1 used for testing

Figure 13: Image2 used for testing

The results are presented in Table 2 and Table 3. These results are strongly influenced by the processor model used, the operating capacity of the computer, the load of the processor, the image type, so it was used more complex images, generated from fractals processing. Tables above represent the processing time for compression and decompression resulted from previous images, as a simple example.

Table 2: Value of time (in milliseconds) using different wavelet families, for compression and recover the previous images (weak image-wi).

S. No.	Biorthogonal				
	Wavelet	**Compression time I1**	**Compression Time I2**	**Recover Time I1**	**Recover time I2**
1	Bior 1.1	4833	5687	8514	9214
2	Bior 1.3	4837	5702	8758	9238
3	Bior 1.5	4843	5714	8689	9249
4	Bior 2.2	4902	5723	9316	9789
5	Bior 2.4	4910	5731	9373	9890
6	Bior 2.6	4920	5744	9409-wi	9909-wi
7	Bior 2.8	4931	5752	9412-wi	9972-wi
8	Bior 3.1	4842	5701	9201-wi	9321-wi
9	Bior 3.3	4947	5768	9663-wi	9233-wi
10	Bior 3.5	4856	5777	9823-wi	9993-wi
11	Bior 3.7	4928	5789	9834-wi	9999-wi
12	Bior 3.9	4801	5794	9987-wi	Wi
13	Bior 4.4	4934	5722	8452	9162
14	Bior 5.5i	4900	5701	7333	9223
15	Bior 6.8	4890	5710	8590	9200

Table 2 a. Biorthogonal

S. No.	Coiflets				
	Wavelet	**Compression time I1**	**Compression Time I2**	**Recover Time I1**	**Recover time I2**
1	Coi 1	5003	6123	7901	8301
2	Coi 2	5022	6201	7943	8312
3	Coi 3	5058	6333	7945	8320
4	Coi 4	5070	6302	7956	8333
5	Coi 5	5001	6358	7949	8310

Table 2 b. Coiflets

S. No.	Daubechies				
	Wavelet	**Compression time I1**	**Compression Time I2**	**Recover Time I1**	**Recover time I2**
1	Db 01	5210	5911	8522	9530
2	Db 02	5220	5926	8534	9620
3	Db 04	5336	5938	8866	9803
4	Db 05	5398	5998	9372	9850
5	Db 06	5440	5940	9743	9905
6	Db 08	5601	6001	9060	wi
7	Db 10	5613	6013	wi	wi
8	Db 15	5350	5950	wi	wi
9	Db 16	5522	5922	wi	wi
10	Db 32	5803	6022	wi	wi

Table 2 c. Daubechies

This time is strongly influenced by factors such as image size, their quality, but there are in conclusion the results of a calculation based on the set of selected filter. Since the actual implementation is in C ++ it can be said that research can take into new implementations based on another technology also based on parallel programing.

5. CONCLUSIONS

The result of this study is integrated in some applications treating in different contexts the image processing topic. The capacity to generate and keep certain images, view and processing others, understanding and studying the compression models, all these are simple operations that can improve a lot of applications today, when we talk about image processing. We use daily standards such as png or jpeg without asking what technologies they use. The studies proposed in work highlight some significant improvement in lossless image compression. Lossless compression is used in cases where it is relevant that the original and the compressed data be the same, or where deviations from the original data could be deleterious. Typical examples are executable programs, text documents, and source code. The benefits of parallel programming in this area should be taken into account, bringing them more compression improvement of existing systems. Also consider that this is a very important use today to store images in large databases and to use the web where time and space are important. This study in this area is useful and how was presented with these issues may be completed by further studies to generate results getting better.

REFERENCES

[1] M. J. Weinberger, G. Seroussi, and G. Sapiro. The LOCO-I Lossless Image Compression Algorithm: Principles and Standardization into JPEG-LS. IEEE TRANSACTIONS ON IMAGE PROCESSING, 9(8):1309–1324, 2000.

[2] D. D. Shuai. Parallel lossless data compression: A particle dynamic approach. In Proceedings of the 4th international conference on Intelligent Computing: Advanced Intelligent Computing Theories and Applications - with Aspects of Theoretical and Methodological Issues, ICIC '08, pages 266–274, 2008.

[3] I. Tabus and J. Astola. Adaptive boolean predictive modelling with application to lossless image coding. In In SPIE - Statistical and Stochastic Methods for Image Processing II, pages 234–245, 1997.

[4] A. J. Penrose and N. A. Dodgson. Error resilient lossless image coding. In In ICIP, Kobe, pages 426–429, 1999.

[5] A. P. Neil. Extending Lossless Image Compression. PhD thesis, University of Cambridge, 2001.

[6] Olivier Rioul and Martin Vetterli, "Wavelets and Signal Processing", IEEE Trans. on Signal Processing, Vol. 8, Issue 4, pp. 14 - 38

[7] D. S. Taubman, "High performance scalable image compression with EBCOT", IEEE Transaction Image Processing, Vol. 9, No. 7, pp. 1158– 1170, July 2000

[8] M. Antonini, M. Barlaud, P. Mathieu, and I. Daubechies, "Image Coding Using Wavelet Transform," IEEE Trans. on Image Processing, Vol. 1, No.2, pp. 205-220, April 1992

[9] J. Liao . "Wavelet filter evaluation for image compression". al., August 1995, IEEE Trans. Image Process., Vol. 4, pp. 1053–1060

[10] Priyanka Singh, Priti Singh, Rakesh Kumar Sharma "JPEG Image Compression based on Biorthogonal, Coiflets and Daubechies Wavelet Families", International Journal of Computer Applications (0975 – 8887) *Volume 13– No.1, January 2011*

[11] S. W. Smith. The scientist and engineer's guide to digital signal processing. California Techn. Publ., San Diego, CA, USA, 1997.

[12] G. Weinh, H. Stögner, and A. Uhl. Experimental study on lossless compression of biometric sample data. In Image and Signal Processing and Analysis, 2009. ISPA 2009., pages 517–522, 2009.

[13] G. Schaefer, R. Starosolski, and S. Ying Zhu. An evaluation of lossless compression algorithms for medical infrared images, 2005.

[14] G. Roelofs. PNG: The Definitive Guide. O'Reilly & Associates, Inc., Sebastopol, CA, USA, 1999.

[15] D. Santa-Cruz and T. Ebrahimi. An Analytical Study of JPEG2000 Functionalities. In IEEE ICIP, pages 49–52, 2000.

[16] D. Santa-Cruz, T. Ebrahimi, T. Ebrahimi A, J. Askelof, M. Larsson B, and C. A. Christopoulos B. JPEG2000 still image coding versus other standards. Howpublished = Public Draft FCD 14495, ISO / IEC JTC1 SC29 WG1 (JPEG / JBIG), 2000.

System for data aquisition with real-time complex processing of a bearing vibration

Popescu Ion Marian

Department of Automation, Energy and Environment, University Constantin Brâncuşi, Targu Jiu, Romania (*e-mail: po_marian@yahoo.com*)
*Postdoctoral Researcher at University of Craiova, Craiova, Romania (*e-*mail: pmarian@automation.ucv.ro*)

Abstract: The current technical possibilities, based at hardware level, on the development of a high power computing for microprocessor systems, to which are added consistent software tools have led to increasing complexity of information processing in two aspects that are in opposition: working in real-time and complexity of processing. The current performance in the processing of real-time information, and automatic control are possible due to a very dedicated connections between hardware and software. The idea of using FPGA technology in conjunction with microprocessors and higher-level software, allows the design of information processing applications in real time with high complexity.

Keywords: real-time processing, FPGA, bearing vibration

1. INTRODUCTION

This paper presents the aspects of hardware and software implementation level, of a system of real-time acquisition and processing of vibration signals, from two bearings placed on the same axis. Due to industrial environmental conditions, to which are added mechanical vibrations in the structure in which you can find a actuation structure, it is not possible to mount in installation of a computer for vibration signal processing. Vibration signal is a dynamic signal, and a great length cable connection between the transducer and data acquisition system, would perform filtering for the high frequency harmonics and could compromise the information [1], [2], [3].

Also, the data acquired are very more and are difficult to store, but even so, further processing would mean that it is not processing in real-time. The system hardware and software, provided by National Instruments, allows overcoming these impediments. CompactRIO hardware platform, through which a designer can develop applications for acquisition and very complex processing of data in real time, to which are added spatial positioning near to the industrial process, represent a solution. The results of processing are used to obtain real-time decision at this level or are transmitted to the higher level for a more complex decision.

The main causes of a bearing defects [4], [5], [6], [7] are excessive loading in stationary or dynamic regime, inadequate lubrication, external contamination, improper installation, improper size, exposure to vibration, passing electric current through the bearing [2]. In each of those cases of a failure, it emits vibrations that require specific techniques for diagnostic / monitoring.

Also, a vibration sources are multiple, and processing in parallel and in real-time of the information from multiple sensors placed in the installation can lead at realization of a real predictive maintenance [8], [10].

The solution proposed in this paper focuses on the possibilities of complex processing in real time and obtain results in the field of predictive maintenance will be developed later.

2. ACCOMPLISHING OF AN EXPERIMENTAL MODEL

The experimental model is formed from an actuation motor and a shaft, on which are mounted two bearings, one now, and one with visible defects as in *Fig.1.* The vibrations are seised using piezoelectric sensor whose output signal is applied to a signal conditioning circuit, in order to be then converted to a digital signal using an data acquisition system. The resulting digital signal is transmitted to a computer system for processing and to obtain information about the operating status of the system under observation. To achieving mechanical part of the experimental model, shown in *Fig.1.* have been use in a single row two ball bearings the type of 6308C3, which were mounted at the ends of a shaft, actuated by an AC motor via a belt and toothed wheel and will generate a speed, the shaft bearings that are positioned, by 1750 rotations / minute. To make comparison between a vibration signal originated from a defective system with a signal from a system OK, the two mounted bearings were one new and the other with a high degree of wear.

The degree of wear of the second bearing was accentuated supplementary by hitting balls with a hammer. The experimental mechanical system thus obtained will be used as a real process for testing and validation at acquisition system at hardware and software level based on equipment produced by the company National Instruments.

Fig.1. Structure of the experimental model

3. IMPLEMENTATION OF DATA ACQUISITION SYSTEM, AND COMPLEX PROCESSING IN REAL-TIME

The data acquisition system is based on the idea developed by National Instruments company [9] with PAC platform (Programmable Automation Controller). NI PACs, programmed with NI LabVIEW software, combine the reliability and ruggedness of a programmable logic controller (PLC), the performance and openness of the PC, and the flexibility of custom field-programmable gate array (FPGA) circuitry. So, the NI PAC technology of can help to optimize an existing automation system with advanced measurements, enhance the functionality of PLC-based control system, or design a new control and monitoring system.

This system [9] has a robust construction that allows placing it in an industrial environment near to the physical process. The novelty that it brings, is the possibility of complex signal processing at this level without having required signal transmission at distance to be processed by a powerful computing system. Thus the processing results are obtained in real time, which leads to obtaining plant complex decisions, all in real time. Also, it eliminates the need for storage and transmission of large amounts of data (vibration signal samples) for complex processing to be carried out later. Further processing of data stored obviously not done in real time.

The characteristics of the system are shown in *Fig.2.* NI cRIO-907x integrated systems combine an industrial real-time controller and reconfigurable field-programmable gate array (FPGA) chassis for industrial control and monitoring applications. The NI cRIO-9074 integrated system features an industrial 400 MHz real-time processor and an eight-slot chassis with an embedded, reconfigurable 2M gate FPGA chip. The systems feature built-in nonvolatile memory and a fault tolerant file system.

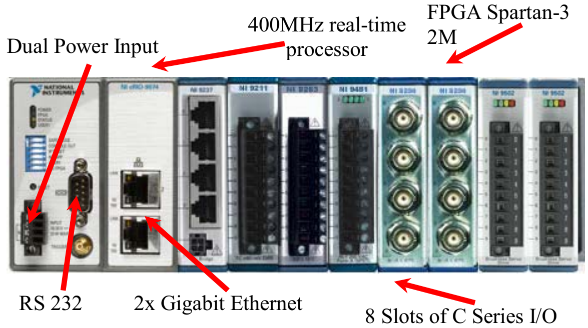

Fig.2.The NI CompactRIO 9074 system

The system architecture presented in *Fig.3.* is based on inserting a FPGA circuit between microprocessor architecture NI-9074 system and the data aquisition system. In general, a microprocessor architecture involves an operation of extracting an instruction from memory, decoding, processing, submission results in memory. In contrast, the execution of an instruction at a FPGA circuit, is performed directly at the hardware level, with the lowest possible processing time. Also, at the FPGA circuit, is realized the processing of a multiple acquisition channels simultaneously [8], [9], enabling higher processing complexity for information sampled from the real process.

FPGAs are reprogrammable silicon chips. In contrast to the processors found in usual computer, which run software application in predefined circuitry, programming an FPGA rewires the chip itself to implement your functionality directly in hardware [9]. FPGAs offer several advantages for embedded test, monitoring, and real-time control applications.

With reconfigurable field-programmable gate array (FPGA) technology [9], can perform high-speed signal aquisition, very complex processing in real-time, very precise synchronization of the application in relation to certain events, parallel processing of more signals from sensors (practically simultaneously) placed in the installations. For control systems, can also run advanced control algorithms [8] directly in the FPGA chips to minimize latency and maximize loop rates. Actual advanced control solutions require complex mathematical processing, and real-time execution, which comes with an important support this architecture. NI FPGA hardware platforms combine modular I/O, real-time processing, and NI LabVIEW programmable FPGAs. Also, the development of the processing in real time using a high level development environment (such as LabVIEW development environment [9]), brings an increase productivity at software level, and implementation of complex mathematical processing.

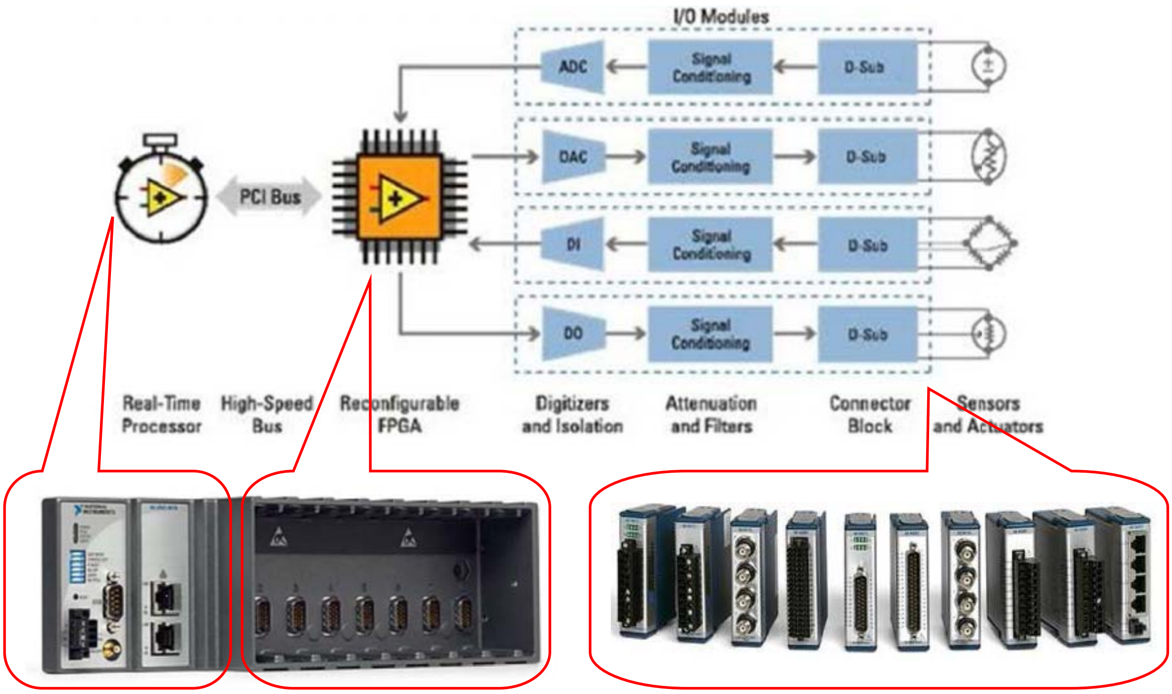

Fig 3. The new concept of platform PAC- Programmable Automation Controller [NI www]

Signal acquisition module for vibration NI-9234, presented in *Fig.4*, is a 4-channel C Series dynamic signal acquisition module for making high-accuracy audio frequency measurements from integrated electronic piezoelectric (IEPE) and non-IEPE sensors with NI CompactRIO systems [9]. The NI 9234 delivers 102 dB of dynamic range and incorporates software-selectable AC/DC coupling and IEPE signal conditioning for accelerometers and microphones. The four input channels simultaneously digitize signals (24-bit resolution) at rates up to 51.2 kHz per channel with built-in anti-aliasing filters that automatically adjust to your sampling rate.

Fig 4. The acquisition Module NI-9234

Fig 5. PCB accelerometers 352C33

Vibration sensors which are used, presented in *Fig.5.*, are accelerometers of the type 352C33 produced by the PCB Piezotronix Company and are mounted one on each bearing through some permanent magnets. The principal characteristics are Sensitivity 10 mV/g, Measurement Range ± 50 g pk, Broadband Resolution 0.00015 g rms, Frequency Range (± 5%) 0.5 to 10k Hz, Resonant Frequency > 50 kHz.

Organizing application at software level, is based on a project in LabView 2013 development environment, according to *Fig.6.* that takes into account hardware configuration.

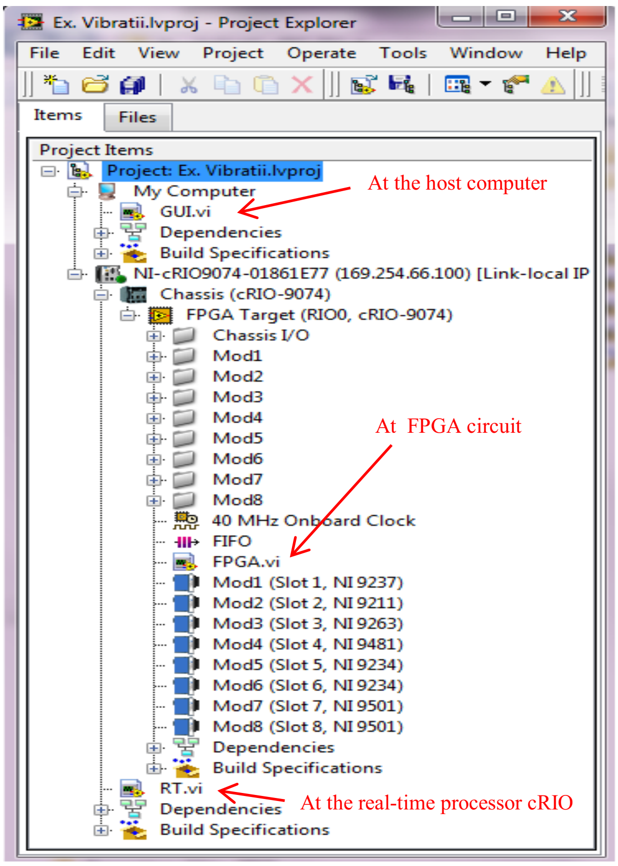

Fig.6. Acquisition and processing application

Corresponding FPGA circuit, we have FPGA.vi file, that will be compiled and loaded just in the FPGA circuit. The structure of this file, and libraries of graphical functions that can be used in FPGA are presented in *Fig.7*.

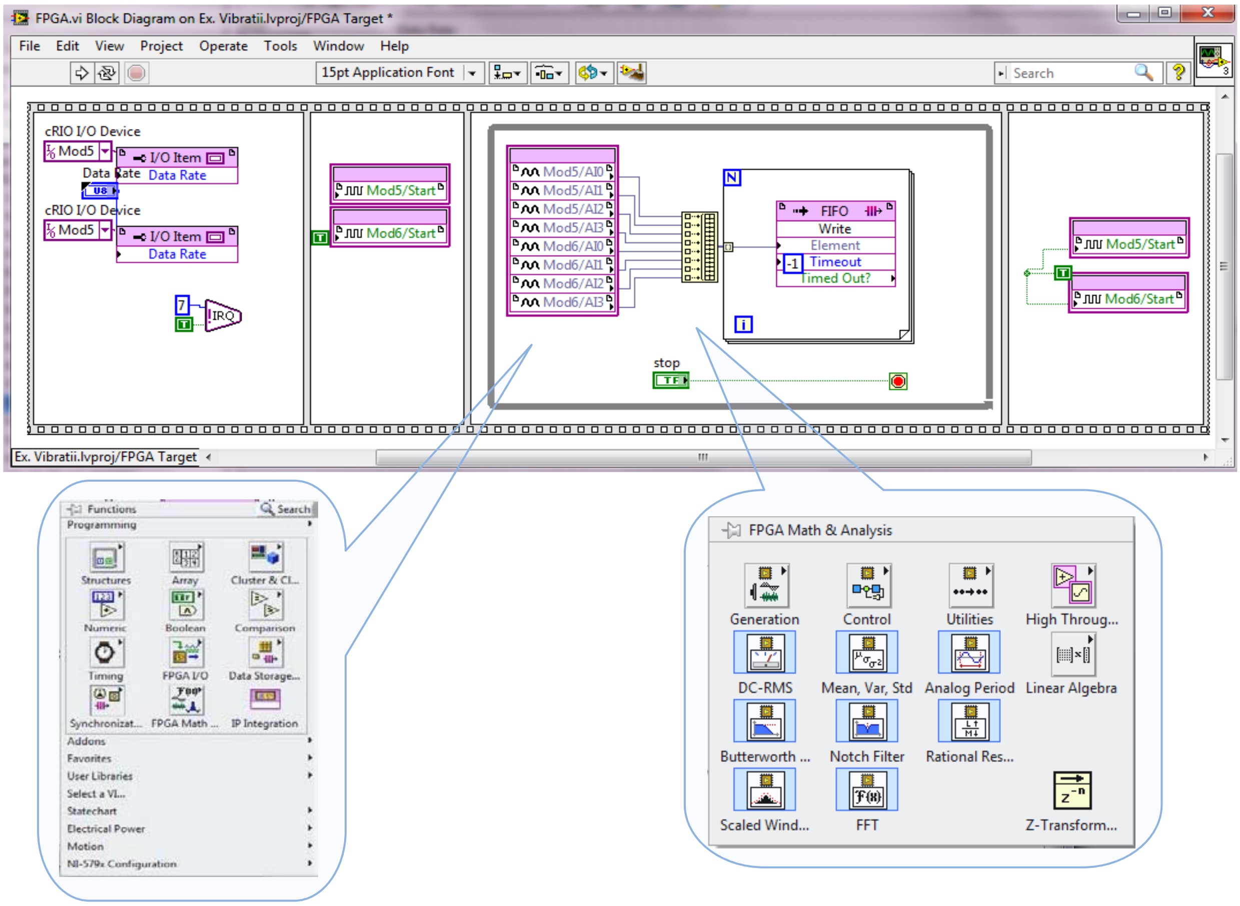

Fig.7. Acquisition and processing application on the level of FPGA circuit, the FPGA.vi file

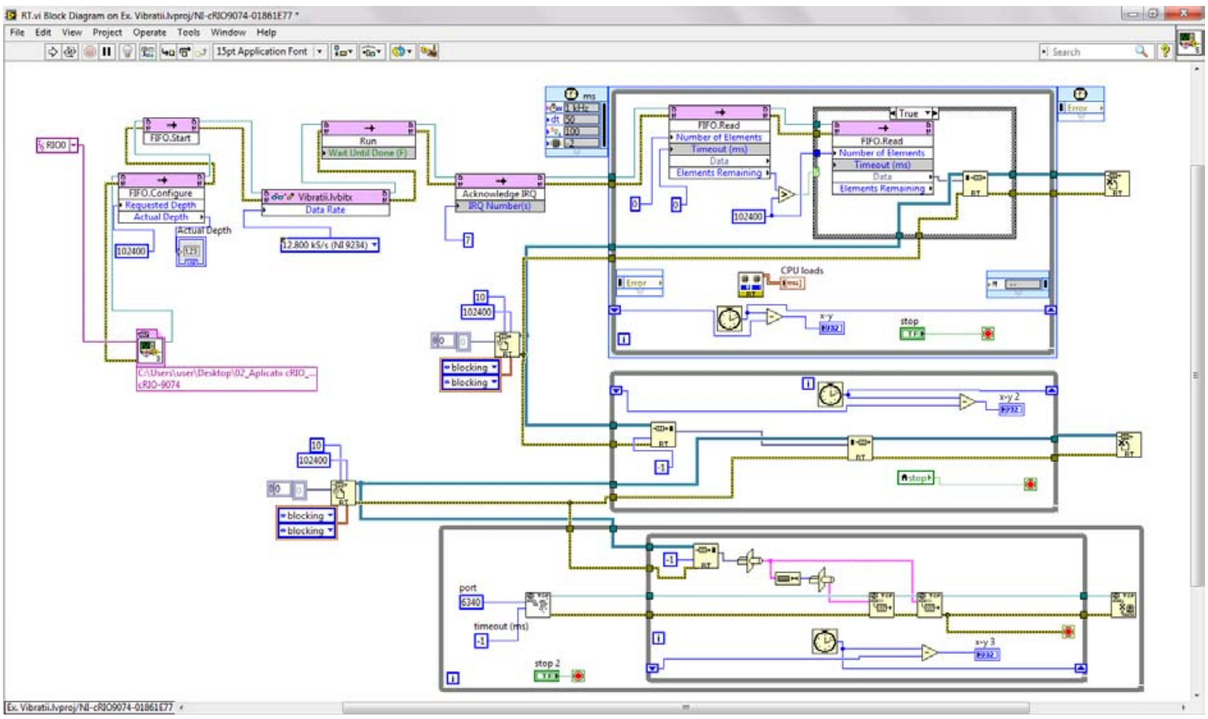

Fig.8. The acquisition and processing application, at the level of of real-time processor NI-cRIO9074, the RT.vi file

The complex processing that can be made are: signal generation, interpolation functions, linear and nonlinear control, PID, work with matrices, trigonometric functions, z-transform, Fourier transform, various filters, timed loops, timers for real-time communication functions, and so on.

The RT.vi file, presentet in *Fig.8.* corresponds to the processor that work in real time at the level of CompactRIO system that can perform complex operations [9], specific CISC processors. At the level of this processor is performed real time processing results management and obtaining appropriate decisions and communicating with a computer system on a higher level, for coordination. The RS 232 serial port can connect a display screen that can be shown diverse local information.

The GUI.vi file, presentet in *Fig.9.*, is the virtual instrument, which represents the application being run on the host computer. It can perform additional processing functions over signals sampled, of the results received from NI CompactRIO system [9], processing / presentation information at a SCADA / HMI system, a database management.

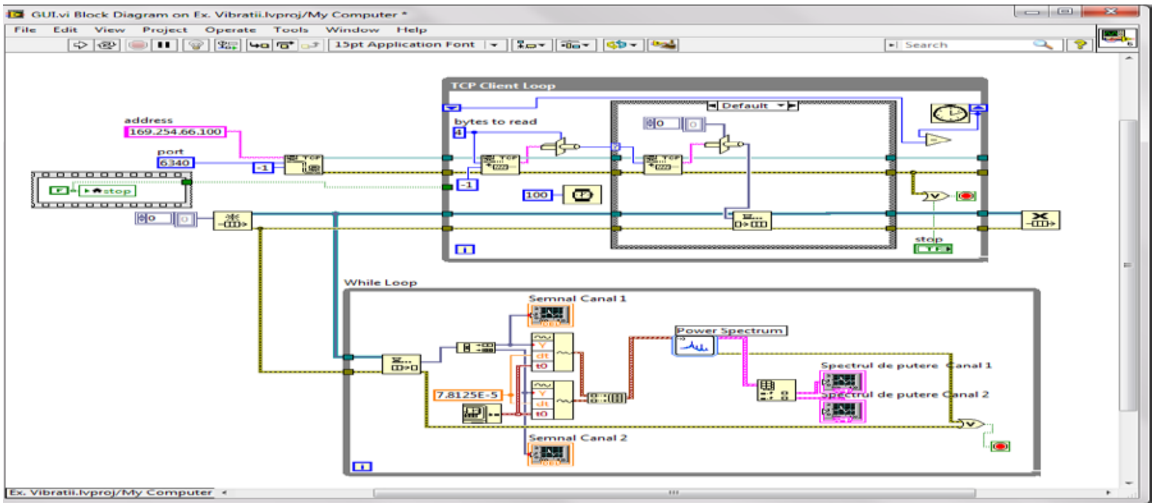

Fig.9.Aplicatia de achizitie si prelucrare la nivelul calculatorului gazda, fisierul GUI.vi

4. EXPERIMENTAL RESULTS

The graphical representation of the vibration signals acquired on each bearing, and the power spectrum after enveloping, are shown *in Fig.10.*

The paper presents study of the implementation and processing, and the results represent signals acquired through FPGA circuit, taken from real-time system NI-cRIO 9074 and sent to the host computer.

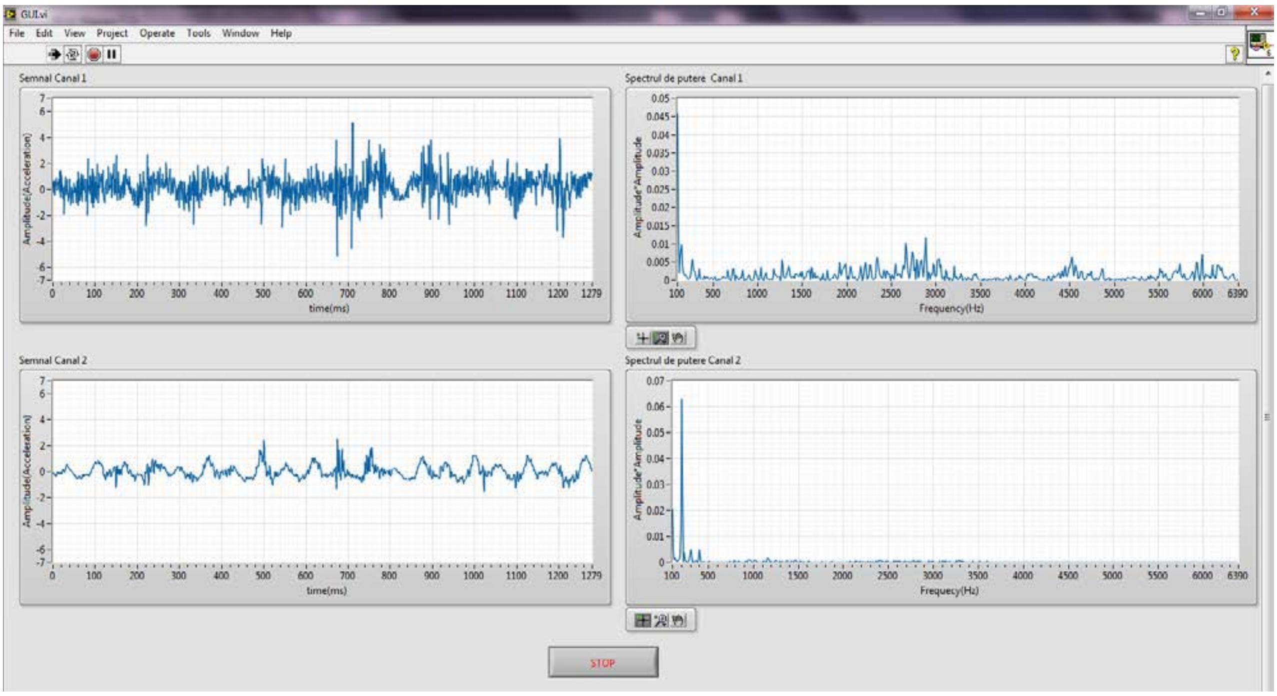

Fig.10. Acquired vibration signals and power spectrum accordingly the two bearings: one new and the other with visible defects

The fourier transform for processing of signals is performed at the level of the host computer. Further developments will use this approach to hardware and software for full processing FPGA circuit level.

5. CONCLUSIONS

As a final conclusion, the complex processing in real-time vibration signals is a difficult enough problem which must take into account the following aspects:

- The data acquisition system must meet the powerful real-time facilities because the vibration signal may have a highly dynamic evolution. Such sampling frequency must be relatively high.
- Most mechanical systems that generate vibrations have imperfections in their structure, to which are add the fact that mechanical vibrations in a structure have more degrees of freedom and speed of transmission through the structure.
- The vibration transducers introduce distortions of amplitude and phase, which should take into account by the acquisition system.
- Any data acquisition system (including transducer) and the vibration signal processing, requires laborious calibration on the stands specially designed for a specific type of application.
- The structures of analysis and processing on-line vibration signals are very difficult to realize [8] because, in a machine, the point where vibration measurement is performed, is away from the processing system and connection cables introduce additional distortions.

Most applications for predictive maintenance, vibration-based signal processing from a mechanical structure, focuses on the study of mechanical structures considered good, which is considered as a the reference for other structures in operation.

The complexity of the information contained herein vibration signal associated with the idea of complex processing performed in real time opens the way for research towards the development of advanced processing methods.

ACKNOWLEDGMENT

This work was supported by the strategic grant POSDRU/159/1.5/S/133255, Project ID 133255 (2014), co-financed by the European Social Fund within the Sectorial Operational Program Human Resources Development 2007-2013.

REFERENCES

[1] Grofu F., Popescu M., Popescu L., Data Acquisition System for Vibration Signal, *International Journal of Computers, Communications & Control*, ICCC Publications, 1-3 June, Băile Felix - Oradea, Romania, 2006, pp. 251-255.

[2] Popescu M., Runceanu A., Vibration Signal Processing by Deconvolution Method, *International Joint Conferences on Computer, Information, and Systems Sciences, and Engineering (CISSE 2009)*, December 4-12, 2009, University of Brigeport, USA, Volume 1, Technological Developments in Networking, Education and Automation, IETA 09, pp. 393-398.

[3] Popescu I. M., Real-Time acquisition and processing of a vibration signal, *14th Geoconference on Informatics, Geoinformatics and Remote Sensing*, 2014, pp. 303-310, ISSN 1314-2704, DOI:10.5593/sgem2014B21, Section: Informatics.

[4] Sawalhi N., Randall R.B., Simulating gear and bearing interactions in the presence of faults, Part II: Simulation of the vibrations produced by extended bearing faults, *Mechanical Systems and Signal Processing*, vol. 22 (2008), pp. 1952–1966, doi:10.1016/j.ymssp.2007.12.002.

[5] Robert B. Randall, Jerome Antoni, Rolling element bearing diagnostics, *A tutorial, Mechanical Systems and Signal Processing*, vol. 25 (2011), pp. 485–520, doi:10.1016/j.ymssp.2010.07.017.

[6] N. Sawalhi, R.B. Randall, Vibration response of spalled rolling element bearings: Observations, simulations and signal processing techniques to track the spall size, *Mechanical Systems and Signal Processing*, vol. 25 (2011), pp. 846–870, doi:10.1016/j.ymssp.2010.09.009.

[7] Idriss El-Thalji, ErkkiJantunen, A summary of fault modelling and predictive health monitoring of rolling element bearings, *Mechanical SystemsandSignalProcessing60-61(2015)252–272*, http://dx.doi.org/10.1016/j.ymssp.2015.02.008

[8] Zhifen Zhang, HuabinChen,Yanling Xu, Jiyong Zhong, Na Lv, Shanben Chen, Multisensor-based real-time quality monitoring by means of feature extraction, selection and modeling for Al alloy in arc welding, *Mechanical Systems and Signal Processing*, vol. 60-61 (2015), pp. 151–165, http://dx.doi.org/10.1016/j.ymssp.2014.12.021

[9] http://www.ni.com/compactrio/

[10] http://www.spminstrument.com/Measuring-techniques/

Traction Asynchronous Motor Fed by Power Converter Controlled by Direct Torque Control Method

Răzvan Prejbeanu*

**RELOC S.A., 109, Bd. DECEBAL, 200746*
CRAIOVA, ROMANIA (e-mail: razvan.prejbeanu@relocsa.ro)

Abstract: In the case of asynchronous motor with squirrel cage, rotor currents cannot be measured, and the implementation of vector control (field - oriented control of stator, rotor or magnetization fluxes) requires information about the module and the phase (position) of the stator, rotor respectively magnetization phasors fluxes. The control is performed in the reference systems joined with the stator, rotor or magnetization fluxes, resulting the stator currents components. Direct torque control (DTC) method describes how the torque and the speed are directly adjusted by the electromagnetic status of the motor, similar to a direct current (DC) motor, unlike the traditional pulse width modulation (PWM) mode which uses the motor control by adjusting frequency and voltage from the output of the converter. DTC is the first technology that enables control by means "real" motor torque and flux control variables.

Keywords: converter, asynchronous motor, control, torque, regulator.

1. INTRODUCTION

Methods type DTC and field oriented control (FOC) ensure more precise control of torque than the scalar methods (type U/f = constant) and permit good reliability for the proposed dynamics driving; at the same time they reduce all instability of the transient regimes and increase the energy efficiency.

In terms of simplifying the control diagrams, DTC control has an important advantage over to FOC control type. An important advantage of driving with scalar control is also the possibility to control several motors in parallel or, in case of failure, to replace the original motors with other new ones with unknown parameters.

Regarding the other two types of controls, and particularly the FOC control, these skills are not possible because the motor parameters are essential to control and we cannot speak about multiple motors systems yet.

1.1 DTC control technique

According to the principle of operation of asynchronous motor, the greater is the slipping determined as the difference between the speed of the rotating field and the mechanical speed rotor ω_r, the higher is the generated torque. Fundamentally, DTC consists in controlling the speed of progress of the stator flux (which is the speed of the rotating field ω_0) and its future position, knowing the current position depending on the torque that the motor should develop.

The necessary torque to be developed can be the result of a simple proportional – integral (PI) regulator, which compares the rotor speed target with the current value, as in the case of vector adjustment.

The control system is extremely simple and the adjustment is made up of a flux and torque estimator whose control magnitudes outputs are control values for the bi-positional flux comparator and of the respective tri-positional to the torque. The obtained values for flux and torque are inserted in a table where control angle values are obtained for the transistors inverter.

2. TECHNICAL CONSIDERATIONS

2.1. Possible situations

There are three possible situations [2]:

a) the developed torque is too small: flux phasor must advance (Fig. 1a);
b) the developed torque is enough: flux phasor must maintain their position (Fig. 1b);
c) the developed torque is too high: flux phasor must delay (Fig. 1c).

At the same time, the flux value must be steady and kept (for a given operating mode). This means that the peak of the flux phasor must describe a circle with a radius equal to the required flux (Fig. 2).

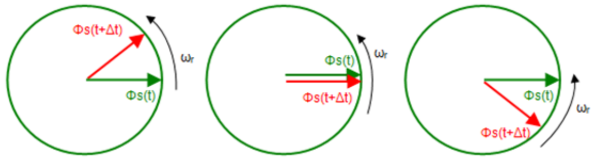

a) b) c)

Fig.1. Comparison between the present and the prescribed speed

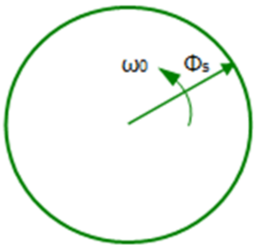

Fig. 2. Flux phasor

2.2. Methods to determine the flux amount

Stator flux value and position can be determined by direct measurement or estimation. Direct measurement would require special construction motors which have incorporated flux transducers (Hall probes, measuring windings).

To avoid such solution, and in order to be able to use the control method of any existing motor, the flux stator estimation using the measured stator values of voltage and current, based on the relation (1), is preferred [2]:

$$\underline{\Phi}_S = \int (\underline{u}_S + R_S \cdot \underline{i}_S)dt \tag{1}$$

where: $\underline{u}_s$ are voltage vectors, and $\underline{i}_s$ are stator current vectors:

$$u_s = u_{s\alpha} + j_{us\beta}, \tag{2}$$

$$i_s = i_{s\alpha} + j_{is\beta} \tag{3}$$

expressed in the fixed system, jointly and severally liable with the stator.

The stator flux is practically achieved by the composition of the two components:

$$\Phi_{s\alpha} = \int (u_{s\alpha} + R_s \cdot i_{s\alpha})dt \tag{4}$$

$$\Phi_{s\beta} = \int (u_{s\beta} + R_s \cdot i_{s\beta})dt \tag{5}$$

resulting:

- the module of the stator flux:

$$\left|\underline{\Phi}_s\right| = \sqrt{\Phi_{s\alpha}^2 + \Phi_{s\beta}^2} \tag{6}$$

- the position of the stator flux:

$$arctg\left(\frac{\Phi_{s\beta}}{\Phi_{s\alpha}}\right) \tag{7}$$

- electromagnetic torque developed by the motor:

$$m_C = \frac{3}{2}p(\Phi_{s\alpha} \cdot i_{s\alpha} - \Phi_{s\beta} \cdot i_{s\beta}) \tag{8}$$

That means that, only measuring the phase voltages and currents, the value and the position of the stator flux and the instantaneous electromagnetic torque developed by the motor can be reconstituted. In practice, taking into account that the motor is powered by a three-phase voltage inverter, it is only necessary to measure the phase currents in the intermediate circuit and the voltage *U*, the phase voltages resulting on the inverter topology [8].

2.3. Types of inverter voltage control

The amplitude and the position of the stator flux phasor can be controlled only through the stator voltage.

For the motor fed by a three-phase voltage inverter (which has only eight distinct states, due to the operation of the switching contacts), the stator voltage can be written as follows [10]:

$$u_S = u_{S\alpha} + ju_{S\beta} = \frac{3}{2}(u_A + a \cdot u_B + a^2 \cdot u_C) \tag{9}$$

$$a = c^{j\frac{2\pi}{3}} \tag{10}$$

and can occupy only eight positions (Fig. 3).

Keeping (approximately) constant the stator flux amplitude and controlling its speed can be achieved only by the appropriate choice of one of the eight topologies [1]. The selected status depends on the necessary tendencies evolution for both - flux amplitude and electromagnetic torque. There are two possible topologies that correspond to the null phasor (state 0: $K_A = K_B = K_C$ = OFF and state 7: $K_A = K_B = K_C$ = ON). Choosing one of them depends on the current status of the inverter so the null state commutation to be achieved only commuting a few contacts.

2.4. The choice of inverter topology

There is no predefined strategy of PWM for DTC [9]. Inverter topology is determined, each time, depending on the necessary tendencies of development of the flux amplitude and electromagnetic torque. The algorithm for the determination of the inverter topology suppose on each interval of PWM, the next steps:

2.4.1. Determination of instantaneous values of the stator voltage

Taking into account the actual inverter topology and the instantaneous measured DC link voltage U, the instantaneous values of the stator voltages $u_{s\alpha}$ and $u_{s\beta}$ are determined:

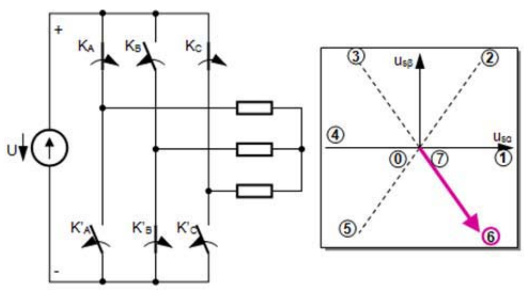

Fig. 3. The positions of the stator voltage

$$\begin{bmatrix} u_{s\alpha} \\ u_{s\beta} \end{bmatrix} = \frac{2}{3}\begin{bmatrix} 1 & -\frac{1}{2} & -\frac{1}{2} \\ 0 & \frac{\sqrt{3}}{2} & -\frac{\sqrt{3}}{2} \end{bmatrix}\begin{bmatrix} \frac{2}{3} & -\frac{1}{3} & -\frac{1}{3} \\ -\frac{1}{3} & \frac{2}{3} & -\frac{1}{3} \\ -\frac{1}{3} & -\frac{1}{3} & \frac{2}{3} \end{bmatrix}\begin{bmatrix} s_A \\ s_B \\ s_C \end{bmatrix}\frac{U}{2} \qquad (11)$$

State values $s_{A,B,C}$ are considered "1" for $K_{A,B,C}$ = ON and "0" for $K_{A,B,C}$ = OFF.

2.4.2. Determination of the stator current instantaneous values

On the basis of the instantaneous measured values of the phase currents i_{sA}, i_{sB}, i_{sC}, the values of the stator current $i_{s\alpha}$ and $i_{s\beta}$ will be calculated instantaneous [3].

$$\begin{bmatrix} i_{s\alpha} \\ i_{s\beta} \end{bmatrix} = \frac{2}{3}\begin{bmatrix} 1 & -\frac{1}{2} & -\frac{1}{2} \\ 0 & \frac{\sqrt{3}}{2} & -\frac{\sqrt{3}}{2} \end{bmatrix}\begin{bmatrix} i_{sA} \\ i_{sB} \\ i_{sC} \end{bmatrix} \qquad (12)$$

Remark: It is enough to measure the instantaneous values only of the two phase currents; the third phase value could be calculated with the equation (13):

$$i_{sC} = -i_{sA} - i_{sB} \qquad (13)$$

2.4.3. Determination of the stator flux components values

The stator flux components from the two axes are calculated as follows [8]:

$$\begin{aligned} \Phi_{s\alpha} &= \Phi_{s\alpha o} + (u_{s\alpha} - R_s \cdot i_{s\alpha})\mathrm{T_s} \\ \Phi_{s\beta} &= \Phi_{s\beta o} + (u_{s\beta} - R_s \cdot i_{s\beta})\mathrm{T_s} \end{aligned} \qquad (14)$$

then the modulus of the stator flux:

$$|\underline{\Phi}_s| = \sqrt{\Phi_{s\alpha}^2 + \Phi_{s\beta}^2} \qquad (15)$$

and electromagnetic torque developed by the motor:

$$m_c = \frac{3}{2} p(\Phi_{s\alpha} \cdot i_{s\beta} - \Phi_{s\beta} \cdot i_{s\alpha}) \qquad (16)$$

3. CONTROL STRATEGY

The block diagram (made of six main blocks) is shown in Fig. 4. The induction motor, the converter phase, the three-phase rectifier diodes blocks are provided from the SimPowerSystems library [6].

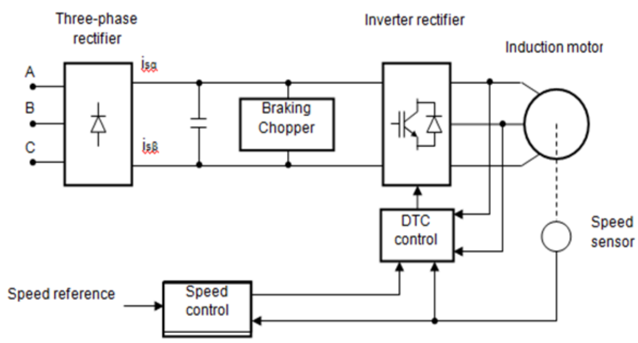

Fig. 4. The block diagram of DTC

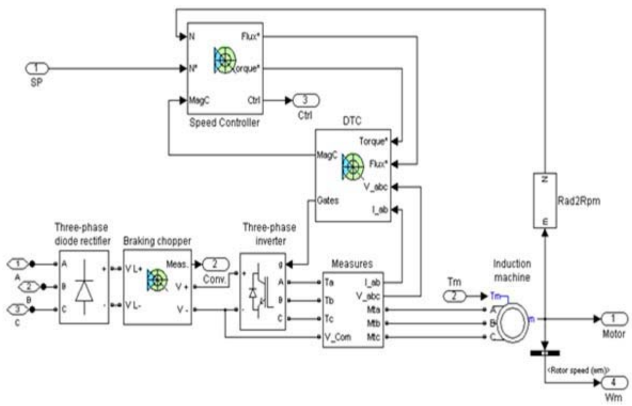

Fig. 5. The Simulink functional diagram

The functional schematic Simulink diagram is presented in Fig. 5 [4, 5].

The speed controller and the controller model are specific to the DTC library and presented below.

3.1. Speed controller

The speed controller is based on a PI regulator, which is shown in Fig. 6. The prescribed and measured speed values determined torque magnitude command controller. At the output of this regulator is a torque prescribed value applied to DTC control unit by a block of limitation. Speed signal is applied to a first order low pass filter and thereby determines the prescribed signal flux.

3.2. DTC controller

DTC regulator and flux control contains five main blocks, as shown in Fig. 7. These blocks are described below.

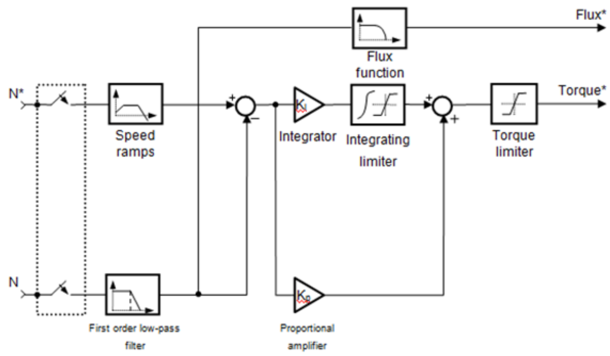

Fig. 6. Speed regulator diagram

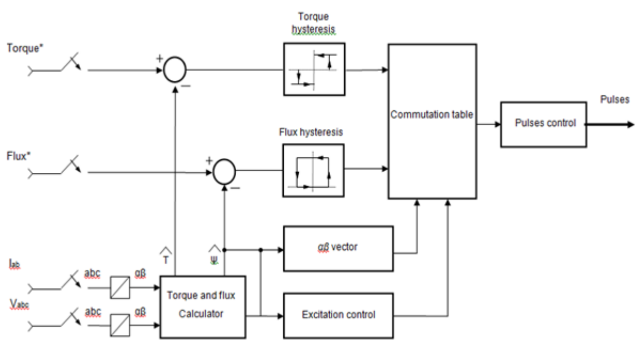

Fig. 7. DTC diagram regulator

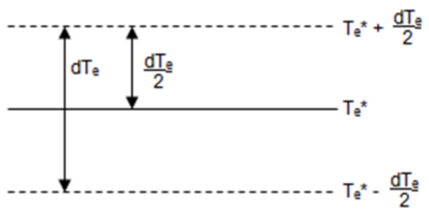

Fig. 8. Electromagnetic torque working band

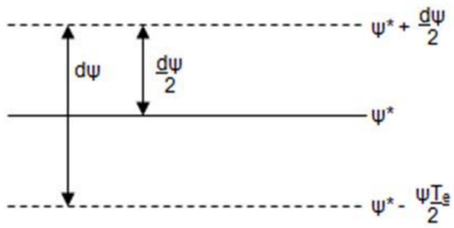

Fig. 9. Definition of working flux band

The torque and flux calculator unit is used to estimate the $\alpha\beta$ components for motor torque and electromagnetic flux. This calculator is based on the motor equations. $\alpha\beta$ vectors unit is used to find the plane (α, β) flux vector in which it evolves. Plan (α, β) is divided into six different areas at intervals of 60 degrees.

Hysteresis torque and flux blocks contain a comparator with hysteresis on two levels for flux control and a comparator with hysteresis for torque control on three levels. Hysteresis comparators description is presented below. The amount of the bandwidth is distributed symmetrically around the prescribing torque (Nm). Fig. 8 shows a case where the point of prescribing torque is T_e* and the bandwidth torque is set to dT_e.

In the same way the value of the bandwidth flux is distributed symmetrically around the prescribing ψ*, and the flux bandwidth is set to dψ (Fig. 9).

4. SIMULATION, RESULTS AND DISCUSSION

Using DTC control for asynchronous motor type MABT10 very small differences between the current motor stator with saturation and without saturation are obtained. Both values are for rated voltage and torque value at $1.5U_n$ [7].

In the case of supplying from the power voltage source, the motor saturation does not play an important role, unless the situation when the power supplying system has a sudden overvoltage variation. It was further considered that the asynchronous motor operates without saturation. The technical data used in the simulation are shown in Fig. 10. First of all they relate asynchronous motor data for the studied MABT10 motor, and then - the main parameters of the converter and of the intermediate circuit, as well as the regulator parameters: time, amplification and filtration constants.

A starting regime in nominal load with simulation for slipping during acceleration is given in Figs. 11-12. Slipping is simulated by a sudden drop in the motor load, which occurs in practice when a vehicle loses adherence.

Simultaneously with the torque decreasing, the stator current also decreases and returns to initial value only after the resumption of adhesion. During the slipping, the speed of the rotor slightly exceeds the prescribed value, on one hand due to the asynchronous motor characteristics, and on the other hand due to more performing control acuity than the control type U/f.

The following parameters are important for the control:
- proportionality and integration constant;
- acceleration of the vehicle;
- torque and flux constant for hysteresis control;
- initial value and maximum torque limits.

When performing an analysis of the behaviour by the detail of the skating, it is found that the vehicle loses grip when the resisting torque greatly decreases; there is a slight increase in the rotor speed that is matched by the control with DTC.

Fig. 10. The rated data for the motor type MABT10 in the case of DTC implementation

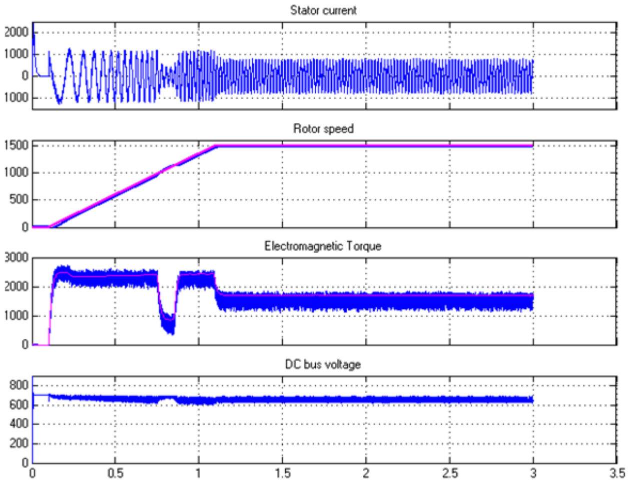

Fig. 11. Waveforms for rated speed and slipping/sliding torque

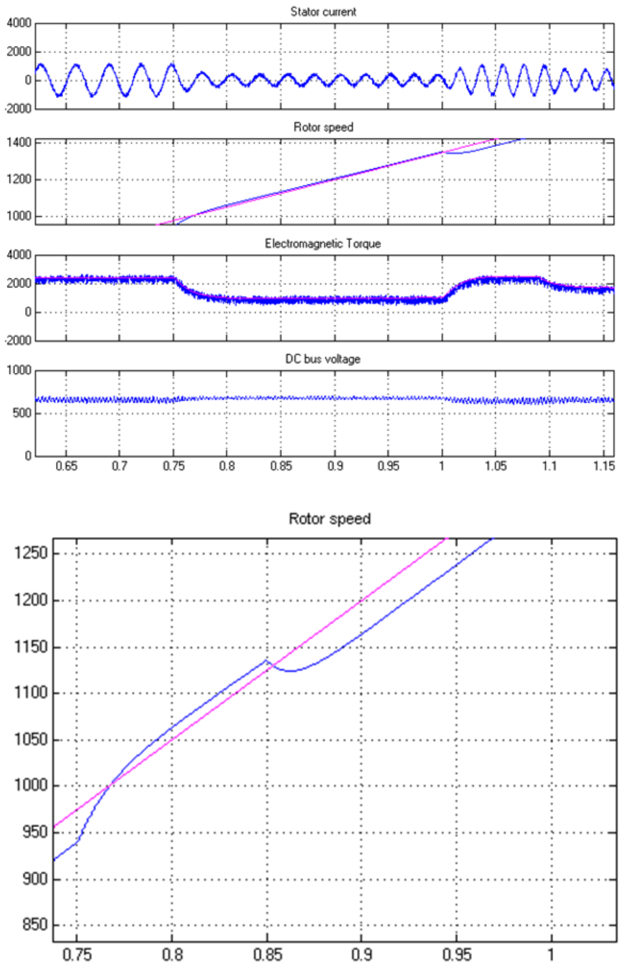

Fig. 12. Details of achieved slipping/sliding area, for waveforms given in Fig. 11

After returning of adhesion or after the increase of the value of the torque at the initial value, a decreasing speed to the initial value before starting the slipping is put into evidence. Simultaneously with the decrease of the torque value, a similar decrease of the stator current is found (Fig. 11).

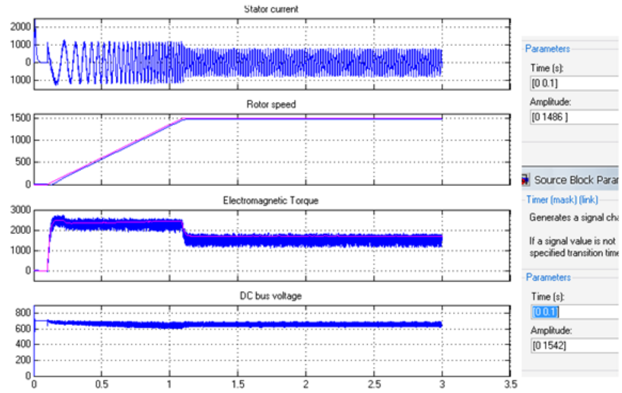

Fig. 13. Rated speed and rated torque waveforms

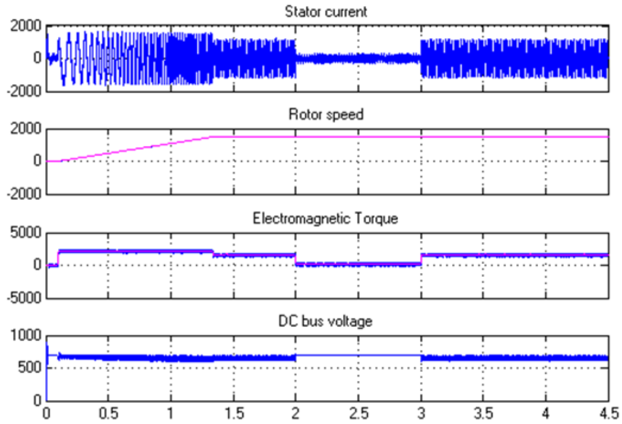

Fig. 14. Waveforms for different torque variations

The corresponding diagrams are shown in Fig. 13 which presents a slipping situation at full speed. As it was shown above, the speed has a slight increasing trend, but it is limited because of the control precision.

The waveforms for different variations of the torque are presented in figure 14.

The diagrams of the stator current, rotor speed, electromagnetic torque and intermediate circuit voltage when the vehicle accelerates from zero to the maximum motor speed, operates at constant speed, brakes and then reverses completely the direction of movement, without brake chopper, are shown in Fig. 15.

During braking, DC link voltage values increase due to the regenerative brake system; they can reach dangerous levels for the integrity of the traction converter.

For the control of the dangerous voltages during braking, a braking chopper (whose working was described previously) is introduced. Basically, during the braking process, the voltage is "consumed" by a resistor so dimensioned that the intermediate circuit voltage is maintained within acceptable limits (Fig. 16).

In the case of the descent slope with braking, the recovered energy is considerably higher and the voltage increases more. When the vehicle goes up a hill, the braking torque helps the process which takes less time and less energy is recovered.

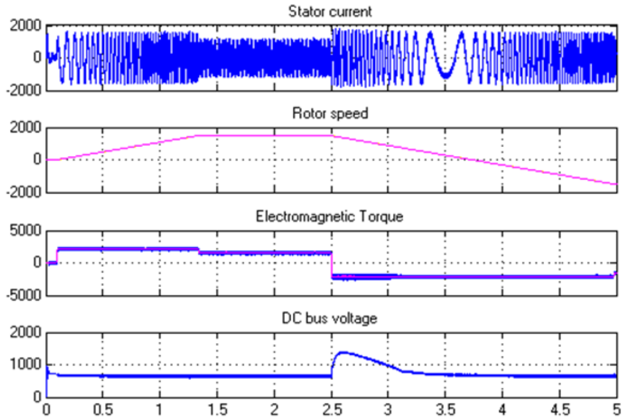

Fig. 15. Waveforms for the reversal of direction and torque without braking chopper

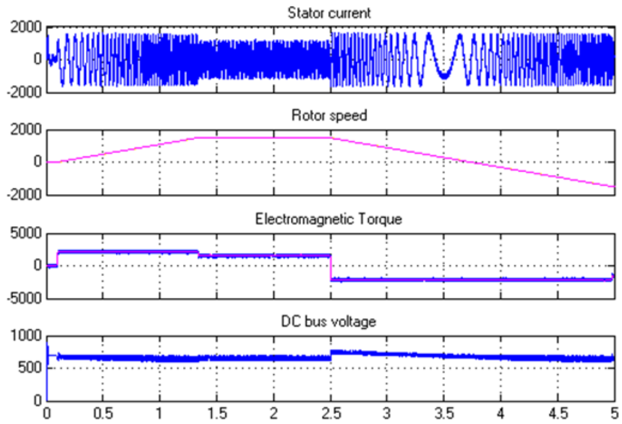

Fig. 16. Waveforms for the reversal direction and torque variation with brake chopper

5. CONCLUSIONS

The simulation software Matlab-Simulink is a powerful tool which helps for calculating and dimensioning drives (in this case for the railways) and which, together with qualitative and quantitative analysis of the present situation, allowed the analysis of the traction motor dynamic regimes submitted.

In order to properly size a drive for some railway vehicles we must take into account the following: the prescription of the limit values of the electromagnetic torque, the polynomial approximation of the decreasing motor flux, the vehicle acceleration, the inverter switching frequency, the maximum vehicle load and the profile route.

The following results were registered for DTC:

- high accuracy for the speed control;
- the stator current is more stable than in the case of the control *U/f = constant*;
- the electromagnetic torque does not present oscillations and the initial overcontrol is small;
- the vehicle slipping was simulated and the dynamic response of the drive is satisfactory.

DTC control method is a newer version, relatively easier than the field oriented control, but it has better performance than the scalar control in what concerns torque control at lower frequencies (in particular).

REFERENCES

[1] *** (2011). *Direct torque control - the world's most advanced AC drive technology*. Company catalogue: ABB drives.

[2] Ivanov, S., Grenier, D., Labrique, F., Resende, M., Robyns, B. (2008). Online Interactive Lessons on the Principle of the Direct Torque Control of the Induction Machine. *Wseas Trans. Advances in Engineering Education*, vol. 5, issue 5.

[3] Leonhard, W. (1992). *Control of Electrical Drives*, Springer Verlag.

[4] *** (2004). *Matlab, Language of Technical Computing*, version 7, 2004.

[5] *** (1992). *Matlab User's Guide*, The Math Works, Inc. Natick, Massachusetts.

[6] Munoz-Garcia, A., Lipo, T.A., Novotny, D.W. (1998). A new induction motor open-loop speed control capable of low frequency operation, *IEEE Trans. on Industry Applications*, vol. 34, no. 5.

[7] Murphy, J.M.D., Turnbull, F.G. (1988). *Power Electronics Control of AC Motors*, A. Wheaton and Co. Ltd., Exeter, England.

[8] Phan, Q.D., Phuong, L.M., Nguyen, X.B. (2007). Direct Torque Control Method with Modified Switching Table for low-cost inverter – induction motor drive. In: *Proc. ISEE'07*, HCMUT Univ. of Technology Vietnam.

[9] Vault, B., Heckenkamp, D., King, T. (1999). Selection of Short – Circuit Protection and Control for Design E Motors. *Industry Applications Magazine*, vol. 5, no. 3.

[10] Whitaker, J.C. (1996). *The Electronics Handbook*, IEEE Press.

Image Processing Using Frequency Separation Technique

Virginia Maria Radulescu*,

* *Department of Automatic Control, University of Craiova, Craiova, Romania*

(e-mail: virginia@automation.ucv.ro)

Abstract:

The evolution of creation and use of high-quality images of the last few years requires an updated and continuously study in the field of image processing. In the following are discussed issues related to the treatment and improvement of the quality of the images. It is proposed a technique that treats images in terms of technical issue, which is based on its frequency in the decomposition. The study will also present examples of implementation of these methods and their results.

Keywords: image, processing, analysis, model, frequency methods.

1. INTRODUCTION

The study of the representation of images has been a continuous concern both in the world of artists and in the world of science. The speed with which things are developing in all fields has also made their mark in the representation of images. We are surrounded by images and their processing is needed to be able to be integrated into existing applications.

We first list the different types of images that we may have to process. In order to be processed by a computing system, an image must be represented by a discrete ensemble of values, the pixels. Each pixel is associated with one or several values depending on the chosen representation.

The most elementary representation corresponds to the binary image, for which each pixel can take only one value among two. For monochrome images, each pixel can take one value among N. N is generally a power of 2, thus facilitating the image representation in the computer. For example, for a grey-level image, each pixel can take one value among 256: this value is then encoded by a data byte. This representation is frequently used and finds a justification involving the human visual system and the physical characteristics of the image support. This point is detailed in the Sampling and quantization section.

A tri-chrome image (or colour image) is a superposition of three grey-level images corresponding to three basic colours. For images that will be displayed on a computer screen, the RGB (red, green, blue) representation is used. Each pixel of a tri-chrome image is thus associated with a triplet of values corresponding to the luminance of the basic colours.(Savakis, Etz, Loui, 2000)

This representation is not the only one allowing colour images to be processed by a computing system. An alternative consists in using indexed colour images, associating the matrix of pixels with a colour table (colour map). More precisely, in this case, each pixel value is an index pointing to the colour table. The colour table is composed of three columns corresponding to the three basic colours. The number of rows in the table is equal to the total number of colours used for the representation. The indexed colour representation is more cost-effective in terms of memory occupancy than the RGB representation since the number of colours is voluntarily limited. Therefore, it is also less precise in terms of image definition.

Images obtained through snapshots in the visible range are not the only ones to find applications, and multi-spectral images are a generalization of the previous case. They are represented by n tables of numbers.

Let us end this section by mentioning some quantitative information regarding image representation in the computer. An image is composed of a pixel matrix of I rows by J columns, where each pixel value is encoded in n bits.

Crt. No.	Bits representation	Image representation
1.	1 bit	2 colours / white & black
2.	4 bits	2^4 colours / tones of grey
3.	8 bits	2^8 colours / tones of grey
4.	16 bits	2^{16} colours / tones of grey
5.	24 bits	2^{24} colours / tones of grey
6.	32 bits	2^{32} colours / tones of grey

For example, a mono-chrome image 512x512 for which each colour is encoded in 8 bits requires 176 KB of data for storage. Such an image is represented on figure 1. On figure 2, we represented the same image after applying the JPEG algorithm. This later image is stored in a memory space of only 25 KB.

Fig. 1. Image 1 – original codification.

Fig. 2. Image 1 - JPG codification.

2. IMAGE PRECESSING ISSUES

Digital image processing is the use of computer algorithms to perform image processing on digital images. As a subfield of digital signal processing, digital image processing has many advantages over analogue image processing; it allows a much wider range of algorithms to be applied to the input data, and can avoid problems such as the build-up of noise and signal distortion during processing.

2.1 Image representation

An image as defined in the "real world" is considered to be a function of two real variables, for example, *imag*(x_1,x_2) with x as the amplitude (e.g. brightness) of the image at the real coordinate position (x_1,x_2). Further, an image may be considered to contain sub-images sometimes referred to as regions of interest or simply regions. This concept reflects the fact that images frequently contain collections of objects each of which can be the basis for a region.

An example of two-dimensional signal is a grayscale image, where x_1 and x_2 represent the horizontal and vertical coordinates, and *imag*(x_1,x_2) represents some measure of the intensity of the image at location (x_1,x_2). This example can also be considered in discrete-time (or rather in discrete space in this case): digital images are made up of a discrete number of points (or pixels), and the intensity of a pixel can be denoted by *imag_d*$[z_1,z2]$.

Digital image processing is an important example of applied numerical computing. There are at least the following three reasons why people want to transform and compute with the numbers in an image:

- Enhancement: improving or changing a picture in different way;
- Compression: reducing the storage required, usually to economize on storage or speed up transmission;
- Recognition: automatically recognize objects, like faces or missile installations. Clearly, this application is in its early stages. (Kou, 1995).

A useful method to express a digital image is to use Fourier Transforms. Fourier analysis is used in image processing in much the same way as with one-dimensional signals. However, images do not have their information encoded in the frequency domain, making the techniques much less useful. For example, when the Fourier transform is taken of an audio signal, the confusing time domain waveform is converted into an easy to understand frequency spectrum. In comparison, taking the Fourier transform of an image converts the straightforward information in the spatial domain into a scrambled form in the frequency domain. In short, don't expect the Fourier transform to help you understand the information encoded in images.

A given function or signal can be converted between the time and frequency domains with a pair of mathematical operators called a transform. Let us consider the given function *imag*(x_1,x_2) - a set of sine and cosine functions having particular frequencies are chosen for image representation. These are termed the basis functions of the representation. A weighted sum of these basic functions is called a Fourier series. The weighting factors for each sine and cosine function are known as the Fourier coefficients.

$$imag(x_1,x_2)=\sum_{x_1=0}^{\infty}\sum_{x_2=0}^{\infty}\left(a_{u,v}\cos\left(\frac{2\pi(ux_1+vx_2)}{lung}\right)+b_{u,v}\left(\frac{2\pi(ux_1+vx_2)}{lung}\right)\right) \quad (1)$$

where *lung* is the period (length of the cycle, or dimension for an image), u and v are the number of cycles fitting into one horizontal and vertical period, respectively of *imag*(x_1,x_2) and the coefficients $a_{u,v}$ and $b_{u,v}$ determine the relative contributions of each basis image to the representation. So we could regard the Fourier series representation of $imag(x_1,x_2)$ as a pair of two-dimensional arrays of coefficients, each of infinite extent. Still an image has a finite representation and in what will follow it will be shown it forms.

Let it be a two dimensional image of length *lung*. In these conditions the above equation (1) it becomes:

$$imag(x_1,x_2)=\sum_{x_1=0}^{lung}\sum_{x_2=0}^{lung}\left(a_{u,v}\cos\left(\frac{2\pi(ux_1+vx_2)}{lung}\right)+b_{u,v}\left(\frac{2\pi(ux_1+vx_2)}{lung}\right)\right) \quad (2)$$

or

$$imag(x_1,x_2)=\frac{1}{lung}\sum_{x_1=0}^{lung}\sum_{x_2=0}^{lung}imag(x_1,x_2)e^{-2i\pi((ux_1+vx_2)/lung)} \quad (3)$$

In what will follow it will be present a 2D image conversion in the frequency domain. The representation was made given that we know the fact that an image is a finite collection of data, which will lead to a representation of Discrete Fourier Transform (DFT) type. The output of the transformation represents the image in the Fourier or frequency domain, while the input image is the spatial domain equivalent. In the Fourier domain image, each point represents a particular frequency contained in the spatial domain image.

The DFT represents the sampled Fourier Transform and therefore does not contain all frequencies forming an image, but only a set of samples which is large enough to fully describe the spatial domain image. The number of frequencies corresponds to the number of pixels in the spatial domain image, e.g. the image in the spatial and Fourier domain is of the same size. For a square image of size *lung*×*lung*, the 2D DFT is given by equation (4). So, an example is the Fourier transform, which converts the time function into a sum of sine waves of different frequencies, each of which represents a frequency component. The 'spectrum' of frequency components is the frequency domain representation of the signal. (Gonzalez, 2002):

$$F(x_1,x_2)=\frac{1}{MN}\sum_{x_1=0}^{lung}\sum_{x_2=0}^{lung}imag(x_1,x_2)e^{-i2\pi(x_1a/lung+x_2b/lung)} \quad (4)$$

The inverse Fourier transform converts the frequency domain function back to a time function. A spectrum analyser is the tool commonly used to visualize real-world signals in the frequency domain.

In electronics, control systems engineering, and statistics, the frequency domain refers to the analysis of mathematical functions or signals with respect to frequency, rather than time. We can simply say that a time-domain graph shows how a signal changes over time, whereas a frequency-domain graph shows how much of the signal lies within each given frequency band over a range of frequencies. A frequency-domain representation can also include information on the phase shift that must be applied to each sinusoid in order to be able to recombine the frequency components to recover the original time signal (Smith, 2003).

Likewise, we don't look to the frequency domain for filter design in what concern images – at list not for now. The basic feature in images is the edge, the line separating one object or region from another object or region. Since an edge is composed of a wide range of frequency components, trying to modify an image by changing the frequency spectrum is generally not productive. Image filters are normally designed in the spatial domain, where the information is encoded in its simplest form. Think in terms of smoothing grand edge enhancement operations (the spatial domain) rather than high-pass and low-pass filters (the frequency domain).

In spite of this, Fourier image analysis does have several useful properties. For instance, convolution in the spatial domain corresponds to multiplication in the frequency domain. This is important because multiplication is a simpler mathematical operation than convolution. As with one-dimensional signals, this property enables FFT convolution and various deconvolution techniques. Another useful property of the frequency domain is the Fourier Slice Theorem, the relationship between an image and its projections (the image viewed from its sides). This is the basis of computed tomography, an x-ray imaging technique widely used medicine and industry (Gonzalez, Woods, 2007).

The frequency spectrum of an image can be calculated in several ways, but the FFT method presented here is the only one that is practical. The original image must be composed of N rows by N columns, where N is a power of two, i.e., 256, 512, 1024, etc. If the size of the original image is not a power of two, pixels with a value of zero are added to make it the correct size. We will call the two-dimensional array that holds the image the real array. In addition, another array of the same size is needed, which we will call the imaginary array.

The recipe for calculating the Fourier Transform of an image is quite simple: take the one-dimensional FFT of each of the rows, followed by the one-dimensional FFT of each of the columns. Specifically, start by taking the FFT of the N pixel values in row 0 of the real array. The real part of the FFT's output is placed back into row 0 of the real array, while the imaginary part of the FFT's output is placed into row 0 of the imaginary array. After repeating this procedure on rows 1 through N-1, both the real and imaginary arrays contain an intermediate image. Next, the procedure is repeated on each of the columns of the intermediate data. Take the N pixel values from column 0 of the real array, and the N pixel values from column 0 of the imaginary array, and calculate the FFT. The real part of the FFT's output is placed back into column 0 of the real array, while the imaginary part of the FFT's output is placed back into column 0 of the imaginary array. After this is repeated on columns 1 through N-1, both arrays have been overwritten with the image's frequency spectrum.

Since the vertical and horizontal directions are equivalent in an image, this algorithm can also be carried out by transforming the columns first and then transforming the rows. Regardless of the order used, the result is the same. From the way that the FFT keeps track of the data, the amplitudes of the low frequency components end up being at the corners of the two-dimensional spectrum, while the high frequencies are at the center. The inverse Fourier transform of an image is calculated by taking the inverse FFT of each row, followed by the inverse FFT of each column (or vice versa).

Now the question arises as to what would be still useful application of Fourier Transform analysis of images. As I mentioned earlier, the implementation of an image in the complex domain brings with it several advantages in image analysis. Some of these advantages will be:

- easier to remove undesirable frequencies.
- faster perform certain operations in the frequency domain than in the spatial domain.

3. PRACTICAL ALGORITHM FOR IMAGE PROCESSING

Frequency Separation technique is virtually a process of decomposing of the image data into spatial frequencies, so that we can edit image details in the different frequencies independently. There can be any number of frequencies in each image, and each frequency will contain certain information (based on the size of the details). Typically, we break down the information data in our images into high and low frequencies.

Like in music any audio can be represented in sine waves, we can also break up an image into low and high frequency sine waves.

For example: *high frequencies* in an portraiture image will contain information about fine details, such as skin pores, hair, fine lines, skin imperfections (acne, scars, fine lines, etc.). *Low frequencies* are the image data that contains information about volume, tone and colour transitions. In other words: shadows and light areas, colours and tones. If one looks at only the low frequency information of an image, he might be able to recognize the image, but it will not hold any precise detail. A simple representation of all above it will be presented on figure 3.

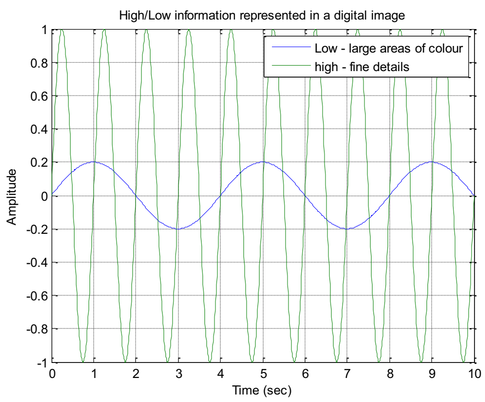

Fig. 3. A simple interpretation of informations from a digital image

Next you will be presented with the above mentioned method. First to get a result as correctly and completely, you must understand fully what they understand by breaking down the information contained in an image. It is important to understand how to transpose the term separation in frequency domain analysis of digital images. It was established that they will share a picture in low frequencies and high frequencies, respectively. This so-called Division represents the key to the method.

After splitting we get basically two images, all digital, which contain only certain information from the original image. The first separate image will match low frequency pattern, for example. Define low frequencies of paternal image that you want to extract information that varies slowly or less - low frequencies correspond to slowly varying information (e.g., continuous surface, tones, etc.). As for the high frequency pattern, it will be the image that will contain information about edges, visible changes of contrast, details - high frequencies correspond to varying quickly information (e.g., edges).

Next will be presented with three images, with which he worked. The image in figure 4 represents the original image that has been analysed and the analysis it was determined that it is necessary to apply an algorithm to improve the qualities of this image. The separation methods in frequency were applied and thus have obtained the two images in Figure 5 and Figure 6.

Fig. 4. Original image

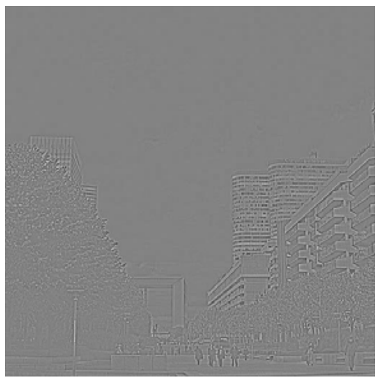

Fig. 5. High pass image

Fig. 6. Low pass image

From this point you can move on to the actual processing of the image. Through processing, but in this case it shall be understood that the process of repairing the image details. The details of large surfaces, colour tones, etc. will be obtained by processing the image as "Low pass" and in the "High pass" will be extracted information as well as finesse large contrasts, edges, etc. After obtaining the desired results in the two pictures will switch to their overlapping and getting the final result.

4. CONCLUSIONS

Many times, image processing tasks are best performed in a domain other than the spatial domain. Exactly this wants to emphasize and work towards. The good result obtained by using the method outlined here makes this one modern. The finesse with which you can work and the accuracy with which you can highlight information from any image shows the qualities of this method. Key steps you must follow in its application are simple and easy to work with:

1. Transform the image
2. Carry the tasks in the transformed domain.
3. Apply inverse transform to return to the spatial domain.

REFERENCES

Kou, W. (1995), *Digital Image Compression: Algorithms and Standards*, Kluwer, Boston.

Savakis, A.E., Etz, A.E.,Loui, A. C.,(2000). Evaluation of image appeal in consumer photography, *Proceedings of SPIE - Human Vision and Electronic Imaging*, Vol. 3959, 111-120.

Smith, S.W. (2003). *Digital Signal Processing: A Practical Guide for Engineers and Scientists*, Newnes, Boston.

Gonzalez, R.C., Woods, R.E. (2007). *Digital Image Processing (3rd Edition)*, Prentice Hall, United States.

Hlawatsch, F., Auger, F.,(2008). *Time-Frequency Analysis*, ISTE Ltd, Great Britain.

Sonka, V., Boyle, M., Hlavac, R. (2014). *Image Processing, Analysis, and Machine Vision,* Cengage Learning Inc.

Gonzalez, R.C., Woods, R. E., (2002). *Digital Image Processing,* Pearson Education, Asia.

Bhattacharya, S., Mali, K., (2014). Comparative Study of Different Filters on Images in Frequency Domain, *International Journal of Advanced Research in Computer Science and Software Engineering*, Volume 4, Issue 8, ISSN: 2277 128X

Improved Smith predictor structures applied in electric plant control

Ionuţ Cristian Reşceanu*, Cristina Floriana Reşceanu*

*University of Craiova , Faculty of Automation, Computers and Electronics
(e-mail: {resceanu , cristina} @robotics.ucv.ro)

Abstract: This paper presents studies regarding remote control of some electric rotating machines – the DC motor and the synchronous generator, using the improved dynamic Smith predictor and double Smith predictor structures. The synchronous generator and the DC motor are studied based on transfer functions (model). One of the most important aspects when applying such control strategies is the study of network delays which is largely depicted here in a large number of simulations. The paper also contains an amply detailed case study performed on a Quanser SRV-02 servo motor controlled via Matlab® and Wincon®. For comparison, we use a non-predictor structure in order to underline the improvements brought on by using the presented Smith predictor configurations.

Keywords: networked control system (NCS), Smith predictor, networked induced delay.

1. ASPECTS REGARDING NETWORKED CONTROL SYSTEMS (NCS)

Networked control systems (NCS) are feedback control systems in which the control loops are achieved through a real-time network. One of the most important features in NCS is the exchange of information between the control system components (usually sensors, actuators and controllers).

The use of NCS is encouraged mainly because of the reduced amount of wiring involved, improved diagnosis abilities and improved speed of response.

Achieving a control loop through a communication network makes the analysis of a networked control system a complex procedure. A disadvantage of NCS is that conventional control theory is hard to apply because of the presence of simplifying assumptions which make the calculi easier to perform. Aspects of conventional control must be closely studied before applying them in NCS.

The following issues may affect the functions of a NCS. Equal distance sampling cannot be insured mainly because of non-deterministic factors during a transmission process. As a result, the NCSs will have a time varying model with direct consequence on the stability analysis. If the control loop achieved in a NCS contains more than one independent plant which is subject to the control activity, then a network scheduling mechanism must be implemented. Network scheduling sets a transmission priority list in order to deal with concurrent transmissions. Another issue describing NCS is the network induced delay (controller to actuator delay and sensor to controller delay) which appears while exchanging information through a shared medium. Another aspect to be dealt with is the packet loss rate. In order to improve this rate, a reliability of the transmissions paths must be enforced. The last aspect is related to the plant output/s which may be transmitted using multiple network packets. The idea is that at the time of the control calculation all packets must be transmitted in order to achieve the control purpose.

Current implementations of NCSs include heterogeneous network architectures (Zhang, 2001).

2. INTRODUCTION TO SMITH CONTROL

The systems that use a Smith predictor are the kind of systems which use a model of the controlled process in order to “predict” certain evolutions that influence the application of adequate commands.

These systems were later developed by Manfred Morrari in the so called Internal Model Predictive Control systems (Marin, 2004).

The plant model plays a decisive role in the control action. The chosen model must be capable of reflecting the process dynamics in order to accurately predict future outcomes. The model also needs to be easily implemented and understood.

The main idea of this technique is to substitute the conventional controller C(s) with a new design $C^*(s)$ in such a way that closed loop control of the process dynamics without delay can be achieved. Given a process, with a delay of τ seconds, Smith proposed that a new controller $C^*(s)$ be introduced in the closed loop with the delayed process $G(s)e^{-\tau s}$ as can be seen in figure 1a.

The effect of the Smith controller $C^*(s)$ is to eliminate the delay from the control loop as can be seen in figure 1 b. and to effectively realize the control of the non-delayed process dynamics $G(s)$ using a conventional controller $C(s)$.

Many slow processes can be described through models of the following form:

$$H(s) = G(s)e^{-\tau s} \tag{1}$$

Where $G(s)$ is rational and strictly proper and τ is the delay (dead time). A conventional control structure like in figure 1a induces infinity of poles in the system. Thus, $H_0(s)$ is:

$$H_0(s) = \frac{C(s)G(s)e^{-\tau s}}{1 + C(s)G(s)e^{-\tau s}} \tag{2}$$

In order to eliminate the unwanted effect of the delay from the process model, a separation of the delay inside the model is attempted and also the use of variable $y(t)$ instead of $y(t-\tau)$ is realized. The structure of the control system, in this case, is the one presented in figure 1b with the following transfer function:

$$H_0^*(s) = \frac{C^*(s)G(s)e^{-\tau s}}{1 + C^*(s)G(s)e^{-\tau s}} \tag{3}$$

Imposing the condition that the structures have the same input-output behavior, we obtain:

$$H(s) = H_0^*(s) \tag{4}$$

The predictive control algorithm (Smith predictor) will be defined by the following transfer function:

$$C^*(s) = \frac{C(s)}{1 + C(s)G(s)(1 - e^{-\tau s})} \tag{5}$$

For the design of the control system any known method for non-delayed systems can be used in order to determine $C^*(s)$.

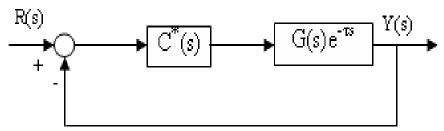

a.

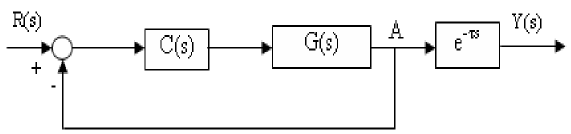

b.

Fig.1. The Smith controller and its equivalent conventional controller

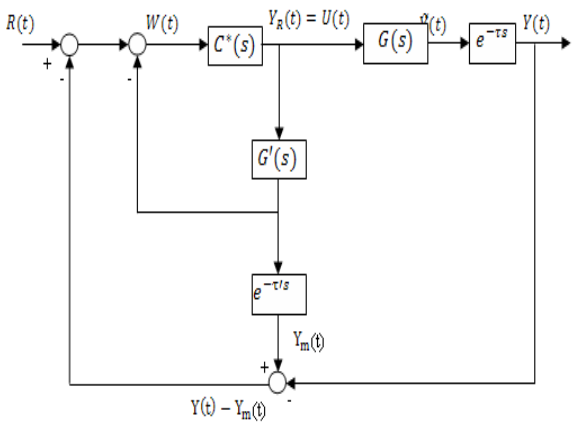

Fig.2. Smith Predictor classic configuration

3. IMPROVED SMITH PREDICTOR AND DOUBLE SMITH PREDICTOR STRUCTURES

The Smith configurations used for the electric plant control are shown in the figures below (Du, 2007):

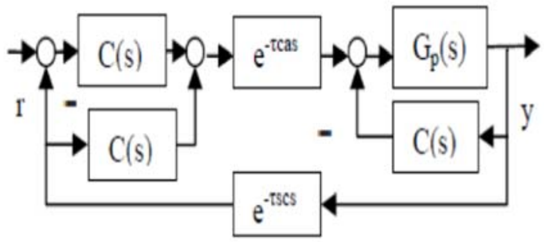

Fig.3. NCS with improved Smith predictor

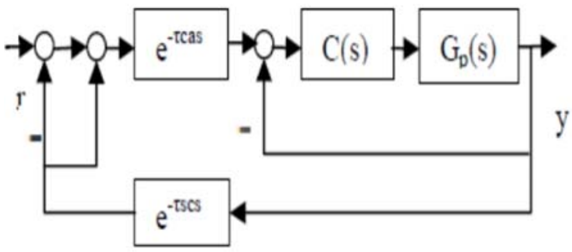

Equivalent control system

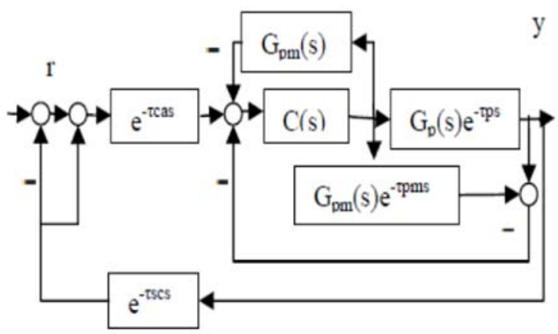

Fig. 4. Double Smith predictor configuration

The closed loop transfer function of the system is as follows:

$$y(s)/r(s)=e^{-\tau cas}C(s)G_p(s)e^{-\tau ps}/ \\ (1+C(s)G_{pm}(s)+C(s)(G_p(s)e^{-\tau ps}-G_{pm}(s)e^{-\tau pms})) \qquad (6)$$

If τpm = τp, Gpm(s) = Gp(s), the prediction models can accurately approximate true models, the above equation (5) is reduced to:

$$y(s)/r(s)=e^{-\tau cas}C(s)G_p(s)e^{-\tau ps}/(1+C(s)G_p(s)) \qquad (7)$$

The improved Smith dynamic prediction compensator can cancel effects of the delays which include network induced delay τsc, τca and controlled plant delay τp in the closed loop system. It realizes double Smith dynamic prediction compensations.

4. CASE STUDY: QUANSER SRV-02 PLANT CONTROL

We demonstrated the findings of the simulations above on the Quanser SRV-02 plant which is a common servo-motor used for diverse laboratory activities.

In the demonstration below we are going to use two Simulink subsystems which are very important: a subsystem representing the real plant (blue) and a subsystem representing the plant model (green).

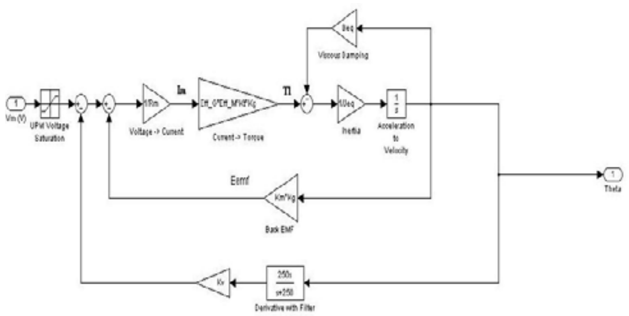

Fig. 5. The model for the Quanser plant (all the coefficient values are stated in a special configuration file).

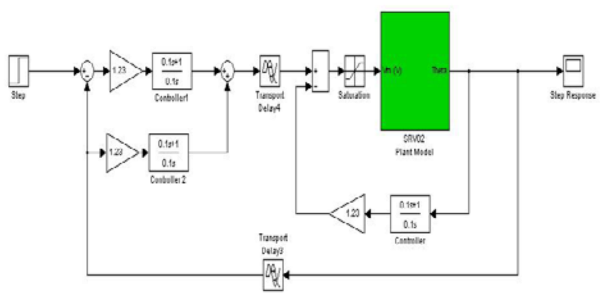

Fig. 6. Improved Smith predictor structure using the subsystem which describes the model of the SRV-02 plant.

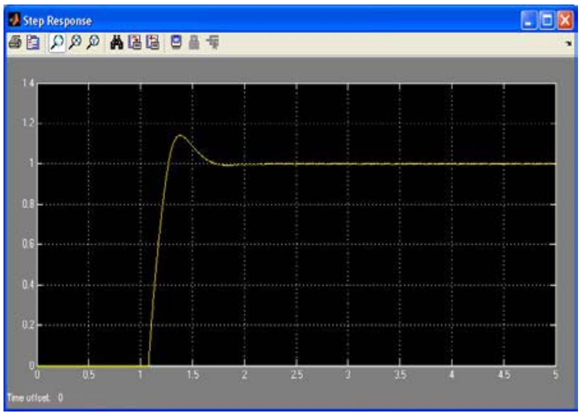

Fig.7 Step response of the configuration presented in Fig.8

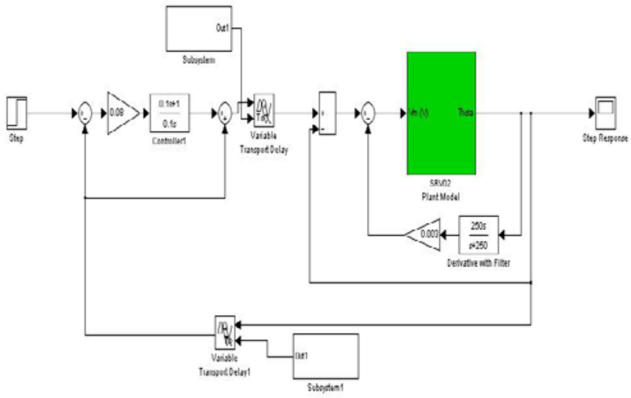

Fig. 8. Improved Smith predictor in case of variable delay and using the Quanser SRV-02 model plant

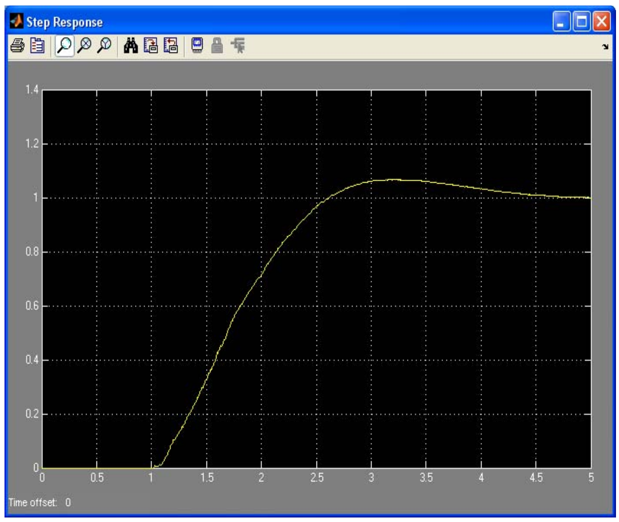

Fig. 9. Step response for the configuration presented in Fig.10

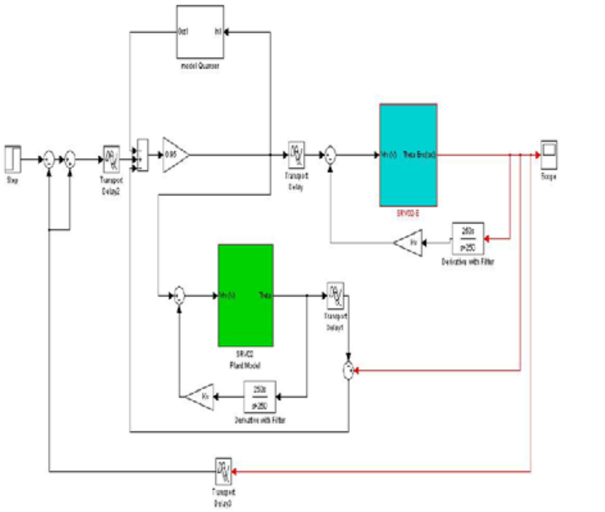

Fig. 10. Double Smith predictor used for the control of a Quanser SRV-02 plant

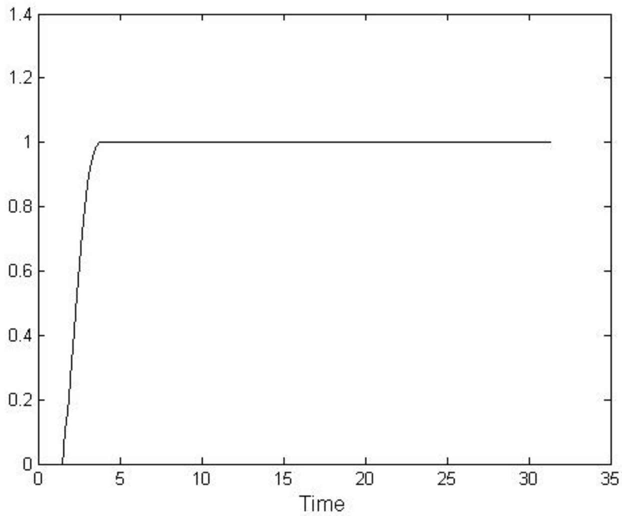

Fig. 11. Step response with a frequency of 0.1 Hz

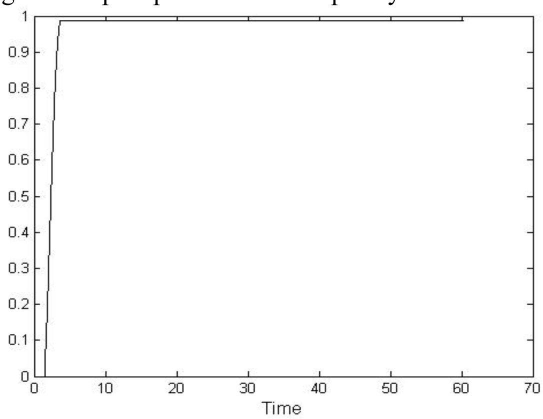

Fig. 12. Step response at a frequency of 0.05 Hz

In the following paragraph we will present another application characteristic to the Quanser SRV-02 plant – position control. For comparison we will use non-predictor configurations presented below.

The response will be presented using several frequencies in order to achieve better control.

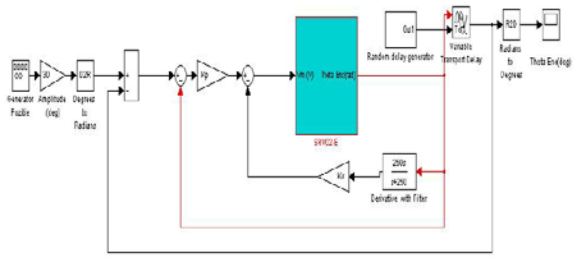

Fig.13. Non-predictor structure used for the position control of the real plant

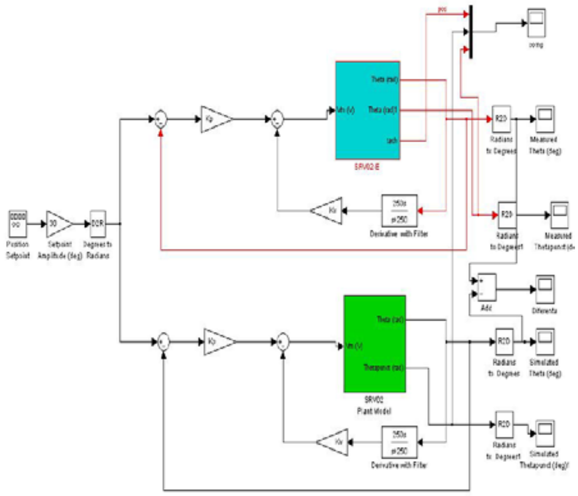

Fig. 14. Non-predictor configuration implying a comparison between the model plant and the real system

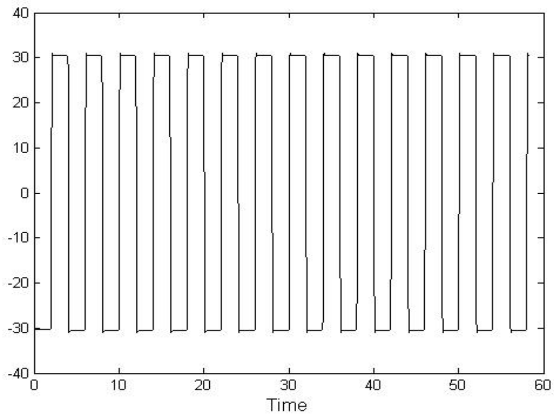

Fig. 15. Position control between 30º and -30º with a frequency of 0.25 Hz using a non-predictor structure

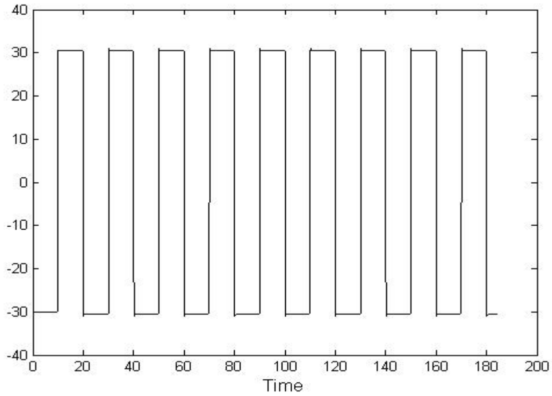

Fig. 16. Position control between 30º and -30º with a frequency of 0.05 Hz using a non-predictor structure

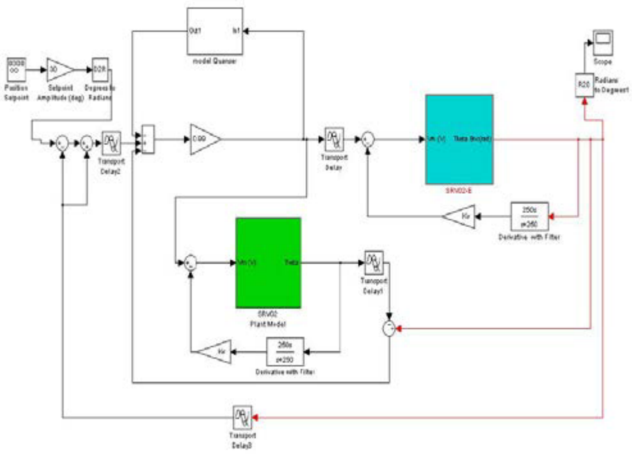

Fig. 17. Double Smith predictor structure for the control of the position of the Quanser SRV-02 plant

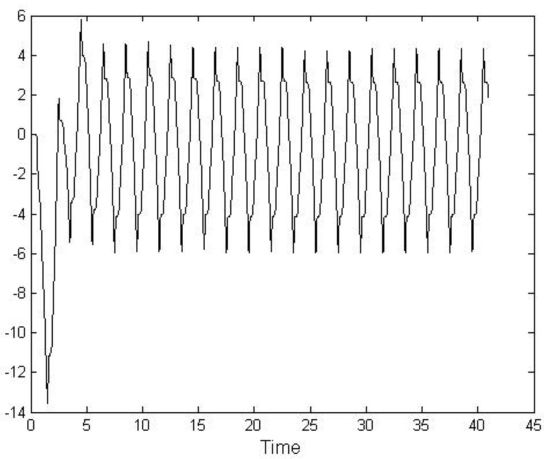

Fig. 18. Position control between 30º and -30º with a frequency of 0.5 Hz using a double Smith predictor structure

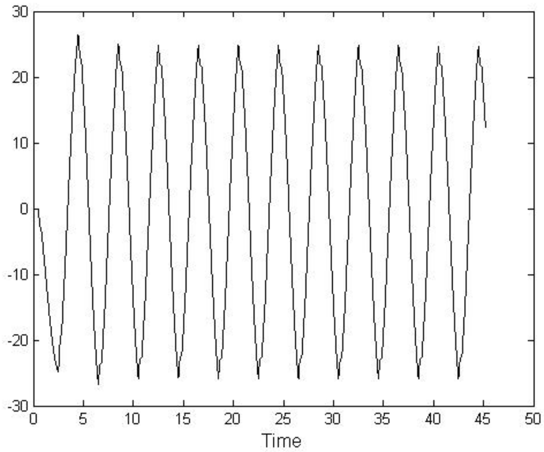

Fig. 19. Position control between 30º and -30º with a frequency of 0.25 Hz using a double Smith predictor structure

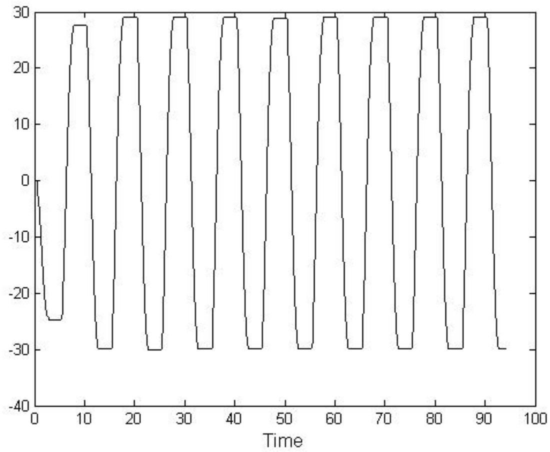

Fig. 20. Position control between 30º and -30º with a frequency of 0.1 Hz using a double Smith predictor structure

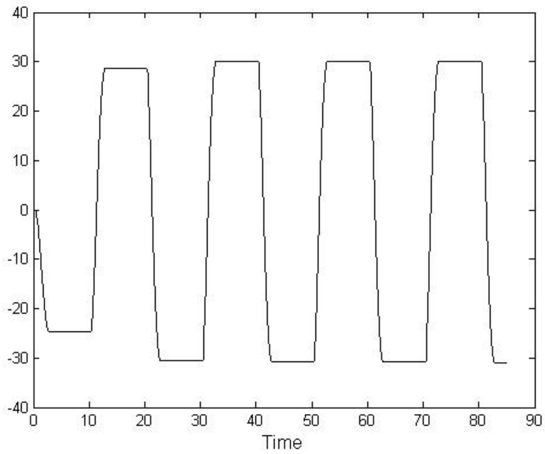

Fig. 21. Position control between 30º and -30º with a frequency of 0.05 Hz using a double Smith predictor structure

In the figures above, it can be seen that for a frequency of 0.5 Hz compensation cannot be achieved under any circumstances. Only for a frequency of 0.1 Hz and below the signal can be contained. Thus, the appropriate frequency requirements must be obtained in order to achieve the correct compensation

5. CONCLUSIONS

Regarding the simulations performed in the first part of this paper, we can clearly state that a networked control system affected by random communication delay responds slower to a predictive control structure than a system with a fixed communication delay. This slow response is due to the fact that the dynamic compensation is much harder to achieve because of the random delay.
The double Smith predictor structure achieves a better dynamic compensation than the improved Smith predictor structure.

The conclusion of the case study implying the Quanser SRV-02 plant is that the delay occurrence frequency is high and the process time constant is low and thus the compensation will not be fully achieved.

The case study performed on the Quanser SRV-02 plant through Matlab and WinCon reveals that in the case of the double Smith predictor configuration the compensation is fully achieved. Thus, in appropriate frequency requirements and with a fixed delay, the position control of the Quanser SRV-02 plant doesn't need a complex controller. In predictive structures, the controllers used can be calculated through heuristic methods because the predictive structures imply a thorough compensation within themselves.

ACKNOWLEDGMENT

This work was supported by the strategic grant POSDRU/159/1.5/S/133255, Project ID 133255 (2014), co-financed by the European Social Fund within the Sectorial Operational Program Human Resources Development 2007 – 2013.

REFERENCES

Aström K.J., Hang C.C. and Lin B.C. (1994). A New Smith Predictor for Controlling a Process with an Integrator and Long Dead-Time, *IEEE Transaction on Automatic Control*, 39(2), pp. 343-345.

Du F., Wencai D., Zhi L. (2009). New Smith Predictor and Nonlinear Control for Networked Control Systems, *Proc. of the International MultiConference of Engineers and Computer Scientists*, March 18-20, Hong Kong, Vol. 2, pp. 1184-1188.

Du F., Qian Q. (2007). Study of NCS with Improvement Smith Predictor and Fuzzy Immune Control, *Proc. of the International Conference on Intelligent Systems and Knowledge Engineering*, Chengdu, China.

Marin C. (2004). *Sisteme neconventionale de reglare automata,* Ed. Sitech, Craiova.

Truxal J.G., Shooman M.J., Blesser W.R. , Clark J.W. (1967). *Remote Control*, in the Handbook of Telemetry and Remote Control, Mc-Graw Hill, New-York, pp 1-169.

Velagic J. (2008). Design of Smith-like Predictive Controller with Communication Delay Adaptation, *World Academy of Science, Engineering and Technology*, no. 47, pp 199-203.

Zhang W. (2001). *Stability Analysis of Networked Control Systems,* Case Western Reserve University, Ph. D. Thesis.

*** IEEE Standard Dictionary of Electrical and Electronic Terms, the Institute of Electrical and Electronic Engineers, Inc., New York.

*** Matlab User Guide.

*** Quanser Consulting Inc., SRV-02 series, Rotary Experiment #1, Position Control.

*** Quanser Consulting Inc., SRV-02 series, User Manual, WinCon 5.0 User Manual.

Nonlinear dynamics in biotechnological processes: Analysis and case studies

Monica Roman*

**Department of Automation and Electronics,*
University of Craiova, A.I. Cuza 13, RO-200585, Craiova, Romania
(e-mail: monica@automation.ucv.ro)

Abstract: This paper presents the dynamics analysis of some biochemical processes under different reaction kinetics, highlighting the influence of physical chemical factors over the evolution of the process run. The models of reaction kinetics are integrated in the general pseudo bond graph models of the biochemical processes as bond graph elements, underlining and using the modularity advantage of bond graph modeling methodology. First, a prototype bioprocess is used in order to analyze the behavior of some process parameters under the influence of substrate and biomass concentrations on the specific growth rate. Second, some of these reaction kinetics are considered for the analysis of a more complex bioprocess of lipase production. The simulations are performed in 20sim modeling and simulation environment.

Keywords: nonlinear systems, modeling, biotechnology, bond graphs.

1. INTRODUCTION

In the last decades, numerous results related to the modeling, identification and control of biotechnological processes have been reported in research papers and various industrial applications (Bastin and Dochain, 1990; Julien and Whitford, 2007; Dochain, 2008; Selișteanu *et al.*, 2014). One of the most important problems in this area concerns the modeling and analysis of biological phenomena inside bioprocesses, especially regarding the development of some estimation and control algorithms.

The bioprocesses are nonlinear systems, with interconnections, uncertainties and absence of low-cost instrumentation. The bioprocess modeling necessitates efforts to understand the interconnections between several compartments and the associated propagation or growth phenomena. A classification of model types which can be used in control is as follows (Julien and Whitford, 2007): heuristic or mass/energy conservation balances; qualitative models and fuzzy logic; black-box models and neural networks; statistical models.

In this work, the mass/energy conservation balance method will be used. In this modeling paradigm, the dynamical models can be obtained via classical approaches (such as the modeling method of Bastin and Dochain, 1990), or by using an alternative modeling procedure: the bond graph method (Karnopp *et al.*, 1990; Borutzky, 2010).

One of the important issues in the bioprocess modeling is the kinetics description. The kinetic rates models are strongly nonlinear and often their analytical expressions are hard or even impossible to obtain. In the last decades (even the last century) several types of models were proposed for the specific growth rates associated to different bioprocesses (Monod, 1942; Andrews, 1969; Bastin and Dochain, 1990). From the well known Monod law to Haldane kinetics, Contois or Tessier laws, various expressions were proposed to describe the influence of substrate, biomass, product concentrations, pH, temperature, etc. on the kinetics. Because the implementation of control schemes requires the achievement of simple and practical models, the analysis of reaction kinetics and of the whole dynamics of the process has a key role in the bioprocess modeling.

A suitable modeling environment for bioprocesses is the bond graph method. This technique, initiated by Paynter in 1961, was applied in the past especially to mechanical and electrical processes. The method was extended later to hydraulic and thermal systems (Karnopp *et al.*, 1990; Thoma and Ould Bouamama, 2000), and in the last period to thermodynamics, chemistry and biology. The method application to chemical and biochemical processes requires a modified bond graph approach, which is based on the so-called pseudo bond graphs (Heny *et al.*, 2000; Couenne et al., 2006; Roman et al., 2009). The pseudo bond graph approach uses variables with physical correspondence different from power, variables that substitute the classic bonds. For instance, the chemical potential is replaced by the concentration of the reactant or reaction products.

In this work, the dynamics analysis of some bioprocesses under different reaction kinetics is widely studied. The models of reaction kinetics are integrated in the pseudo bond graph models of the bioprocesses as bond graph elements. First, a batch prototype bioprocess is used to analyze the behavior of some process parameters under the influence of substrate and biomass concentrations on the specific growth rate. Second, various reaction kinetics are considered to analyze a complex bioprocess of lipase production. Several simulations are performed in 20sim modeling and simulation environment.

2. REACTION KINETICS MODELS

The specific growth rate μ is an important parameter in biomass growth, product formation and substrate consumption. Experimental results shown that this parameter varies in time and it is influenced by a lot of physical-chemical and biological factors such as: substrate concentration, biomass concentration, product concentration, dissolved oxygen concentration, temperature, pH, etc., and consequently it is highly nonlinear:

$$\mu(\cdot) = \mu(S, X, P, C, T, pH, ...) \tag{1}$$

or

$$\mu(\cdot) = \mu(S)\mu(X)\mu(P)\mu(C)\mu(T)\mu(pH)... \tag{2}$$

where *S*, *X*, *P*, *C* have the above mentioned signification.

Next, several models of the specific growth rate influenced by substrate and biomass concentrations are presented.

2.1 The influence of substrate concentration

The most common analytical model of the specific growth rate is the Monod law, also known as Michaelis-Menten law, describing the relation between the substrate concentration and μ as follows (Monod, 1942):

$$\mu(S) = \mu^* \frac{S(t)}{K_M + S(t)} \tag{3}$$

where μ^* is the maximum specific growth rate and K_M is the Michaelis-Menten (Monod) constant. The specific growth rate – substrate concentration in the Monod case is depicted in Fig. 1 (for $\mu^* = 0.02 \ h^{-1}$, $K_M = 2g/l$). It can be observed the typical saturation behavior.

Another model that relates the specific growth rate and substrate concentration was proposed by Tessier (Bastin and Dochain, 1990):

$$\mu(S) = \mu^*(1 - \exp(-S(t)/K_M)) \tag{4}$$

A common profile of the specific growth rate in this case is given in Fig. 2.

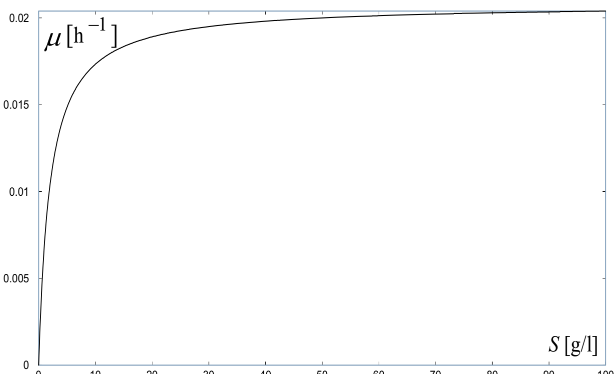

Fig. 1. Specific growth rate: Monod.

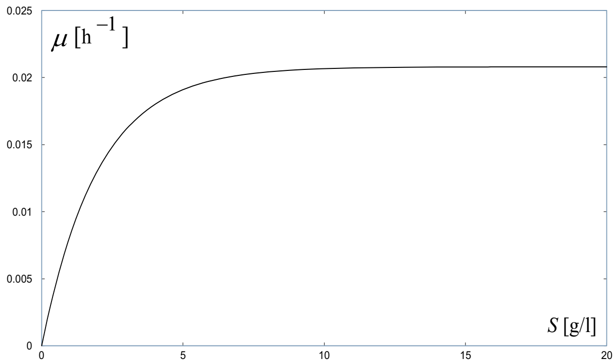

Fig. 2. Specific growth rate: Tessier.

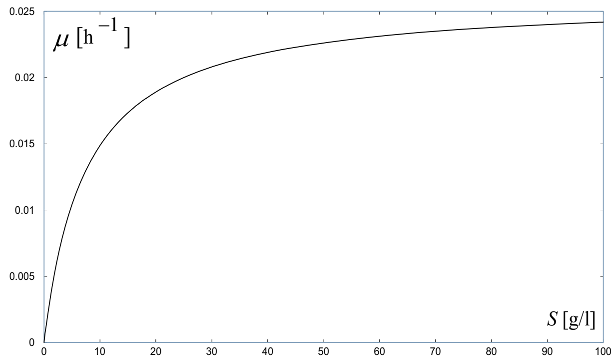

Fig. 3. Specific growth rate: Yue.

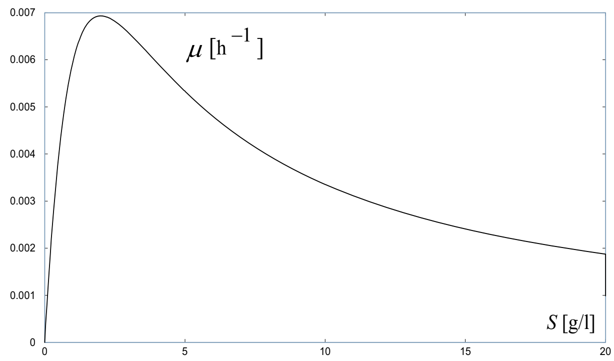

Fig. 4. Specific growth rate: Haldane.

A different model was proposed by Yue, which presents the specific growth rate as function of the influent substrate, according to the following relation:

$$\mu(S) = \mu^* \frac{S(t)}{K_{in}(S_{in} - S(t)) + K_M + S(t)} \tag{5}$$

The profile of this kinetic law is presented in Fig. 3 (for the parameters $\mu^* = 0.025 \ h^{-1}$, $K_M = 2g/l$, $K_{in} = 0.1$, $S_{in} = 100g/l$).

The main disadvantage of the above presented models is that the possible inhibition effects of substrate on the microbial growth that appear at high substrate concentrations are not taken into account. One model that describes the inhibitor effect is the Haldane law (Andrews, 1969):

$$\mu(S) = \mu_0 \frac{S(t)}{K_M + S(t) + S(t)^2 / K_I} \tag{6}$$

where $\mu_0 = \mu^*\left(1 + \sqrt{K_M / K_I}\right)$, K_M is the Michaelis-Menten constant and K_I is the inhibition constant.

The specific growth rate described by the Haldane law has a profile that expresses the inhibitory effect of the substrate in excess (Fig. 5, $\mu^* = 0.025\ h^{-1}$, $K_M = 2g/l$, $K_I = 1g/l$).

2.2 The influence of biomass concentration

At high concentrations of biomass, its growth is slowed down, and one of the models that highlight the influence of biomass concentration on the specific growth rate was developed by Verhulst:

$$\mu(X) = \mu^*(1 - aX(t)) \tag{7}$$

where a is the inhibition constant.

Contois proposed a model for the specific growth rate as function of substrate and biomass concentrations (Contois, 1959):

$$\mu(S, X) = \mu^* \frac{S(t)}{K_M X + S(t)} \tag{8}$$

Another model for the specific growth rate as function of substrate and biomass concentrations was given by Staniskis and Levisauskas:

$$\mu(S, X) = aS(t) - bX(t) \tag{9}$$

where a and b are constants.

Some of the models presented in this section will be used for the modeling of two biotechnological processes: the prototype microbial growth bioprocess and the lipase production bioprocess.

3. MODELING AND DYNAMICS ANALYSIS OF THE PROTOTYPE MICROBIAL GROWTH PROCESS

The simple microbial growth reaction represents a prototype reaction, present in almost every bioprocess. The reaction scheme of this bioprocess is (Bastin and Dochain, 1990; Dochain, 2008):

$$S \xrightarrow{\varphi} X\ , \tag{10}$$

where S is the substrate, X is the biomass and φ is the reaction rate.

For the modeling of the microbial growth process the pseudo bond graph approach was used, tacking into account the basics of bond graph methodology and the pseudo bonds adapted for biochemical processes. The effort and flow variables are in this case concentration and mass flow (Roman *et al.*, 2009).

In the case of the batch bioreactor, there is no influent into or effluent flow from the bioreactor and the biomass X is periodically collected. The modeling procedure starts with the reaction scheme and taking into account the mass transfer through the batch bioreactor. The model is presented in Fig. 5. The directions of half arrows correspond to the run of the reaction, from the substrate S towards biomass X.

In this pseudo bond graph model, the mass balances of the components involved in the bioreactor are represented by two 0-junctions: one for substrate and one for biomass.

The accumulations of substrate S and biomass X in the bioreactor are modeled using capacitive elements C and the reaction kinetics are encapsulated into the MR element.

By writing the constitutive equations of each element the dynamical model of this prototype bioprocess is obtained (Roman *et al.*, 2009):

$$\begin{aligned} \dot{S}(t) &= -\varphi, \\ \dot{X}(t) &= \varphi. \end{aligned} \tag{11}$$

Various simulations were performed for the dynamical model (11), taking into account that the reaction rate φ can be expressed as $\varphi(X, S) = \mu(S) \cdot X$, where μ is the specific growth rate.

In Figs. 6 and 7, the time profiles of the substrate and of the biomass concentration, respectively, are given, for different specific growth rate models: Monod, Tessier, Yue and Haldane.

The typical behavior of this kind of process can be noticed in all situations: the substrate consumption associated with the biomass growth. It should be mentioned that the dynamical behavior strongly depends on the parameter values but also on the initial conditions.

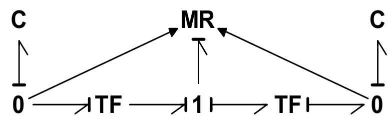

Fig. 5. Pseudo bond graph model of the batch prototype bioprocess.

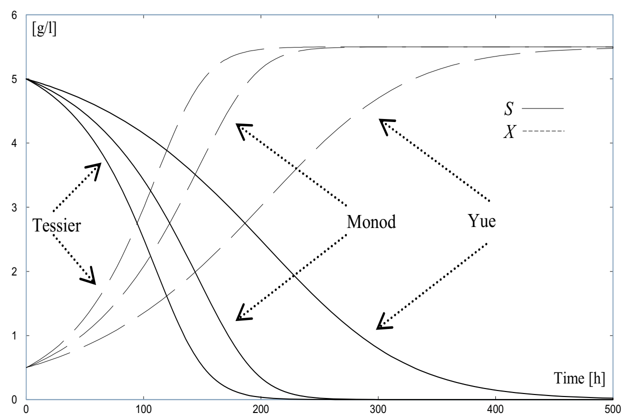

Fig. 6. Substrate and biomass concentrations for the prototype bioprocess: Monod, Tessier and Yue.

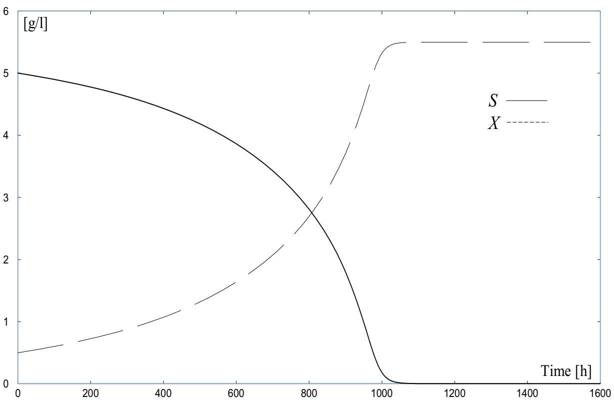

Fig. 7. Substrate and biomass concentrations: Haldane.

4. MODELING AND DYNAMICS ANALYSIS OF LIPASE PRODUCTION BIOPROCESS

In this section, the lipase production from olive oil by *Candida rugosa*, which takes place into a batch reactor, is modeled and analyzed. The process is characterized by the growth of microorganisms on two substrates that are produced by the hydrolysis of a primary complex organic substrate. Actually, it is represented by three-step reaction network (Chen and Bastin, 1996; Bernard and Bastin, 2005):

a) The hydrolysis:

$$k_1 S_1 + E \xrightarrow{\varphi_1} S_2 + k_2 S_3 + E \qquad (12)$$

b) The growth on substrate S_2 (glycerol):

$$k_3 S_2 + k_4 O \xrightarrow{\varphi_2} X + k_5 P \qquad (13)$$

c) The growth on substrate S_3 (fatty acids):

$$k_6 S_3 + k_8 O \xrightarrow{\varphi_3} X + k_7 E + k_9 P \qquad (14)$$

In this reaction scheme S_1 is the primary substrate, i.e. the olive oil (which is made of several compounds, especially triglycerides), S_2 and S_3 represents the secondary substrates (the glycerol and the fatty acids), E is the enzyme (lipase), X is the biomass (*Candida rugosa*), O is the dissolved oxygen and P is the dissolved carbon dioxide. φ_1, φ_2 and φ_3 are the reaction rates and $k_i, i = \overline{1,9}$ are the yield coefficients.

In order to obtain the pseudo bond graph model of batch lipase production process, the reaction scheme and the properties of batch bioreactor were used. The directions of half arrows correspond to the run of the reactions, from the reactants towards the reaction products for each reaction. The pseudo bond graph model is presented in Fig. 8.

The mass balances of the components involved in the bioreactor are modeled by two 7-junctions corresponding to each reaction component.

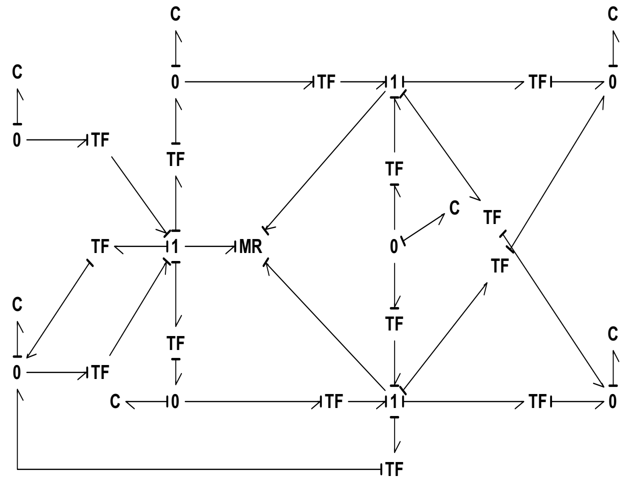

Fig. 8. Pseudo bond graph model of the lipase production process.

The accumulations of the components in the bioreactor are modeled using 7 capacitive elements C and the reaction kinetics are encapsulated into the MR element. The TF elements are used for the modeling of yield coefficients. Based on the pseudo bond graph model given in Fig. 8, the dynamical model of the bioprocess can be obtained by using the bond graph methodology (Roman *et al.*, 2009). The dynamical model expresses the mass balance of components from the reaction schemes (12)-(14) and consists of seven differential equations which describe the dynamics of concentrations inside the batch process. This model is equivalent with that obtained using classical modeling (see, for example, the continuous model given in (Chen and Bastin, 1996; Bernard and Bastin, 2005; Selişteanu *et al.*, 2014). The dynamical model of the batch lipase production process is:

$$\begin{bmatrix} \dot{S}_1 \\ \dot{S}_2 \\ \dot{S}_3 \\ \dot{E} \\ \dot{X} \\ \dot{O} \\ \dot{P} \end{bmatrix} = \underbrace{\begin{bmatrix} -k_1 & 0 & 0 \\ 1 & -k_3 & 0 \\ k_2 & 0 & -k_6 \\ 0 & 0 & k_7 \\ 0 & 1 & 1 \\ 0 & -k_4 & -k_8 \\ 0 & k_5 & k_9 \end{bmatrix}}_{K} \begin{bmatrix} \varphi_1 \\ \varphi_2 \\ \varphi_3 \end{bmatrix} \qquad (15)$$

In the dynamical model (15), the concentrations of components were denoted with the same symbols as the components. K is the matrix of yield coefficients (called also the pseudo-stoichiometric matrix). The nonlinear (and uncertain) part of the model (15) is represented by the reaction rates φ_1, φ_2 and φ_3. These rates are given in the following general forms:

$$\varphi_1(\xi) = \varphi_1(S_1, E, X) = \mu_1(S_1, E)X \qquad (16)$$

$$\varphi_2(\xi) = \varphi_2(S_2, O, X) = \mu_2(S_2, O)X \qquad (17)$$

$$\varphi_3(\xi) = \varphi_3(S_2, S_3, O, X) = \mu_3(S_2, S_3, O)X \qquad (18)$$

where $\mu_i, i = \overline{1,3}$ are the specific reaction rates.

The specific growth rates are modeled using different configurations of combined and modified kinetics based on Monod, Tessier and Haldane laws.

The pseudo bond graph model was implemented in 20sim modeling and simulation environment, and the simulations were conducted for three reaction kinetics configurations.

The first configuration of the specific growth rates is represented by Monod laws (Bernard and Bastin, 2005):

$$\mu_1(S_1,E)=\mu_1^*\frac{S_1}{K_{m1}+S_1}\frac{E}{K_{m2}+E} \tag{19}$$

$$\mu_2(S_2,O)=\mu_2^*\frac{S_2}{K_{m3}+S_2}\frac{O}{K_{m4}+O} \tag{20}$$

$$\mu_3(S_2,S_3,O)=\mu_3^*\frac{S_3}{(K_{m5}+S_3)(K_{m6}+S_2)}\frac{O^2}{K_{m7}+O^2} \tag{21}$$

where $\mu_i^*, i=\overline{1.3}$ represent maximum specific reaction rates and $K_{mi}, i=\overline{1,7}$ are Michaelis-Menten constants.

The second configuration is based on Tessier laws and Monod-like kinetics:

$$\mu_1(S_1,E)=\mu_1^*(1-\exp(S_1/K_{m1}))\frac{E}{K_{m2}+E} \tag{22}$$

$$\mu_2(S_2,O)=\mu_2^*(1-\exp(S_2/K_{m3}))\frac{O}{K_{m4}+O} \tag{23}$$

$$\mu_3(S_2,S_3,O)=\mu_3^*(1-\exp\left(\frac{S_3}{K_{m5}}\right)\frac{1}{K_{m6}+S_2}\frac{O^2}{K_{m7}+O^2} \tag{24}$$

Finally, the last configuration considered for the specific growth rates is represented by Haldane laws plus Monod-like kinetics:

$$\mu_1(S_1,E)=\mu_1^*\frac{S_1}{K_{m1}+S_1+S_1^2/K_i}\frac{E}{K_{m2}+E} \tag{25}$$

$$\mu_2(S_2,O)=\mu_2^*\frac{S_2}{K_{m3}+S_2+S_2^2/K_i}\frac{O}{K_{m4}+O} \tag{26}$$

$$\mu_3(S_2,S_3,O)=\mu_3^*\frac{S_3}{(K_{m5}+S_3+S_3^2/K_i)(K_{m6}+S_2)}\cdot\frac{O^2}{K_{m7}+O^2} \tag{27}$$

The three possible configurations were simulated and tested for the next parameters values (Bernard and Bastin, 2005): μ_1^* = 0.0208 h^{-1}, μ_2^* = 0.125 h^{-1}, μ_3^* = 0.833 g/(lh), K_{m1} = 2 g/l, K_{m2} = 0.2 g/l, K_{m3}= 1 g/l, K_{m4} = 0.2 g/l, K_{m5} = 1 g/l, K_{m6} = 0.2 g/l, K_{m7} = 2 g^2/l^2, k_1 = 3, k_2 = 0.3, k_3 = 4.54, k_4 = 1.33, k_5 = 0.34, k_6 = 0.5, k_7 = 0.19, k_8 = 0.72, k_9 = 1.24.

Figs. 9-14 present the time evolution of the involved concentrations for three different kinetics configurations given in (19)-(21), (22)-(24), and (25)-(27), respectively. Form the simulations it can be observed that the dissolved oxygen concentration oscillates in the transient regime, regardless of the kinetics reaction models used in simulation. This fact is due to some inhibitory effects of the substrates, but also to the batch operation of the process. The utilization of a continuous operation mode (Chen and Bastin, 1996; Bernard and Bastin, 2005; Selișteanu *et al.*, 2014) can lead to the elimination of some disadvantages and to the improvement of lipase production.

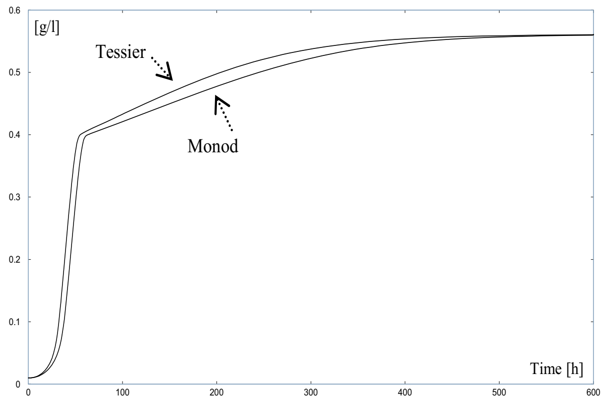

Fig. 9. Lipase concentrations: Monod and Tessier.

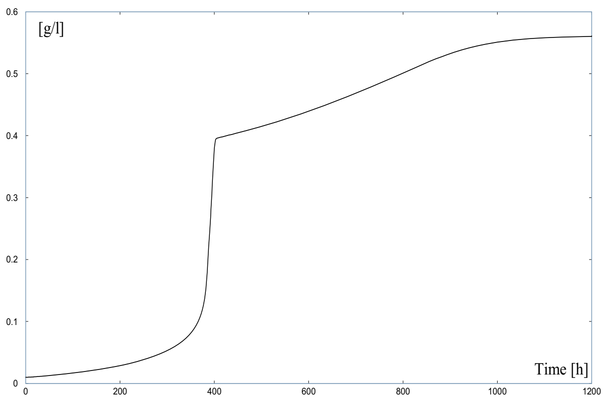

Fig. 10. Lipase concentration: Haldane.

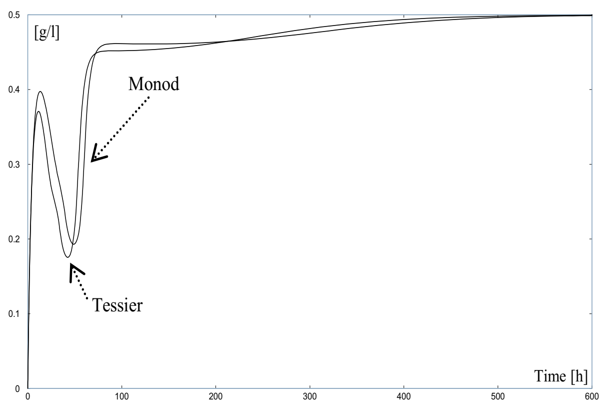

Fig. 11. Dissolved oxygen concentrations: Monod and Tessier.

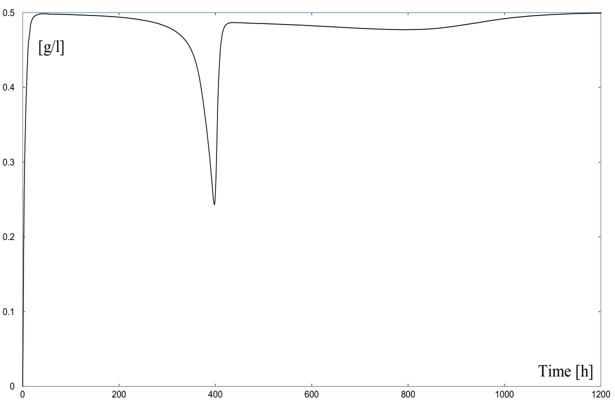

Fig. 12. Dissolved oxygen concentration: Haldane.

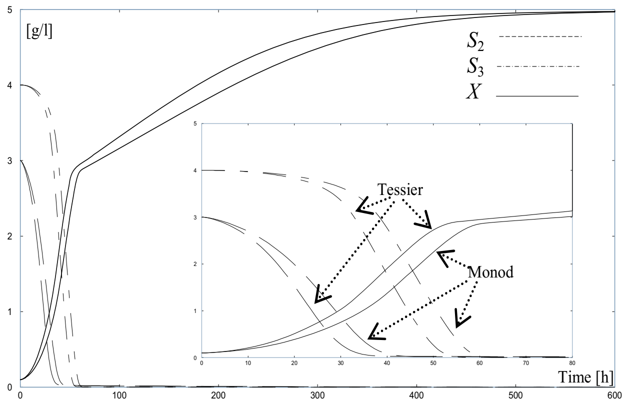

Fig. 13. The concentrations of secondary substrates and of biomass: Monod and Tessier.

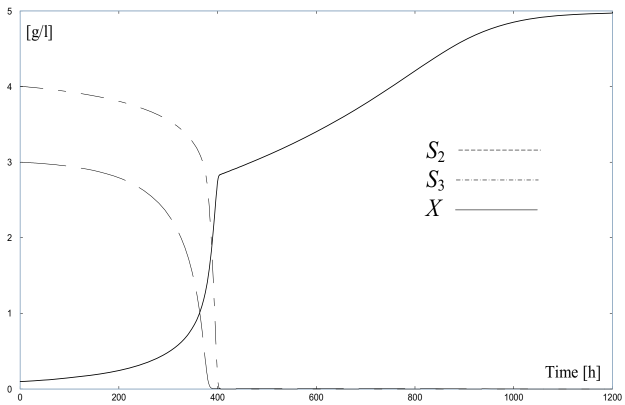

Fig. 14. The concentrations of secondary substrates and of biomass: Haldane.

5. CONCLUSIONS

The pseudo bond graph approach is useful for the extensive study of different kinetics of various bioprocess models. The modularity of bond graph methodology allows the modeling and the simulation of different specific growth rates and of their influence on the overall dynamics of the bioprocess. The simulations were performed on a prototype bioprocess and on a complex lipase production process. This study can be used in order to choose the best kinetic model when some off-line analyses of the concentrations are available.

ACKNOWLEDGMENT

This work was supported by University of Craiova, project no. 17C/2014, and by UEFISCDI, project BIOCON no. 269/2014, PN-II-PT-PCCA-2013-4-0070.

REFERENCES

Andrews, J.F. (1969). Dynamic Model of the Anaerobic Digestion Process. *Am. Soc. Civ. Engng.* 95, 95-116.

Bastin, G., and Dochain, D. (1990). *On-line Estimation and Adaptive Control of Bioreactors*. Elsevier.

Bernard, O., and Bastin, G. (2005). Identification of reaction networks for bioprocesses: determination of a partially unknown pseudo-stoichiometric matrix. *Bioprocess Biosyst. Eng.*, vol. 27, 293-301.

Borutzky, W. (2010). *Bond Graph Methodology. Development and Analysis of Multi-disciplinary Dynamic System Models*, Springer-Verlag.

Chen, L., and Bastin, G. (1996). Structural identifiability of the yield coefficients in bioprocess models when the reaction rates are unknown. *Math. Biosci.*, vol. 132, 35-67.

Contois, D.E. (1959). Kinetics of Bacterial Growth: Relationship Between Population Density and Specific Growth Rate of Continuous Culture. *J. Gen. Microbiol.*, 21, 40-50.

Couenne, F., Jallut, C., Maschke, B., Breedveld, P. C. and Tayakout, M. (2006). Bond graph modelling for chemical reactors. *Math. and Computer Modelling of Dynamical Systems*, vol. 12, no. 2, 159-174.

Dochain, D. (2008). *Automatic Control of Bioprocesses*, ISTE Publishing and Wiley & Sons.

Heny, C., Simanca, D. and Delgado, M. (2000). Pseudo-bond graph model and simulation of a continuous stirred tank reactor. *Journal of the Franklin Institute*, vol. 337, pp. 21-42.

Julien, C., and Whitford, W. (2007). Bioreactor monitoring, modeling, and simulation. *BioProcess Int.*, vol. 5, no. 1, 10-17.

Karnopp, D., Margolis, D., Rosenberg, R. (1990). *System Dynamics: A Unified Approach.* John Wiley & Sons.

Monod, J. (1942). *Recherches sur la Croissance des Cultures Bactériennes*. Hermann, Paris.

Roman, M., Bobaşu, E., Petre, E. Selişteanu, D., Şendrescu, D. (2009). Pseudo Bond Graph Modelling of Some Prototype Bioprocesses. *Control Eng. And Appl. Informatics*, vol. 11, 22-29.

Selişteanu, D., Tebbani, S., Roman, M., Petre, E., and Georgeanu, V. (2014). Microbial production of enzymes: Nonlinear state and kinetic reaction rates estimation. *Biochem. Eng. J.*, vol. 91, 23-36.

Thoma, J., and Ould Bouamama, B. (2000). *Modelling and Simulation in Thermal and Chemical Engineering. A Bond Graph Approach*. Springer.

Author Index